Experimental Investigation of the Performance of Solar Dryer for Miten Shiro *Ingredients* Drying

Yeshiwas Zebene Cherinet

A Thesis Submitted to the Department of Mechanical Engineering

School of Mechanical, Chemical and Materials Engineering

Presented in Partial Fulfillment of the Requirement for the Degree of Master of Science in Thermal Engineering

Office of Graduate Studies
Adama Science and Technology University

June, 2023

Adama, Ethiopa

Experimental Investigation of the Performance of Solar Dryer for Miten Shiro *Ingredients* Drying

Yeshiwas Zebene Cherinet

Advisor: Dr. Addisu Bekele (Associate Professor)

A Thesis Submitted to the Department of Mechanical Engineering

School of Mechanical, Chemical and Materials Engineering

Presented in Partial Fulfillment of the Requirement for the Degree of Master of Science in Thermal Engineering

Office of Graduate Studies

Adama Science and Technology University

June, 2023

Adama, Ethiopia

DECLARATION

I hereby declare that this Master of Science Thesis entitled "*Experimental Investigation of the Performance of Solar Dryer for Miten Shiro Ingredients Drying*" is my original work. That is, it has not been submitted for the award of any academic degree, diploma or certificate in any other university. All sources of materials that are used for this thesis have been duly acknowledged through citation.

Yeshiwas Zebene Cherinet	____________________	________________
Name of the student	signature	date

RECOMMENDATION OF THE ADVISOR

I, the advisor of this thesis, hereby certify that I have read the revised version of the thesis entitled "*Experimental Investigation of the Performance of Solar Dryer for Miten Shiro Ingredients Drying*" prepared under my guidance by **Yeshiwas Zebene Cheinet** submitted in partial fulfillment of the requirements for the degree of Master of Science in Thermal Engineering.

Therefore, I recommend the submission of revised version of the thesis to the department following the applicable procedures.

Dr. Addisu Bekele	____________________	________________
Name of Advisor	Signature	Date

APPROVAL PAGE

I, the advisor of the thesis entitled "*Experimental Investigation of the Performance of Solar Dryer for Miten Shiro Ingredients Drying*" and developed by Yeshiwas Zebene Cherinet, hereby certify that the recommendation and suggestions made by the board of examiners are appropriately incorporated into the final version of the thesis.

Name of Advisor	Signature	Date

We, the undersigned members of the Board of Examiners of the thesis by Yeshiwas Zebene Cherinet have read and evaluated the thesis entitled "*Experimental Investigation of the Performance of Solar Dryer for Miten Shiro Ingredients Drying*" and examined the candidate during open defense. Therefore, this is to certify that the thesis is accepted for partial fulfillment of the requirement of the degree of Master of Science in Thermal Engineering.

Chairperson	Signature	Date
Internal Examiner	Signature	Date
External Examiner	Signature	Date

Final approval and acceptance of the thesis is contingent upon submission of its final copy to the Office of Postgraduate Studies (OPGS) through the Department Graduate Council (DGC) and School Graduate Committee (SGC).

Department Head	Signature	Date
School Dean	Signature	Date
Office of Post Graduate Studies, Dean	Signature	Date

ACKNOWLEDGEMENT

First and foremost, praises and thanks to God, the Almighty, for his blessings throughout my work to complete the thesis successfully. I am truly grateful for his unconditional and endless love, mercy, and grace. Secondly, I would like to express my sincere gratitude to my advisor Dr. Addisu Bekele for the continuous support of my study and research, and for his patience, motivation, and immense knowledge.

Besides my advisor, I would like to thank my instructors Dr. Dawit Gudeta and Dr. Gezahegn Habtamu for their invaluable encouragement and constructive suggestions throughout my academic life. My sincere thanks also go to my colleagues and friends who have supported me throughout this work.

Finally, I must express my very profound gratitude to my parents providing me with unfailing support and continuous encouragement throughout my years of study and through the process of researching and writing this thesis.

ABSTRACT

Miten Shiro which is a product of a mixture of various ingredients is used to make Ethiopian daily dishes. Miten Shiro flour producers mix ingredients like beans, peas, and chickpeas with onion, garlic, and ginger. It is first washed and spread on the ground in a thin layer as it to be dried. However, this process requires a large area, open space, and long drying times. Additionally, due to urbanization, people are now living together in apartments. This makes producing miten Shiro in the home more difficult in urban areas since there is no drying space in apartments. These factors oblige the consumers to buy the product from shops and of-course this is an opportunity for the sellers to produce in large quantities. Therefore, drying these grains hygienically in large quantities and within a short period of time is a requirement for the seller and this can be achieved by using solar dryers. In this study, a solar dryer with spoon-shaped obstacles mounted on the absorber plate is used for drying miten Shiro ingredients and its performance has been investigated experimentally. The experimental results indicated that the average useful heat gain value of 438.7 W and 231.1 W were obtained by the modified and conventional SAHs, respectively. The average thermal efficiency has ranged from 10.27% to 42.6% and from 20.6% to 62% for conventional and modified SAH respectively. Conventional and modified SAHs attained average maximum exergy efficiencies of 2.12% and 3.44% respectively. An average drying chamber useful heat gain value of 170.9 W and 140 W were found with and without enhanced solar collectors. Thermal efficiency value of 28.49% and 23.34% were obtained when it was integrated with the modified and conventional solar air heaters. An average maximum drying chamber exergy efficiency value of 1.22% and 0.73% were found with and without enhanced solar collectors. The moisture content of the product samples was reduced from their initial value to the final value in 18 hours in the drying chamber integrated with enhanced SAH and in 24 hours (three days) in the drying chamber integrated with conventional SAH. The final moisture content value of the multi-grain products was achieved after 34 hours (4 days and 2 hours) by open-sun drying. The overall efficiency of the drying system integrated with the enhanced collector was found to be 6.23%.

Key words: *Solar dryer, miten Shiro, spoon-shaped obstacles, solar collector. air distributor channel*

CONTENTS

LIST OF TABLES

LIST OF FIGURES

LIST OF SYMBOLS AND NOMENCLATURES

ACRONYMS

Symbols	*Description*
SAH	Solar air heater
DTSD	Direct type solar dryer
PBES	Packed bed energy storage
ITSD	Indirect type solar dryer
THPP	Thermo hydraulic performance parameter
SEC	Specific energy consumption

Symbols	*Description*
DPSAH	Double pass solar air heater
PBM	Packed bed material
MMFCSD	Mixed mode forced convection solar dryer
HTR	Heat transfer rate

NOMENCLATURES

Symbols	*Description*	*Units (SI)*
Re	Reynolds number	-
m	Mass	kg
E	Obstacles height	m
H	Duct height	m
$\boldsymbol{P_l}$	Longitudinal pitch	m
$\boldsymbol{P_t}$	Transversal pitch	m
B	The base width of obstacles	m
T	Temperature	^{o}C
M	The moisture content of a product	-
W	Mass of product samples	kg
D	Dry mass of product samples	kg
$\boldsymbol{m_w}$	Amount of water removed from a wet product	kg
$\boldsymbol{M_i}$	Initial moisture content	kg/kg
$\boldsymbol{M_f}$	Final moisture content	kg/kg
$\boldsymbol{M_o}$	Initial mass of product	kg
$\boldsymbol{Q_r}$	Quantity of heat energy for evaporating moisture from the product	J
$\boldsymbol{h_{fg}}$	Latent heat of vaporization	J/kg
$\boldsymbol{T_p}$	Maximum allowable temperature of the product	^{o}C
$\boldsymbol{\dot{V}_{air}}$	Volume flow rate of air	m^3/s
$\boldsymbol{\dot{m}_{air}}$	Mass flow rate of air	kg/s
$\mathbf{V}_{\boldsymbol{air}}$	Total volume of air	m^3
$\mathbf{t}_{\boldsymbol{d}}$	Total time required to dry a given samples	hr
St	Stanton number	-
Q	Convective heat transfer	W/m^2
C_p	Specific heat	J/kgK
$\mathbf{T}_{\boldsymbol{d,max}}$	Air temperature at the collector outlet	^{o}C
$\boldsymbol{T}_{\infty}$	Ambien temperature	^{o}C
H	Efficiency	-
L	Length	m
W	Width	m
Q_u	Useful heat collected by the collector	W

$\boldsymbol{\rho_{gr}}$	Bulk density of the product (wb)	kg/m^3
$\boldsymbol{h_L}$	Layer drying bed thickness	m
ξ	Product porosity	-
$\boldsymbol{\varepsilon_v}$	Loading bed void fraction	%
R_a	Gas constant	J/kgK
RH	Relative humidity	%
P_a	Partial pressure of dry air	Pa
$\boldsymbol{D_p}$	Thickness of the product	m
$\boldsymbol{P_{total}}$	Total energy input to the drying system	MJ
$\boldsymbol{I_b}$	Beam radiation	W/m^2
P	Static pressure	Pa
$\vec{\boldsymbol{F}}$	External body force	N
$\bar{\bar{\boldsymbol{\tau}}}$	Stress tensor	Pa
$\boldsymbol{h}$	Convective heat transfer coefficient	W/m^2K
Nu	Nusselt number	-
K	Thermal conductivity	W/mK
$\boldsymbol{I_o}$	Extraterrestrial solar radiation on a horizontal surface	W/m^2
I	Monthly average hourly global solar radiation on a horizontal surface	W/ m^2
H	Monthly average daily global solar radiation on a horizontal surface	$J/ m^2/day$
$\boldsymbol{M_p}$	Moisture percent	

SUBSCRIPTS AND SUPERSCRIPTS

Symbols	*Description*
G	Vapor
L	Liquid
Min	Minimum
C	Collector
Db	drying bed
Dc	drying chamber
W	Wind

Symbols	*Description*
O	duct with obstacles
S	smooth duct
Max	Maximum
Min	Minimum
P	Product
Co	Cover of the chamber
Ad	Air inside the chamber

GREEK SYMBOLS

Symbols	*Description*	*Units (SI)*
α	absorptivity	-
$\boldsymbol{\theta_z}$	Zenith angle	$(^o)$
$\boldsymbol{\Phi}$	Latitude angle	$(^o)$
δ	Declination angle	$(^o)$
ω	Solar hour angle	$(^o)$
$\boldsymbol{\alpha_s}$	Solar altitude angle	$(^o)$
γ	Surface azimuth angle	$(^o)$

Symbols	*Description*	*Units (IS)*
$\boldsymbol{\gamma_s}$	Solar azimuth angle	$(^o)$
β	Tilt angle	$(^o)$
$\boldsymbol{\theta}$	Angle of incidence	$(^o)$
$\boldsymbol{\omega_s}$	Sun rise and sunset angle	$(^o)$

CHAPTER ONE
INTRODUCTION

1.1 Background

Commercial enterprises in Ethiopia produce a variety of food ingredients and supply them to local customers and also export them abroad. These food constituents mainly include Ethiopian chili pepper (berbere), Shiro (bean, pea, or chickpea powder), Beso (prepared barley powder), Aja (oatmeal), and Miten Shiro (balanced Shiro).

Miten Shiro (balanced Shiro) is a product of beans, peas, chickpeas, red pepper, onion, salt, garlic, and ginger. Beans, peas, and chickpeas are roasted and washed. These moist ingredients are then mixed with red pepper, onion, garlic, and ginger which contain high moisture content (Djaeni et al., 2017). Miten Shiro is dried and milled to make miten Shiro flour which in turn is used to make Shiro wot or Shiro (Ethiopian stew).

Shiro Wot (a thick stew) is a staple in any Ethiopian vegetarian platter. It simmered and served over a thin flatbread called injera with a variety of other vegetarian dishes.

Miten Shiro is suitable and preferable for cooking since it has every ingredient required for Shiro wot making. This will avoid a step-by-step addition of ingredients and lead us to a short cooking time.

Miten Shiro flour is produced, packed, and sold by different Baltina shops throughout the country and in the international market. Producers use the open sun drying technique to dry these daily dish flour moist ingredients after the mixing process is done.

To anyone who produces miten Shiro flour, one of the most serious challenges is the drying process of the moist mixed ingredients. Producers use the open sun drying technique to dry these daily dish flour moist ingredients after the mixing process is done. Traditional open sun drying requires a large area, open space, and long drying times. It is extremely dependent on the availability of sunlight and vulnerable to contamination by fungi, insects, and foreign materials, all of which degrade the quality of the final product. Open sun drying is labor intensive and products being dried are susceptible to spoilage from rain, wind, moisture, and dust (Mustayen et al., 2014).

Local producers claim that the laborious process of sun dehydrating the moist ingredients in miten Shiro during the winter requires more than seven straight days. The sales value is thus decreased as a result. In these circumstances, solar-energy dryers look more and more intriguing as a potential business venture (Ekechukwu & Norton, 1999).

Solar drying is a renewable, eco-friendly, and promising application of solar energy systems technology (Akarslan, 2012). It is the best approach for preserving food, which offers high quality and requires less storage space (El-Sebaii & Shalaby, 2012).

Although solar radiation has been used for drying since antiquity, it has not yet been widely commercialized, especially in the industrial sector. Governments and industries are urged to embrace renewable energies as a clean and sustainable resource because of environmental concerns and harms caused by humans as a result of increased fossil fuel consumption. Thus, it is projected that using solar energy for drying would become necessary in the future due to the limited supply of natural resources and the rising cost of fossil fuels (Pirasteh et al., 2014). Solar energy is a clean and the most plentiful permanent energy source on the planet. The solar drying of food, including agricultural fruits and vegetables, has been covered in a number of recent research (Fudholi et al., 2012). Solar dryers produce high-quality goods by harnessing the free energy of the sun and precisely controlling the radiant heat (El-Sebaii & Shalaby, 2012).

1.2 Working principle of solar dryer

The main principle of solar drying is to collect solar energy by heating the air volume inside the solar air heater duct, then air circulators are used to transport the heated air from the collector to the drying chamber. The solar energy incident on the absorber plate keeps the inner environment warm. The grains to produce miten Shiro are placed in the drying chamber. The air enters the collector duct through a hole between the absorber plate and the base plate. Then, the air flows through the trays to dry the product and ventilates the atmosphere through an air outlet after avoiding the moisture from the surface of the product. An exhaust fan as an active mode is used in this work, which helps to suck the heated air from the solar collector into the drying chamber.

1.3 Statement of the problem

Producers and distributors of Baltina products (constituents for food preparation) face a substantial obstacle during the drying of miten Shiro mixed ingredients. Despite its many disadvantages, the open sun drying method is employed to carry out this vital procedure. Additionally, due to urbanization, people are now living together in apartments. This makes producing miten Shiro in the home a tedious process as it creates a high odor that may disturb the whole floor of the building. These factors oblige the consumers to buy the product from only

Baltina shops. Conversely, the most effective alternative to these disadvantages is solar drying. Therefore, drying these grains hygienically and within a short period is mandatory. Solar drying produces high-quality products by avoiding contamination from dust, insects, wind, rain, and fungi. Furthermore, it entirely removes the necessity for lengthy time consumption, large area demand, and labor intensity compared to the traditional way of drying in an open field.

The performance of solar dryers needs to be improved for them to be energy-efficient, and capable of the fastest drying rates. A solar dryer with spoon-shaped obstacles mounted absorber plate is introduced to maximize the air to be trapped to the absorber plate for maximum convective heat transfer.

1.4 Objectives

1.4.1 General objective

The general objective of the thesis is to investigate the thermal performance of a solar dryer theoretically and experimentally which is used for miten Shiro ingredients drying.

1.4.2 Specific objectives

- To design and develop the prototype of the designed solar air dryer
- To analyze the performance of the solar air heater with an experiment in terms of useful heat gain, energy, and exergy efficiency
- To analyze the performance of the drying chamber with an experiment in terms of useful heat gain, energy, and exergy efficiency
- To compare the solar drying system to be developed with that of the conventional and open sun drying system.

1.5 Significance of the study

Despite, miten Shiro is rich in every ingredient required for Shiro wot (stew) making, it has a long drying time and related problems due to open sun drying of its constituents. This study will avoid the problems related to open sun drying by providing a solar dryer for Miten Shiro ingredients drying.

1.6 Scope and limitations of the study

This study mainly focused on the design, fabrication, and experimental analysis of forced solar air dryer with the suitable material selection. The ingredients are prepared for drying by washing and chopping them. The study also developed a numerical simulation to examine the air flow behavior within a solar air heater with absorber plate mounted spoon-shaped obstacles. A numerical simulation also developed to study the effectiveness of the drying chamber combined with the vertical V-shaped air distributer channel. The developed prototype is constructed from locally available materials and tested under the climatic condition of Adama. The simulation results in this study did not take into account the effect of moist ingredients on various flow parameters.

CHAPTER TWO
LITERATURE REVIEW

2.1 Introduction

World demand for energy is rapidly increasing as a result of population growth and technological advancements. It is abundantly evident that investing in renewable energy is necessary to prevent potential energy crises and reverse climate change after a string of global upheavals (Kannan & Vakeesan, 2016).

Since long ago, foods have been dried using the heat from the sun and the wind. Vegetables and other food crops cannot be adequately dehydrated using the conventional method of open-air sun drying because the end products become polluted. High ambient temperatures and relative humidity increase their deterioration. (Ayensu, 1997). There is a great strive in the field of developing low-cost and heat energy-efficient solar dryers for food production and protection.

This chapter will cover various solar dryers that have been previously built and discuss the requirement for drying.

2.2 Classification of solar dryers

The main goal of drying is to lower the moisture content of products to a position that prevents degradation within a specific time frame, which is typically referred to as the "safe storage period." According to Ekechukwu and Norton (1999), drying is a two-step process that involves both heat transfer from the heating source to the product and mass moisture transfer from the inside of the product to its surface and ultimately to the air outside.

2.2.1 Classification based on operating temperature

All drying systems can be divided into two primary classes, high temperature dryers, and low temperature dryers, principally based on the working temperature ranges. However, the two main classifications of dryers are those that utilize fossil fuels and those that use solar energy. Accordingly, solar energy or fossil fuels are used to power low temperature dryers, while all realistically available designs of high temperature dryers use fossil fuels (Ekechukwu & Norton, 1999).

2.2.2 Classification based on utilization of solar energy

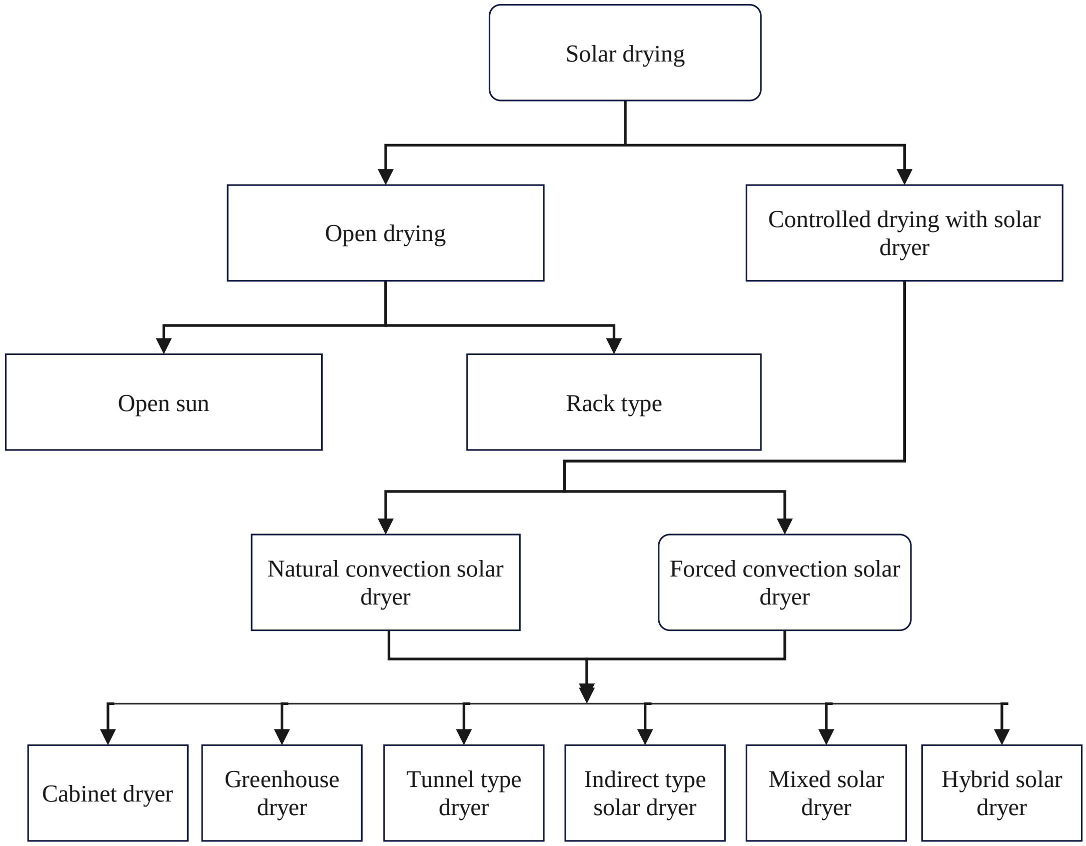

Figure 2. 1: Classification of solar dryer system (Lingayat et al., 2020)

A. Direct type solar dryer (DTSD)

Direct type solar dryers utilize a glass cover to reduce heat losses, and concurrently provide the product with forceful protection from contamination. The aeration required to remove the evaporated water is provided by ascending air forces. However, it is impossible to avoid infestations in this process (Mustayen et al., 2014). This kind of dryer is relatively uncomplicated to construct, affordable, requires less maintenance, and is simple to use (Kumar and Singh, 2020).

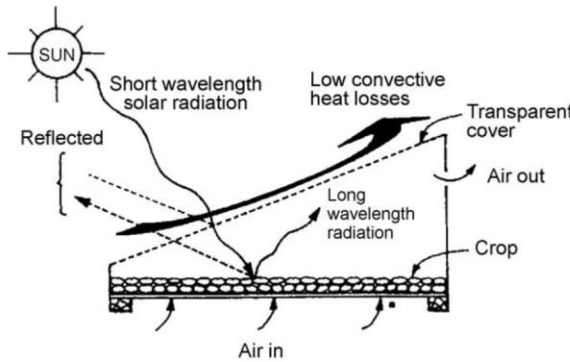

Figure 2. 2: Direct solar dryer working principle (Sharma et al. 2009)

B. Indirect type solar dryer (ITSD)

Indirect type solar dryers are different from direct type solar dryers in terms of moisture removal and heat transfer. This kind of dryer is used to dry products fast. The atmospheric air is heated by a solar air heater before entering the drying compartment. Products are kept dry in the drying chamber while some moisture is removed from them by hot air. Finally, the chimney serves as the air escape for the drying cabin (Kumar and Singh, 2020).

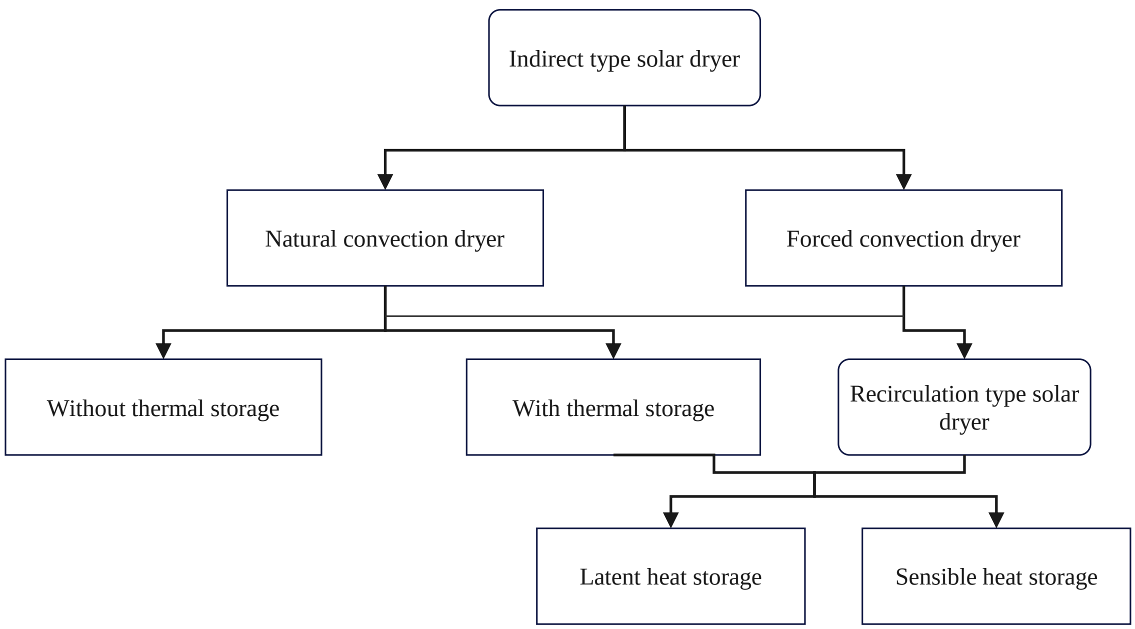

Figure 2. 3: Classification of indirect type solar dryer (ITSD) system (Lingayat et al., 2020)

To reduce crop surface cracking and discoloration, the crop is not exposed to sunlight directly. The products are placed on trays in the drying chamber (Sharma et al. 2009).

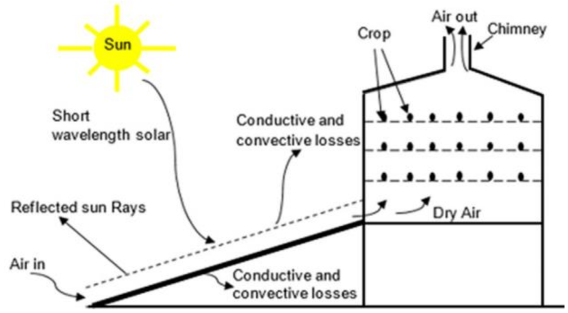

Figure 2. 4: Indirect type solar dryer working principle (Lingayat et al., 2020)

C. Mixed-type solar dryers

Direct and indirect solar dryers are employed in mixed mode solar dryers. In a solar dryer that operates in a mixed mode, solar air collectors heat the incoming air before it enters the drying chamber. The drying chamber has glass sides on several of its sides, which provides additional heating. This method dries the product with hot air and sunlight. Mixed mode solar dryers need less drying time than direct and indirect solar dryers (Kumar and Singh, 2020).

Lakshmi et al. (2019) studied the performance and economic analysis of mixed mode forced convection solar dryers and compared it with open sun drying of stevia leaves. The experimental comparison was carried out under the average solar radiation of 567 W/m^2, ambient temperature of 30 °C, and drying air flow rate of 0.049 kg/s. According to the results obtained the overall dryer efficiency and average exergy efficiency were 33.5% and 59.1%, respectively. Furthermore, the mixed-type forced convection solar drier required substantially less drying time to obtain the required moisture content.

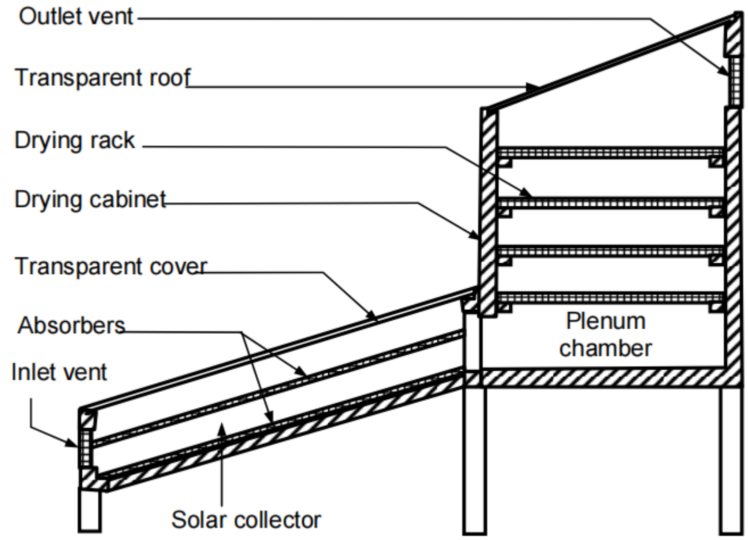

Figure 2. 5: Mixed-mode solar dryer sectional view (Bolaji and Olalusi, 2008)

D. Hybrid solar dryer

Alternative solar energy sources include hybrid solar dryers, which combine solar energy with other energy sources such as fossil fuel, biomass solid fuel, and electrical energy (Pirasteh et al., 2014).

Amer et al. (2010) developed and analyzed the performance of a hybrid solar dryer to dry banana slices. The dryer was used as a solar dryer on usual sunny days and as a hybrid solar dryer on gloomy days. With the aid of electric heaters installed in the water tank and the heat energy that was stored in the water during the day, drying was also done at night. In this investigation, a single layer of banana slices with a thickness of 4-5 mm and an initial moisture level of 75-82% (wet basis) was used. It was noticed that the dryer could hold 30-32 kg of this product. When used exclusively as a solar dryer, the efficiency was determined to be 37.4%, however, it was determined to be 31.7% when water was heated before sunlight and the drying process started with the solar dryer alone. Additionally, it was discovered that when the weather was unfavorable, using an extra heating source (6 kW) for 8 hours with the solar dryer had a 25.3% efficiency.

2.2.3 Classification according to the mode of air flow

Solar dryers can also be divided into natural convection (passive mode) and forced convection (active mode) solar dryers depending on the mode of airflow.

A. Natural circulation type (passive mode)

In a passive solar dryer, the air is heated and circulated naturally by wind pressure, buoyancy force, or a combination of the two. Due to the thermosyphon effect, the heated air rises and is expelled through the roof of the greenhouse (Singh & Gaur, 2020). Dryers for greenhouses and normal and reverse absorber cabinets run in passive mode.

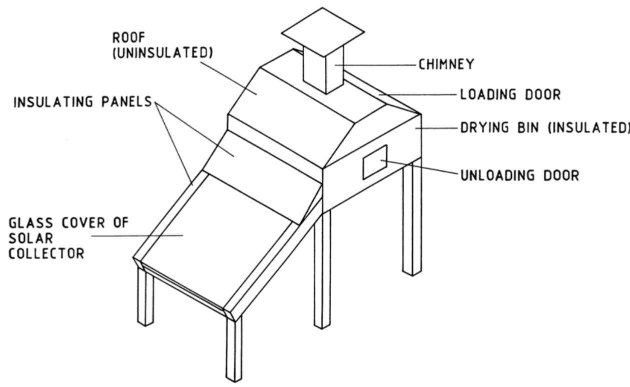

Figure 2. 6: Natural-circulation type solar dryer (Ekechukwu & Norton, 1999)

B. Forced convection type (active mode)

Active solar dryers are made using components like fans or pumps to move heated air produced by solar energy from the solar air heater duct to the drying chamber. Typical active solar dryers only employ solar energy as a heat source; fans and pumps are used for circulating air (Balasuadhakar et al., 2016).

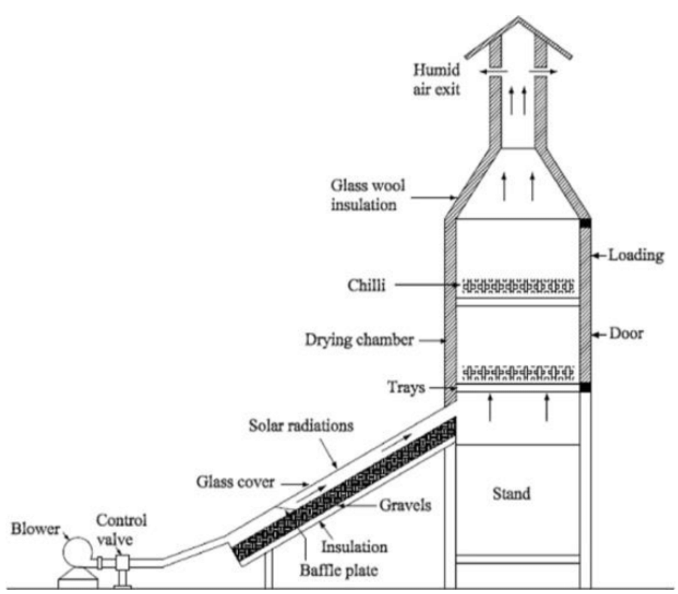

Figure 2. 7:Forced convection solar dryer (Singh & Gaur, 2020)

Mohanraj and Chandrasekar (2008) developed a forced convection type solar dryer for copra drying. With its two sides, the collector was attached to a drying chamber and connected to a centrifugal fan. The sand was used to fill the space between the insulation and the absorber to store heat. The moisture content of the copra in the bottom and top trays was reduced by the drier in 82 hours from 51.8% to 7.8% and 9.7%, respectively. The solar dryer thermal efficiency was determined to be around 24%.

2.3 Solar air heater (SAH)

The most straightforward and effective approach of using solar energy is to transform it into thermal energy for use in heating. A solar air heater is a solar thermal device that utilizes an absorbing media to collect solar energy and uses it to heat the air that is blowing over a surface. Due to their fundamental simplicity, solar air heaters are among the most popular and affordable collecting devices (Varun et al., 2007).

2.3.1 Components of solar air heater

The basic components of solar air heaters are the covering plate, an absorber plate, and insulations. The solar energy that enters the transparent cover of the solar collector is absorbed by the absorber plate, which then distributes the heat to the air.

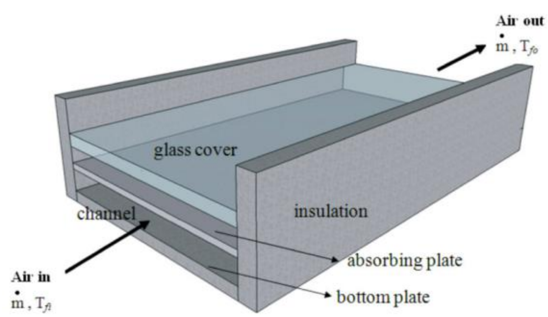

Figure 2. 8: Solar air heater components (Yeh, 2014)

A. Cover plate

A component of a solar air heater, the cover plate (glazing) transports the incident solar radiation to the absorber plate. Glass and plastic are frequently utilized as glazing materials (Bakari et al., 2014).

B. Absorber plate

An absorber plate is a material with a high thermal conductivity that collects the incident solar radiation and transfers it to the air in a solar collector. In order to boost absorption percentage, absorber plates are typically coated black (Sarbu, 2017).

C. Insulation

The greater performance of solar collectors depends on preventing heat losses from absorber plates, either through conduction or convection. The greatest heat resistance is provided by insulation, which reduces this loss. Today, fiber glass, mineral wool, glass wool, and thermo foam are the most used insulation materials (Paneri et al., 2019).

2.3.2 Performance improvement techniques of solar air heaters

The advancement in solar dryer performance has drawn the attention of many different sorts of research. Researchers have discovered that a variety of techniques and approaches might be employed to improve the performance. Increasing the convective heat transfer coefficient with a little pressure drop penalty enhances the heat transfer rate. (Alam & Kim, 2017). They have experimented with several methods to increase the convective heat transfer coefficient. The uses of these distinct strategies are covered in the following subsection.

A. Extended surfaces

Two distinct functions are served by the extended surfaces attached to the absorber plates. They turbulate the flow and also act as fins to increase the area for heat transmission. Various extended surfaces, such as baffles, fins, and corrugated absorbers, have been studied by several researchers (Alam & Kim, 2017).

Bekele *et al.* (2014) experimented to collect data on heat transfer and flow friction from an air heater duct with obstacles positioned in the form of deltas on the absorber surface and with a 6:1 aspect ratio. A uniform heat flux of 800 W/m^2 is applied to the absorber plate. The experiment was carried out by the authors for a Reynolds number (Re) range of 2100 to 30,000, a relative obstacle height (e/H) range of 0.25 to 0.75, a relative obstacle longitudinal pitch (Pl/e) range of 3/2 to 11/2, a relative obstacle transverse pitch (Pt/b) range of 1 to 7/3, and a relative angle of incidence (α) range of 30^o to 90^o. The parameters of P_l/e = 3/2, Pt/b = 7/3, e/H = 0.50, and = 30^o produce the best thermo-hydraulic performance of the solar air heater with delta-shaped obstacles positioned on the absorber plate across the whole examined Reynolds number range. With an incidence angle of 30° and 60°, in particular, they have achieved better results than the other enhancements to heat transfer methods previously used. (Esen, 2008) carried out a thorough experimental energy and exergy analysis for an innovative flat plate solar air heater (SAH) with a number of obstacles and without obstacles. The inlet and outlet temperatures, the temperatures of the absorber plates, the surrounding temperature, and the sun radiation were all measured parameters. The experiments were conducted at different mass flow rates of air and absorber plate levels inside the duct of flow. According to the results, a double-flow collector provided with obstacles performs noticeably better than one without them.

B. Artificial roughness

The surface area for heat transfer is not greatly enhanced by artificial roughness, which is only employed to create turbulence near hot surfaces. The performance parameters of a solar air heater can be significantly enhanced by the application of artificial roughness in the form of extensions and grooves of varied size, form, and orientations on the underside of a heated surface. These laminar sub-layers create heat flow resistance (Kumar et al., 2022).

A comparison of various forms of artificial roughness geometries mounted on the absorbing plate of solar collector and their heat transfer and friction characteristics has been presented by (Gupta & Kaushik, 2009). The performance has been evaluated in terms of energy efficiency, exergy efficiency, and effective energy efficiency has been carried out for various values of the Reynolds number. Six different roughness geometries have been chosen following their capacity to produce turbulence. The researchers discovered that artificial roughness on the surface of the absorbing plate significantly improves efficiency when compared to a smooth surface. Finally, they have concluded that for greater flow cross-sectional areas of solar collector ducts with small Reynolds numbers, the roughened surface will produce more turbulence.

An experimental investigation was conducted by Aboghrara et al. (2017) to determine the jet impingement effect on the corrugated absorbing plate. The results are then compared with conventional solar collectors with flat plate absorbers. Nearly 14% greater thermal efficiency is observed in the proposed design duct than in the smooth duct.

C. Packed bed

In a double-pass solar air heater, a packed bed provides two functions. Due to the huge surface for heat transfer and significant flow turbulence, it first increases the rate of heat transmission. Second, to satisfy demand, the packed bed accumulates thermal energy and releases it continuously into the air. A packed bed further improves the convective heat transfer coefficient since it retains more energy than a collector with a limited height due to the substantial depth of packing material.

A solar dryer that incorporates a packed bed as a thermal energy storage medium to dry orange slices was analyzed for its energy and exergy based performances by (Atalay, 2019). The results showed that the moisture content of the slices was decreased by a solar dryer integrated with a packed bed from 93.5% to 10.28% at the first trial (sunshine hours) and 10.76% at the second experiment (off sunshine hours), respectively. During sunshine hours, the exergy efficiency of the drying system ranged from 50.18 to 66.58%. When utilizing the thermal energy that was previously saved, the exergy efficiency varied between 54.71 and 68.37%.

D. Porous media

Porous media can be used to increase the heat transfer area and enhance the heat transfer rate. Naphon (2005) conducted a numerical investigation to compare the heat transfer characteristics and performance of the double-pass flat plate solar air heater with and without porous media. The implicit method of the finite-difference scheme was applied to solve the developed models. A solar air heater with porous media had a thermal efficiency of 25.9% higher than one without.

E. Phase change materials

Thermal energy can be stored in phase change materials during the day and released at night. Lamrani and Draoui (2020) presented a numerical study of the performance of a passive solar dryer of wood integrated with a thermal energy storage medium. To investigate the dryer thermal performance, numerical simulations were run using the TRNSYS software. The validation showed a good agreement and a maximum relative error of 2.49% obtained. The storage system utilized also reduced the payback period significantly.

Abdu (2021) designed, and experimentally investigated the performance of a solar dryer integrated with a double flow solar collector, baffles, and thermal energy storage. A DPSAH performance was examined with and without baffles. The result showed DPSAH with baffles increased air temperature change, and average thermal and average exergy efficiency of the solar collector increased by 6 ℃, 7%, and 0.53%, respectively.

F. Nanofluids

Over the last few years, the capability to produce tiny particles has increased, and an entirely novel type of solid-liquid mixture termed a nanofluid has arisen. An advanced type of fluid known as a "nanofluid" contains a tiny number of uniformly dispersed nanoparticles (often fewer than 100 nm in size) (Muhammad *et al.*, 2016). Nanofluids can be used to improve the thermal conductivity and heat transmission rate in solar air heaters.

Merdokiyos (2022) developed a solar greenhouse dryer and tested it experimentally to dry 5 kg of washed coffee beans. The output temperature of the collector is increased using a double pass, reverse back reflector, and black ink with 3% concentrated nanofluid paint.

The following is a full summary of the literature investigating the performance of various types of solar dryers for food and crop drying. Tabulation is provided to summarize the works of literature reviewed, listing the methods used and results obtained.

2.4 Drying chamber

A drying chamber is a compartment with trays where the product to be dried by the heated air coming from the SAH is placed. The drying chamber by itself heat further the air coming out of the SAH if it is constructed from a good solar absorptance material. Several researches have been carried out to improve the performance of the drying chamber of solar air dryers.

Sileshi et al. (2022) studied the performance of a mixed-type solar dryer to dry 10 kg of injera with a new feature air distributer channel inside the drying chamber. They have performed a numerical simulation to improve the airflow and air temperature distribution characteristics inside the drying chamber. According to the results, a homogenous air intensity distribution is obtained by the air distributor channel.

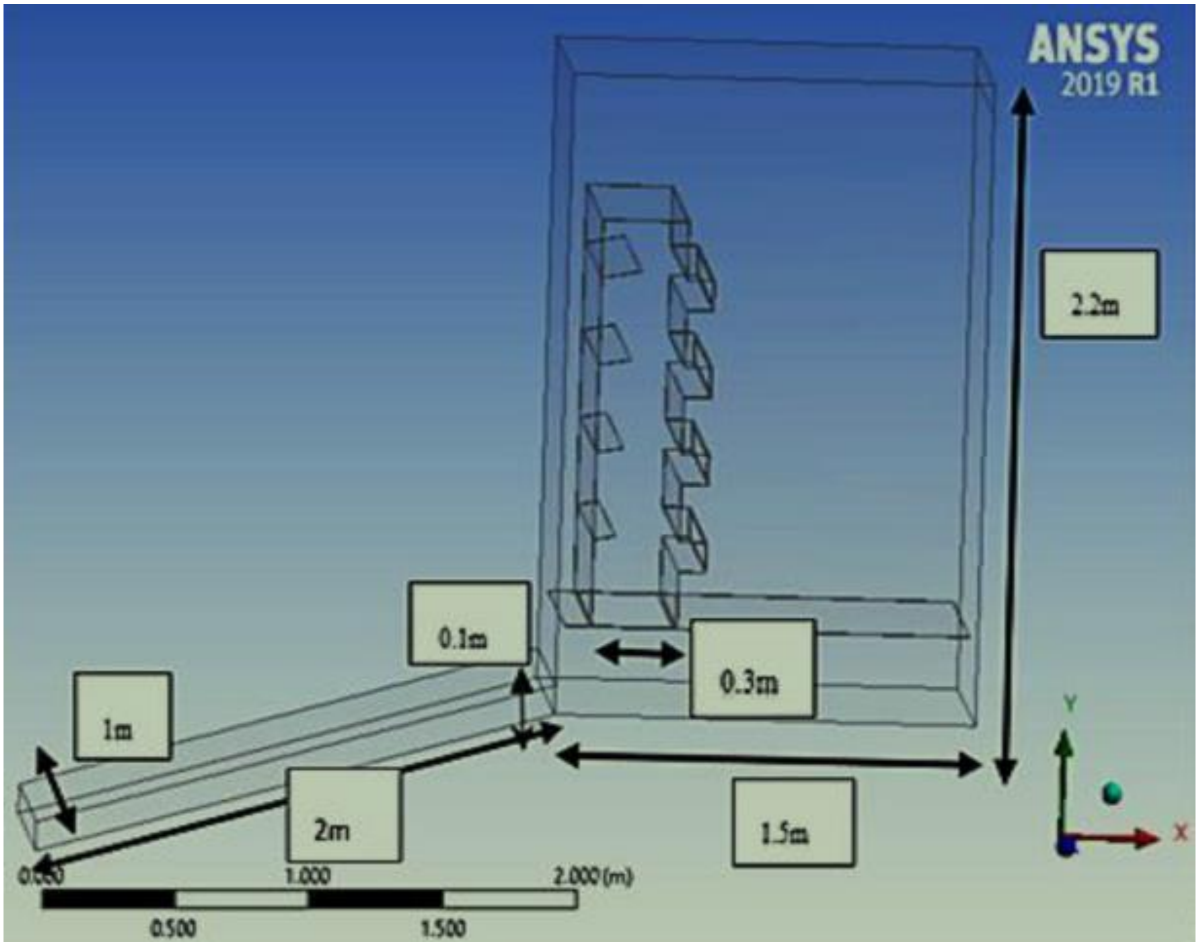

Figure 2. 9: Air distributor channel constructed

2.5 Literature summary and research gap

2.5.1 Literature summary

A comprehensive literature review on the performance of various types of solar dryers for food and crop drying and the effects of various parameters on the drying process has been carried out. Several researchers have strived to enhance the performance of different types of solar dryers by using a variety of ways. Among the methods used to increase the convective heat transfer coefficient are packed bed materials (PBMs), extended surfaces (obstacle ribs and wires), corrugated absorbent surfaces, nanofluid, and jet plate solar air heaters.

2.5.2 Research gap

A properly designed indirect active solar dryer for Miten Shiro ingredients which are used for miten Shiro preparation has not been done yet. All these grains have different moisture content. Thereby, an experimental performance investigation was performed as all the grains reach their suitable moisture content.

A few attempts had been made to trape the maximum amount of the airflow inside the duct of the SAH as it impinges with the high temperature absorber plate to enhance the convective heat transfer. Moreover, there is a very limited number of papers discuss the improvement of air flow distribution inside the drying chamber.

To fill the gaps listed a new feature obstacle and air distributing system is expected from this investigation.

Table 2. 1: Summary of the literature reviewed

Authors	Classification	Analysis	Performance evaluation	Modifications
Bekele *et al.* (2014)	Forced convection type SAH	Experimental	$\frac{Nu_o}{Nu_s} = 5.88, \frac{f_o}{f_s} = 3.47, \frac{St_o/St_s}{f_o/f_s^{1/3}} = 3.89$	Delta-shaped obstacles mounted on the absorber surface
Esen, (2008)	Forced convection type SAH	Experimental	Maximum efficiency of 60.97% with a 0.025 kg/s mass flow rate is obtained using delta-shaped obstacles.	Triangular obstacles, delta-shaped and rectangular ones with triangular tips are used for comparison.
Ozgen et al. (2009)	Forced convection type SAH	Experimental	The mean efficiency for a 0.05 kg/s mass flow rate is 55% for a staggered arrangement of the cans.	Aluminum cans mounted on the absorber plate
Aboghrara et al. (2017)	Forced convection type SAH	Experimental	A maximum thermal efficiency of 68% is obtained for a mass flow rate of 0.028Kg/s.	Jet impingement on the corrugated absorber plate
Naphon (2005)	Forced convection type SAH	Numerical	25.9% higher thermal efficiency than that without porous media	Porous media
Merdokiyos (2022)	Forced convection-type solar greenhouse dryer	Experimental and Numerical	Mean efficiency of the greenhouse=21.5% Mean efficiency of the solar collector=42.1%	Reverse back reflector, nanofluid, TES
Atalay (2019)	Forced convection solar dryer	Experimental and Numerical	The maximum exergy efficiency of 68.37%	Packed bed
Kumar and Layek (2019)	Forced convection type SAH	Experimental and Numerical	Thermal and exergy efficiency increased by 1.81 and 1.8 times higher than without the roughness	Twisted rib roughness

CHAPTER THREE
MATERIALS AND METHODS

This chapter introduces the methods employed to get through the work and the materials and equipment used. The techniques and models used have also been completely addressed.

3.1 Introduction

The primary methodology used in the current work uses theoretical and experimental analysis. For the evaluation of every component, governing equations are used to explain the theoretical approach. The methods for presenting and evaluating results from experiments, as well as the materials and equipment used, are all discussed in this section. These methods will be used for the experimental investigation and performance assessment of the current solar dryer.

3.2 Materials and equipment

The materials, measuring tools, and components of the system needed to build the experimental prototype are purchased from the local markets. Materials utilized to build the experimental setup were chosen based on cost-effectiveness, local availability, and specialist properties for unique applications. The primary components and measuring tools used in the experiment are listed below.

Materials;

- **Galvanized iron sheet**: used for constructing the absorber plate.
- **Rectangular iron**: used for constructing the greenhouse, and enhanced solar collector supporter.
- **Transparent Glass**: used for covering the solar collector.
- **Black paint:** used to paint the absorber plate and the drying chamber to increase the absorbance of the absorber plate.
- **Insulators:** used for covering the base of the absorber plate to reduce thermal heat loss.
- **Fan:** used for initiating the air flow through the dryer by creating a pressure difference.

Measuring instruments;

- **Digital weight balance:** to measure the mass of products.
- **Thermocouple wires:** to measure the temperature of products and components.
- **Digital thermometer:** to measure ambient temperature and for calibration.

3.3 Methodology

This study focuses on theoretical and experimental analysis to evaluate the performance of a technically upgraded solar dryer for Miten Shiro ingredients drying. The theoretical approach analyzes the components of the dryer using governing equations. The prototype was built for the experimental performance investigation after selecting the materials to be used and designing each component. Experimental evaluation was performed by first testing the SAH without applying newly applied spoon-shaped turbulators. Then, the bottom side of the absorber plate was artificially roughened for further heat gain and tested. Figure 3.1 shows the overall methodology to be followed.

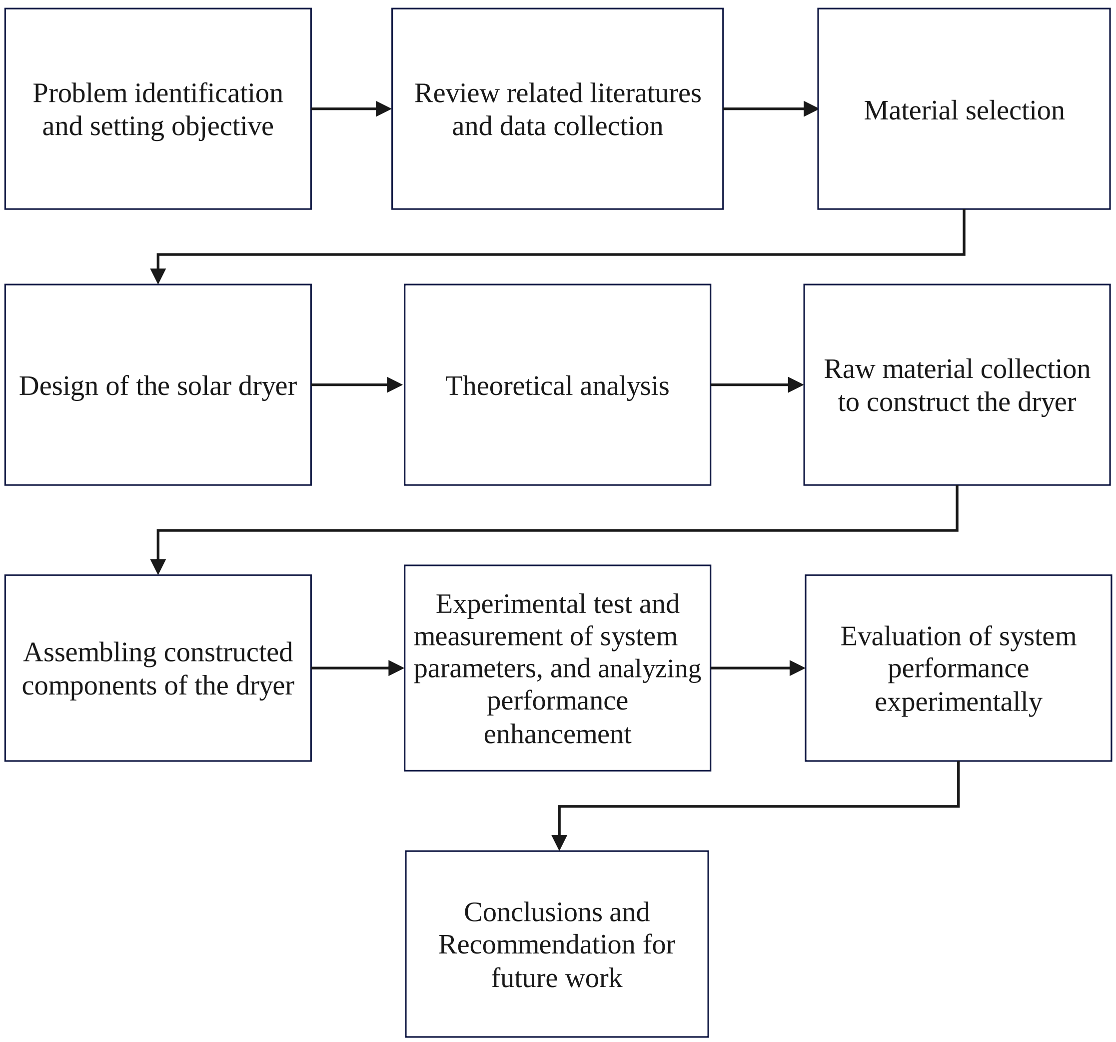

Figure 3. 1: Methodology

3.3.1 Literature review

A thorough analysis of the literature on the effectiveness of various solar dryer types for drying food and crops served as the foundation for the investigation. Effects of various parameters on the drying process, approaches and techniques for performance improvement, the methodology used, the drying time, and the results obtained have all been reviewed. With the information acquired, solar dryer performance improvements were developed for further system development.

3.3.2 Data collection method

The data needed for the entire work is gathered from both primary and secondary data sources. Primary data about the preparation of miten Shiro is collected by visiting the producers. The main information includes its constituents, how they are mixed, how long it takes to dry in the open sun, etc. Further, the moisture content of the ingredients of miten Shiro was determined using an oven. Secondary data are obtained from literature reviews of different books, journals, and websites.

Excel (spreadsheet) is the primary program utilized in this thesis for data storage, estimate, analysis, and interpretation for temperature variation and timely altering of parameters during the experimental tests.

3.3.3 Physical concept

After modifying the design of a solar dryer, a schematic drawing of the system integration and all the components is provided. Using ANSYS SpaceClaim 2021R2 Software, a 3D or pictorial view of the designed solar dryer was developed. Block diagrams of the experimental setup were drawn to understand the experimentation process. The flow process of the system and the working principle were discussed to understand the concept of the system.

3.3.4 Mathematical model

To analyze the performance of a solar dryer, a mathematical model was developed. A drying chamber with two parallel distributors and one without was modeled to compare them in terms of the temperature distribution and flow character. A numerical simulation was also carried out to investigate the flow behavior inside the SAH duct.

3.4 Experimental design procedure

Figure 3.2 describes the experimental flow diagram.

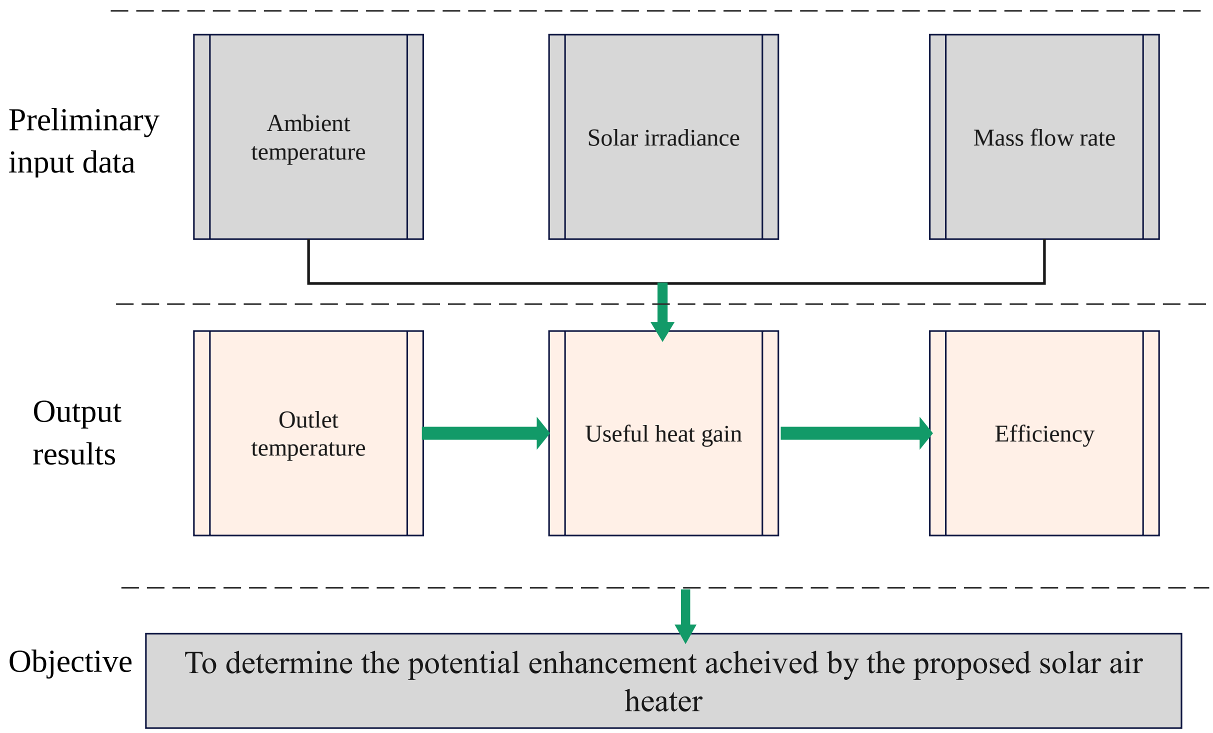

Figure 3. 2: Block diagram of the experimental analysis

CHAPTER FOUR

DESIGN AND THEORETICAL ANALYSIS OF THE SOLAR DRYER

This chapter explains the design of the solar dryer as well as the energy and exergy equations that are utilized for predicting thermodynamic performance. An incident solar radiation through the glass is absorbed by black painted absorber plate. The plate transfers the majority of the energy it absorbs to the air by convection. The hot air is then used in the drying chamber to dry grains which are used for miten Shiro preparation. For the solar dryer to produce hygienic and nutritious products, this is the prerequisite.

4.1 Analysis and estimation of solar radiation intensity

Solar radiation intensity data is necessary to determine the total solar energy incident on the solar collector. Estimation of solar radiation intensity using climatological data is used as an input to the energy and mass balance model.

Adama is located at 8.514477N latitude and 39.269257E longitude. Figures 3.3 and 3.4 illustrate the key ten years of data taken from meteorology for Adama City from 2012 to 2021.

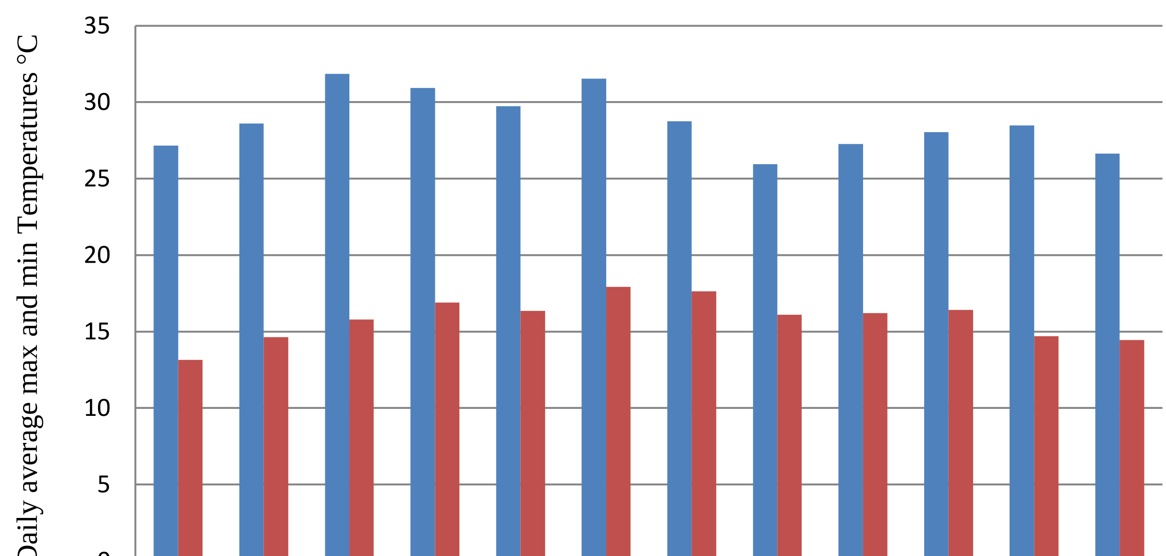

	Januar y	Februa ry	March	April	May	June	July	Auges t	Septe mber	Octob er	Nove mber	Dece mber
Tmax	27.16	28.61	31.85	30.93	29.73	31.53	28.74	25.95	27.26	28.04	28.48	26.63
Tmin	13.15	14.63	15.79	16.89	16.36	17.92	17.63	16.09	16.21	16.42	14.69	14.45

Figure 4. 1: Daily maximum and minimum temperature for Adama

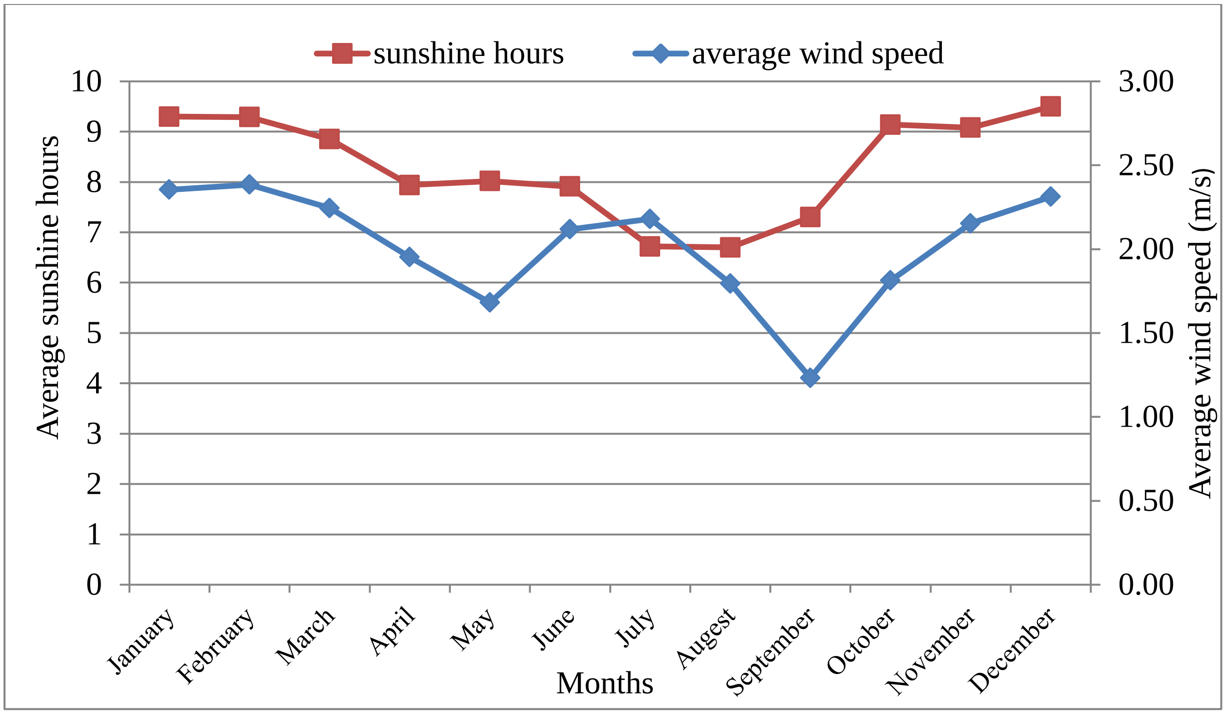

Figure 4. 2: Monthly average sunshine hour and wind speed of Adama

The key meteorological factors that have a significant impact on the performance of the solar collector and drying chamber are ambient temperatures, wind speed, and global irradiation.

4.2 Basic Solar Angles

Latitude angle (ϕ): is an angle that is 0° at the Equator and ranges from -90° at the south pole to 90° at the north pole. (Karney & Deakin, 2009).

Declination Angle (δ): the angular position of the sun at solar noon (i.e., when the sun is on the local meridian) concerning the plane of the equator, north positive; $-23.5^{o} \leq \delta \leq 23.45°$ (Maleki et al., 2017; Venkatachalam et al., 2019). Where n is a day of the year that is counted starting from January 1.

$$\delta = 23.45° \sin (360°(284 + n)/365) \quad (4.1)$$

Hour angle (ω): the angle formed by the solar meridian and the line passing south-north through the center. It decreases at any moment of solar time (t) can be determined by (Venkatachalam et al., 2019):

$$\omega = 15 \times (t - 12)^{o} \quad (4.2)$$

Zenith angle (θz): the angle formed by the Sun's rays and the line perpendicular to a horizontal plane.

$$cos\theta_z = cos\phi cos\delta cos\omega + sin\phi sin \tag{4.3}$$

Solar altitude angle (α_s): the angular relationship between a horizontal plane and the ray of the sun.

$$sin\alpha_s = cos\phi cos\delta cos\omega + sin\phi sin\delta \tag{4.4}$$

Surface azimuth angle (γ): the deviation of the projection on a horizontal plane of the normal to the surface from the local meridian, with zero due south, east negative, and west positive; $-180^o \leq \gamma \leq 180^o$.

Solar azimuth angle (γ_s): the angular displacement from the south of the projection of beam radiation on the horizontal plane. Displacements east of south are negative and west of south are positive.

$$\gamma_s = sign(\omega)\left[cos^{-1}\left(\frac{cos\theta_z sin\phi - sin\delta}{sin\theta_z cos\phi}\right)\right] \tag{4.5}$$

Tilt angle or slope angle (β):- the angle between the plane of the surface in question and the horizontal surface, $0° \leq \beta \leq 180°$. ($\beta > 90^o$ means that the surface has a downward-facing component.) (Duffie and Beckman, 2013).

$$\beta = \phi + 15 \tag{4.6}$$

The angle of incidence (θ): the angle between the beam radiation on a surface and the normal to that surface (Duffie and Beckman, 2013).

$$cos\theta = \sin\delta\sin\phi\cos\beta - sin\delta cos\phi sin\beta cos\gamma + cos\delta cos\phi cos\beta cos\omega + cos\delta cos\phi sin\beta cos\gamma cos\omega + cos\delta sin\beta sin\gamma cos\omega \tag{4.7}$$

Also,

$$cos\theta = \cos\theta_z\cos\beta + \sin\theta_z\sin\beta\cos(\gamma_s - \gamma) \tag{4.8}$$

Sunrise and sunset angles (ω_s): The sun is said to rise and set when the solar altitude angle is 0.

$$cos\omega_s = -tan\delta tan\phi \tag{4.9}$$

4.3 Estimation of solar radiation

4.3.1 Estimation of the extraterrestrial daily solar radiation on a horizontal surface

The solar radiation (I_o) incident on a horizontal plane in the extraterrestrial region (outside the atmosphere) in W/m^2 can be obtained as follows:

$$I_o = I_{ext} \times cos\theta_z \tag{4.10}$$

The solar intensity on a plane perpendicular to the direction of solar radiation is calculated (Venkatachalam et al., 2019):

$$I_{ext} = I_{sc}\left[1.0 + 0.033\cos\left(\frac{360n}{365}\right)\right] \tag{4.11}$$

Where I_{sc} is the solar constant defined as the radiant solar (energy) flux received in the extraterrestrial region on a plane of the unit area kept perpendicular to the solar radiation at the mean Sun-Earth distance. The value of a solar constant is 1367 W/m^2.

Substituting equation (4.11) and (4.3) in equation (4.10) gives

$$I_o = I_{sc}\left[1.0 + 0.033\cos\left(\frac{360n}{365}\right)\right](cos\phi cos\delta cos\omega + sin\phi sin\delta \tag{4.12}$$

The extraterrestrial radiation on a horizontal surface for a given period from hour angles ω_1 to ω_2 (where ω_2 is larger) can be calculated by integrating equation (4.12) for a period, and it is given by (Duffie and Beckman, 2013).

$$I_o = \frac{12\times3600}{\pi} I_{sc}\left[1 + 0.033cos\left(\frac{360\times n}{365}\right)\right]\left[cos\phi cos\delta(sin\omega_2 - sin\omega_1) + \frac{2\pi(\omega_2-\omega_1)}{360} sin\phi sin\delta\right] \tag{4.13}$$

Integrating the equation above over the period from sunrise to sunset, the daily total extraterrestrial radiation on a horizontal surface gives

$$H_o = \frac{24\times3600}{\pi} I_{sc}\left[1 + 0.033cos\left(\frac{360\times n}{365}\right)\right]\left[cos\phi cos\delta sin\omega_s + \frac{\pi\omega_s}{180} sin\phi sin\delta\right] \tag{4.14}$$

Figure 4.3 shows the monthly average daily extraterrestrial radiation on a horizontal surface.

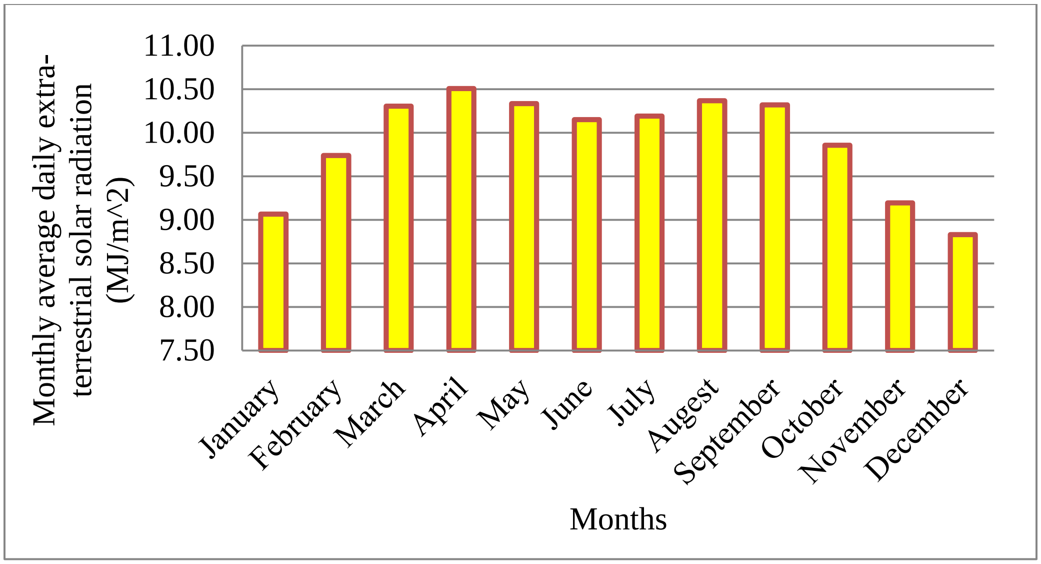

Figure 4. 3: Monthly average daily extra-terrestrial solar radiation for a horizontal surface

4.3.2 Estimation of monthly average daily global radiations on a horizontal surface

The original Angstrom-type regression equation related monthly average daily radiation to clear day radiation in a given location and the average fraction of possible sunshine hours and expressed as follow (Muzathik *et al.*, 2011):

$$\frac{\bar{H}}{\bar{H}_o} = a + b\left(\frac{\bar{n}_s}{\bar{N}_s}\right) \tag{4.15}$$

Where $\bar{n}$ and $\bar{N}$ are the observed monthly average of daily bright sunshine hours and the total length of an average day of the month. $\bar{H}$ and $\bar{H}_o$ are the monthly average of daily total solar radiation on a horizontal surface in the terrestrial and extraterrestrial regions, respectively.

The regression coefficients a and b can be determined by:

$$a = -0.110 + 0.235cos\phi + 0.323\left(\frac{\bar{n}}{\bar{N}}\right) \tag{4.16a}$$

$$b = 1.449 - 0.553cos\phi - 0.694\left(\frac{\bar{n}}{\bar{N}}\right) \tag{4.16b}$$

4.3.3 Estimation of monthly average daily diffuse and beam radiations

The monthly average daily diffuse radiation on a horizontal surface ($\bar{H}_d$) in kW/m^2/day can be determined from the monthly average daily global radiation on a horizontal surface and the number of bright sunshine hours (Bekele et al., 2013).

$$\frac{\bar{H}_d}{\bar{H}} = 0.931 - 0.814\left(\frac{\bar{n}_s}{\bar{N}_s}\right) \tag{4.17}$$

The monthly average daily beam radiation $\overline{H}_b$ on a horizontal surface is the difference between the monthly average daily global and diffuse radiations.

$$\overline{H}_b = \overline{H} - \overline{H}_d \tag{4.18}$$

The monthly average daily global, beam, and diffuse radiations on the horizontal surface of Adama city averaged for ten years of the climatic condition is shown in the figure below.

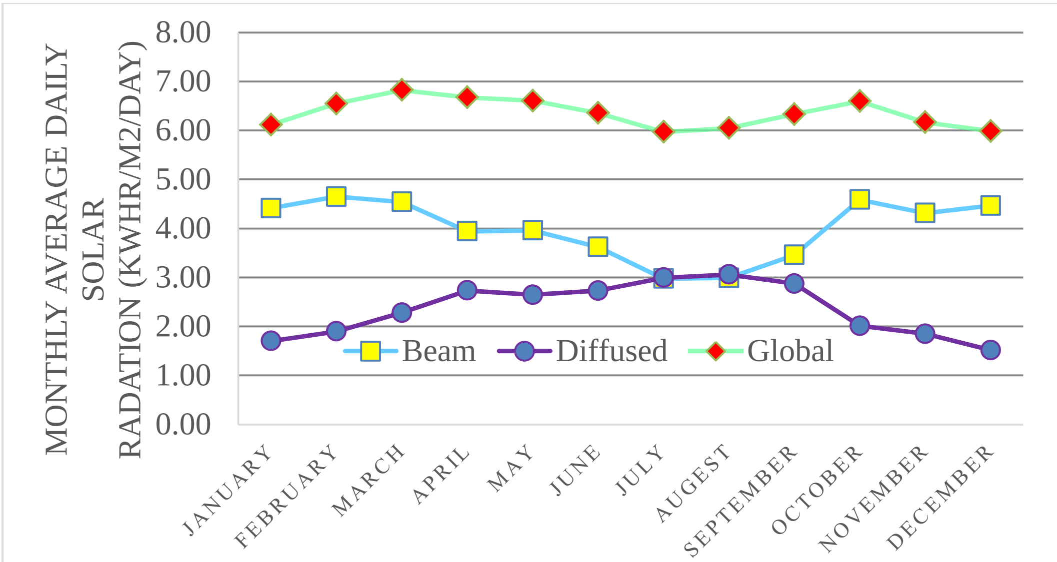

Figure 4. 4: Monthly average daily solar radiation on a horizontal surface

4.3.4 Estimation of monthly average hourly global radiation on a horizontal surface

From the monthly average daily global radiation on a horizontal surface, one can calculate the monthly average hourly global radiation (I) (Bekele et al., 2013). It can be determined by equation (4.19) in W/m^2day:

$$\frac{I}{H} = \frac{\pi}{24}(a + bcos\omega_s)\frac{cos\omega - cos\omega_s}{sin\omega_s - \frac{\pi\omega_s}{180}cos\omega_s} \tag{4.19}$$

The coefficients *a* and *b* are given by

$$a = 0.409 + 0.5016\sin(\omega_s - 60) \tag{4.20}$$

$$b = 0.6609 - 0.4767\sin(\omega_s - 60) \tag{4.21}$$

The diffused component is estimated by the formula from (Liu and Jordan 1960):

$$\frac{\bar{I}_d}{\overline{H}_d} = \frac{\pi}{24}\frac{cos\omega - cos\omega_s}{sin\omega_s - \frac{\pi\omega_s}{180}cos\omega_s} \tag{4.22}$$

In these equations, ω is the hour angle in degrees for the time in question (i.e., the midpoint of the hour for which the calculation is made) and ω_s is the sunset hour angle.

The monthly average hourly beam radiation on a horizontal surface($\bar{I}_b$) is the difference between the monthly average hourly global and diffuse radiations.

$$\bar{I}_b = \bar{I} + \bar{I}_d \tag{4.23}$$

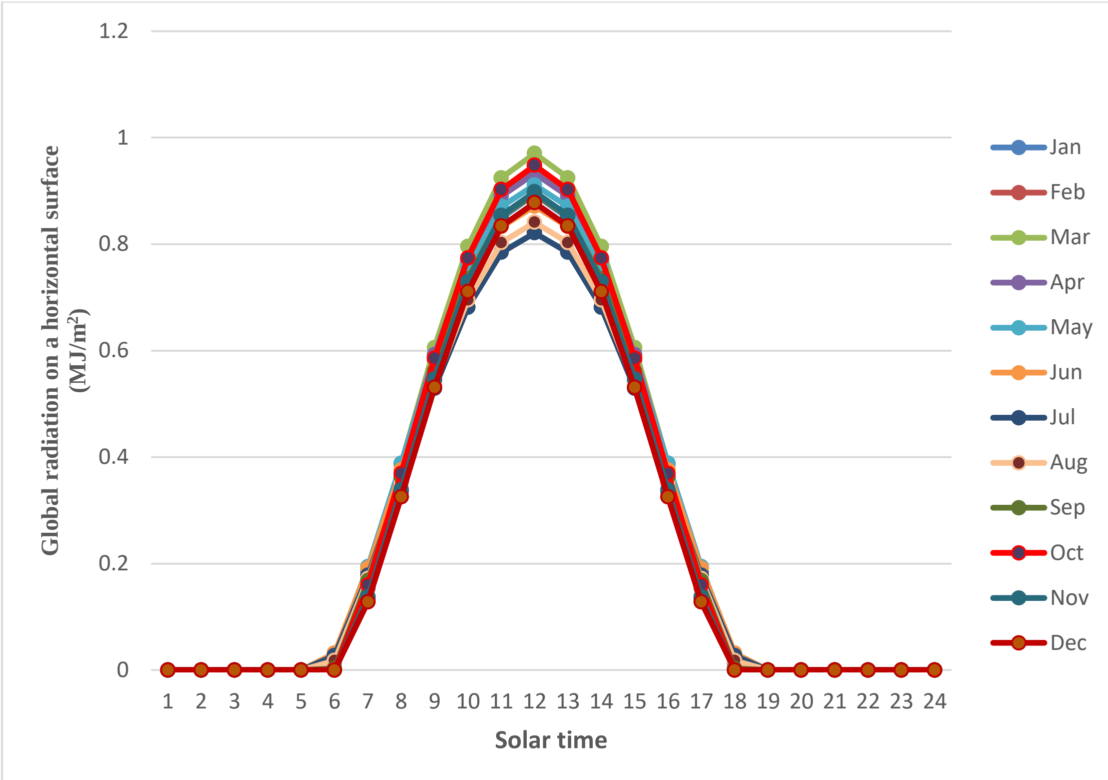

Figure 4. 5: Global radiation on a horizontal surface

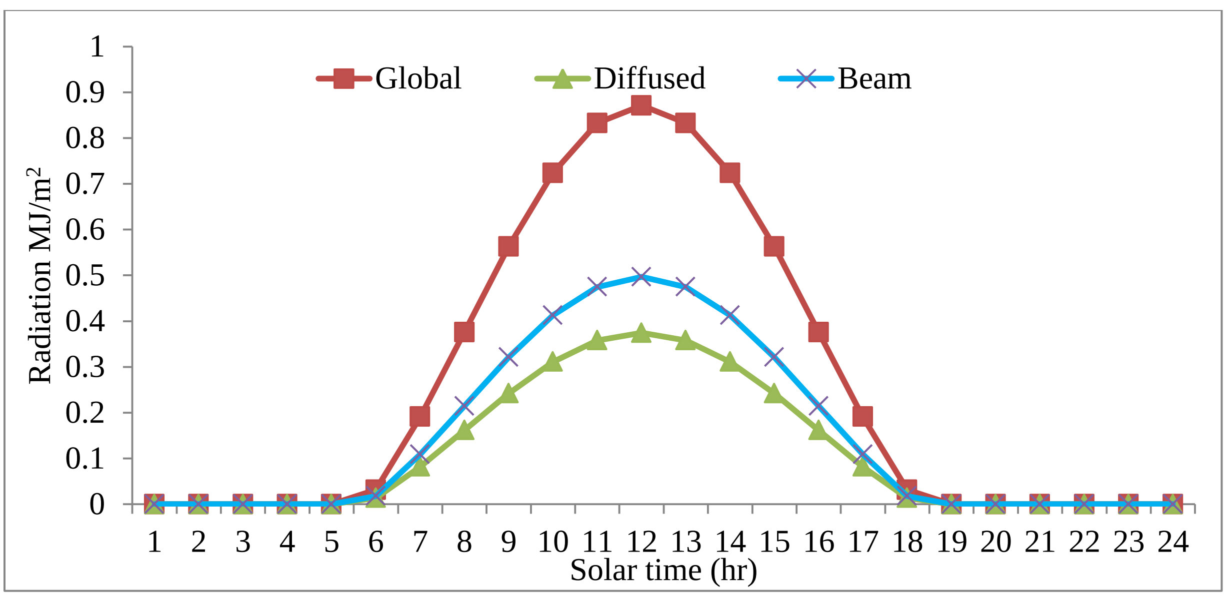

Figure 4. 6: Monthly average hourly Solar potential estimation June 2022 Adama

4.4 Radiation on tilted surfaces

The incident solar radiation on an inclined (tilted) surface is the sum of the solar radiation radiated by various surfaces (from a horizontal surface and surfaces around it) in the form of a beam, diffuse, and reflected solar radiation. The total incident solar radiation on an inclined surface can therefore be represented in terms of the global, beam, diffuse, and total reflected radiation to the tilted surface and can be estimated by equation (Mahian et al., 2017).

$$I_t = I_b R_b + I_d \left(\frac{1+cos\beta}{2}\right) + (I_b + I_d)\rho \left(\frac{1-cos\beta}{2}\right) \tag{4.24}$$

Where:

ρ: reflectivity of the ground and its value is 0.2

R_b: the beam radiation factor (Tiwari and Tiwari, 2016).

$$R_b = \frac{cos\theta}{cos\theta_z} = \frac{\cos(\phi-\beta)cos\delta cos\omega+\sin(\phi-\beta)sin\delta}{cos\phi cos\delta cos\omega+sin\phi sin\delta} \tag{4.25}$$

Substituting equation (4.25) into (4.24), the solar radiation intensity will become:

$$I_t = I_b cos\theta + I_d cos\theta_z \left(\frac{1+cos\beta}{2}\right) + 0.2cos\theta_z (I_b + I_d) \left(\frac{1-cos\beta}{2}\right) \tag{4.26}$$

4.4.1 Estimation of hourly variation of atmospheric temperature

The daily maximum and minimum temperatures can be used to estimate the hourly variation of atmospheric temperature. Day and night time are mathematically described, respectively, as follows (Mavromatidis et al., 2012):

$$T(h) = (T_{max} - T_{min}) sin\left(\frac{\pi \mathrm{m}}{Y+2a}\right) + T_{min} \tag{4.27}$$

$$T(h) = (T_{sunset} - T_{min}) exp\left(\frac{-bn}{Z}\right) + T_{min} \tag{4.28}$$

Where: T(h)= temperature at any hour of the day or night

m= hours from the time the temperature reaches its lowest point to sunset

n= amount of hours from sunset to when the temperature is at its lowest

y= length of the day

z= length of the night

T_{sunset} = temperature at sunset

a= lag coefficient for T_{max}=1.8h

b= night time temperature coefficient =2.2h

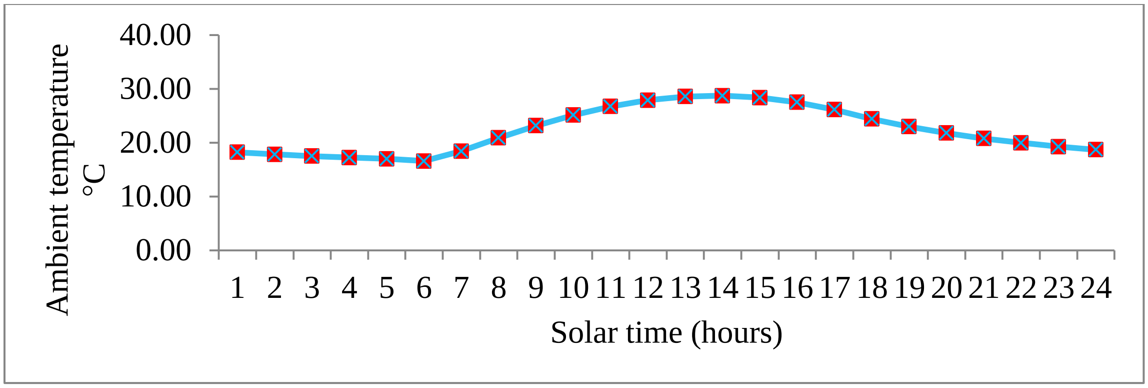

Figure 4. 7: Average daily Ambient Temperature variation for Adama

4.5 Material selection of the solar dryer components

The design parameters affect how well a solar dryer performs. It is essential to take into account several methods to reduce heat losses, increase energy absorption, and shorten the time it takes for the products to dry. The type of material, its thickness, and its strength are vital factors to be taken into account. The decisions and factors taken into account when designing the solar dryer are described in this section.

4.5.1 Transparent cover

The transparent cover is the top cover of a SAH and serves to reduce heat losses by convection and radiation from the absorbing plate. To maximize the solar energy captured, a glass cover is preferred to receive solar radiation from all angles. It is very transparent to solar radiation, opaque to heat energy, protects against being scraped, has great strength over an extended period of time, and is widely accessible.

4.5.2 Absorber plate

The absorber plate is the primary component of a flat-plate solar collector. The goal of an absorber plate is to capture as much solar energy as possible, transmit it to the working fluid, and release as little heat as possible into the environment. Factors to be considered while selecting an absorber plate are absorptivity, thermal conductivity, durability, corrosion resistance, availability, and cost. Galvanized iron sheet metal was selected for this study due to its availability and cost and painted black for better absorption of solar radiation.

4.5.3 Insulation

As a solar dryer is a device that uses solar energy to dry food products, insulation is needed to prevent heat loss and to maintain the temperature inside the dryer. High temperatures can be sustained by insulating materials due to their limited thermal conductivity. Low heat conductivity and local availability are considered while selecting insulation materials. Considering these factors, polyurethane foam and glass wool are selected as insulating materials.

4.5.4 Frame and support

Supports for the trays in solar dryers need to be strong enough to carry the weight of the loaded trays. The frame and support of the SAH were built using square steel pipe and angle iron to sustain its weight.

4.5.5 Sealant material

Sealant materials are used to seal the solar dryer so the air does not enter or does not leave its flow path. Tapes, putty sealant, and silicon sealant are used to seal the dryer gaps and holes drilled for the thermocouple wire. Epoxy is also used to stick the thermocouples on the absorbing plate.

The properties of materials utilized for experimental investigation are described and summarized in Table 4.2.

Table 4. 1: List of materials utilized in this study along with their properties

Components	Material(s)	Properties
Transparent cover	Glass	High thermal conductivity and can withstand wind loads, dust storms, and rainfall
Absorber plate	Galvanized iron	High thermal conductivity, high radiation absorptivity, and resistant to corrosion
Insulator	Glass wool and polyurethane	Low thermal conductivity, affordable, and effective
Frame and support	Square steel pipe and angle iron	Resistant to corrosion with good strength to withstand the system
Sealant material	Silicone sealant and putty sealant	adjust to various circumstances in both low and high temperatures
Obstacles	Thin aluminum sheet	High thermal conductivity, high radiation absorptivity, resistant to corrosion, and easily machineable

4.6 Design of the solar air dryer

The amount of energy required for the drying process, the thermo-physical properties (density, specific heat capacity, and thermal conductivity), and the transport properties (heat transfer and mass transfer coefficient) are the most important variables to take into account when designing solar dryers and evaluating system performance (Mohana et al., 2020). Table 4.3 shows the primary data obtained from laboratory experiments for moisture content analysis.

Table 4. 2: Laboratory results from an oven dryer

Ingredient type	Sample number	Initial mass (grams)	Final mass (grams)	Mass of water removed (grams)
Bean	1	50	36.225	13.775
	2	80	56.8	23.2
	3	130	92.665	37.335
Pea	1	50	34.34	15.66
	2	80	54.2593	25.7407
	3	130	87.756	42.244
Chickpea	1	50	37.3397	12.6603
	2	80	59.5966	20.4034
	3	130	95.534	34.466
Onion	1	25	3.4	21.6
	2	60	7.998	52.002
	3	130	17.65	112.35
Garlic	1	20	7.094	12.906
	2	40	14.26	25.74
	3	90	30.24	59.76
Ginger	1	10	2.016	7.984
	2	20	3.642	16.358
	3	50	8.94	41.06

Figure 4. 8: Laboratory experimentation devices to measure moisture rate a) Digital weight balance calibration b) mass of onion before drying c) mass of onion after drying d) oven dryer

Equations (4.29) and (4.30) can be used to estimate the moisture content of the product (M) on a wet basis and a dry basis, respectively. The mass of product samples (w) and dry mass of product samples (d) were determined.

$$M = \frac{(w-d)}{w}100 \tag{4.29}$$

$$M = \frac{(w-d)}{d}100 \tag{4.30}$$

Table 4. 3: Laboratory experimentation results

Ingredient type	Initial moisture content	Final moisture content
Bean	28.42%	2%
Pea	32%	2%
Chickpea	26.53%	2%
Onion	86.5%	15.59%(Sasongko et al., 2020)
Garlic	65.1%	6.5%
Ginger	81.25%	9.5%

4.6.1 Design of components of the air dryer

Based on the data gathered, it is necessary to specify some basic parameters (assumptions) before estimating and designing the values for the solar air dryer components. Table 4.5 shows the initial assumptions taken for this study.

Table 4. 4: The initial assumption

Parameter	Assumption values
Average ambient temperature	28^oC
Average relative humidity	60%
Average solar radiation	648.3 W/m^2
Sample weight	6kg(2.25kg bean, 1.5kg pea, 0.975kg chickpea, 0.375 kg ginger, 0.45kg onion and garlic)
Critical drying temperature	60^oC
Average bulk density (wb)	610kg/m^3
Loading bed void fraction	0.6
Average porosity	0.46
Layer drying bed thickness	10mm
Length of tray	1m
Width of tray	1m

4.6.1.1 Amount of water removed from the product, kg (m_w)

The mass of water removed from a wet product (m_w) can be calculated by using the initial mass of the product (m_o), the initial and final moisture content(% wet basis) of the product (M_i, M_f) which were shown as (Fudholi et al., 2014):

$$m_w = m_o \left(\frac{M_i - M_f}{100 - M_f}\right) \tag{4.31}$$

Table 4. 5: Mass of water removed from the wet ingredients

No.	Ingredient type	m_w (grams)
1	Bean	606.58
2	Pea	459.18
3	Chickpea	244.05
4	Onion	378.03
5	Garlic	282.03
6	Ginger	297.3

The total mass of water removed from the wet products is:

m_w =2.27kg

4.6.1.2 Amount of heat energy needed to evaporate moisture from a product, $\boldsymbol{Q}_r$

The amount of heat energy needed to evaporate moisture from the ingredients to be dried is given by (Musembi *et al*., 2016):

$$Q_r = m_w h_{fg} \tag{4.32}$$

The latent heat of vaporization can be calculated using the equation given by (Musembi *et al*., 2016).

$$h_{fg} = 4.186 \times (597 - 0.56T_p) \tag{4.33}$$

4.6.1.3 Airflow requirement

Taking an optimum value of the mass flow rate of air ($\dot{m}_{air}$) 0.02 kg/s for a single pass solar collector the volume flow rate of the drying air is calculated from the relation (Abubakar et al., 2018):

$$\dot{V}_{air} = \frac{\dot{m}_{air}}{\rho_{air}} \tag{4.34}$$

The total volume of air (V_{air}) needed to remove the moisture is determined by the equation given by (Abubakar et al., 2018):

$$V_{air} = \dot{V}_{air} t_d \tag{4.35}$$

Where, td is the total time to dry moist ingredients, hrs

4.6.1.4 Sizing of solar air heater

Heat absorbed by the SAH (Qc): the total absorbed thermal energy absorbed by the absorbing medium can be obtained from equation (4.36) (Musembi *et al*., 2016).

$$Q_c = IA_c \tag{4.36}$$

Useful heat gained by the SAH (Qu): It is the energy transferred from the collector to the air, and it is given by Equation (4.37) (Bekele et al., 2014; Montero *et al*., 2010).

$$Q_u = \dot{m}_{air} C_{pa} \left(T_{d,max} - T_\infty\right) \tag{4.37}$$

The efficiency of the SAH (ηc) is defined as the ratio of the useful heat gain to the incident solar radiation and given by (Abuşka, 2018):

$$\eta_c = \frac{Q_u}{Q_c} = \frac{\dot{m}_{air} C_{pa} \left(T_{d,max} - T_\infty\right)}{IA_c} \tag{4.38}$$

Where, η_c is the efficiency of the collector.

Rearranging equation (4.38) for the collector area:

$$A_c = \frac{\dot{m}_{air} C_{pa}\left(T_{d,max} - T_{\infty}\right)}{I\eta_c} \tag{4.39}$$

The surface area of the absorber is given by:

$$A_{ab} = A_c = L_c W_c \tag{4.40}$$

4.6.1.5 Sizing of the drying chamber

The solid density of the wet material is related to its mass and associated volume for calculating the effective drying bed area (A_{db}) given by:

$$A_{db} = \frac{m_o}{\rho_{gr} h_L \xi (1 - \varepsilon_v)} \tag{4.41}$$

Equations (4.42) and equation (4.43) are used to determine the area of the tray, A_t, and the length of the tray, L_t.

$$A_t = \frac{A_{db}}{n} \tag{4.42}$$

And

$$L_t = \frac{A_t}{W_t} \tag{4.43}$$

4.6.2 Performance parameters of the overall drying system

According to Fudholi et al. (2014), the specific energy consumption (SEC) of the solar dryer is calculated by equation (4.44)

$$SEC = \frac{P_{total}}{m_w} \tag{4.44}$$

Equation (4.45) can be used to calculate the total energy input to this drying system as the sum of the incident solar radiation and the electrical energy used by the exhaust fan.

$$P_{total} = \left(IA_c + P_{fan}\right)t_d \tag{4.45}$$

Equation (4.46) is used to determine the overall thermal efficiency of the drying system. It is defined as the proportion of total energy input into the drying system to the energy required to evaporate the moisture from the product.

$$\eta_{system} = \frac{m_w h_{fg}}{P_{total}} \tag{4.46}$$

Table 4.6: Result summary

No.	Equation	Description	Result
1	$m_w = m_o\left(\frac{M_i - M_f}{100 - M_f}\right)$	Mass of water removed from a wet product	2.27kg
2	$h_{fg} = 4.186 \times (597 - 0.56T_p)$	Latent heat of vaporization	2358.4kJ/kg
3	$Q_r = m_w h_{fg}$	Quantity of heat energy required for evaporating moisture from the product	5353.6kJ
4	$T_f = T_\infty + 0.25\left(T_{d,max} - T_\infty\right)$	The temperature of air leaving the drying bed	36^oC
5	$\dot{V}_{air} = \frac{\dot{m}_{air}}{\rho_{air}}$	A volume flow rate of the drying air	$0.0167m^3s^{-1}$
6	$V_{air} = \dot{V}_{air}t_d$	The total volume of air required	$420m^3$
7	$A_c = \frac{\dot{m}_{air}C_{pa}\left(T_{d,max} - T_\infty\right)}{I\eta_c}$	Collector area	$2m^2$
8	$A_c = L_c W_c$	Absorber surface area	$2m^2$
9	$A_c = L_c W_c$	Width of the collector	1.0m
10	$A_c = L_c W_c$	Length of the collector	2.0 m
11	$A_{db} = \frac{m_o}{\rho_{gr} h_L \xi (1 - \varepsilon_v)}$	Effective drying bed area	$5.4m^2$
12	$A_t = \frac{A_{db}}{n}$	Tray area	$1m^2$

The recommended range for the highest temperature at which foods and crops can be dried without losing quality is 50 to 60 ^oC (Tibebu, 2015).

4.7 Conceptual model of the solar dryer

Software called Ansys Space Claim 2021R2 was used to develop the conceptual model of the system. Figure 4.9 shows the pictorial view of the conceptual model with the modification on the absorber plate and the air distributor channel mounted in the drying chamber.

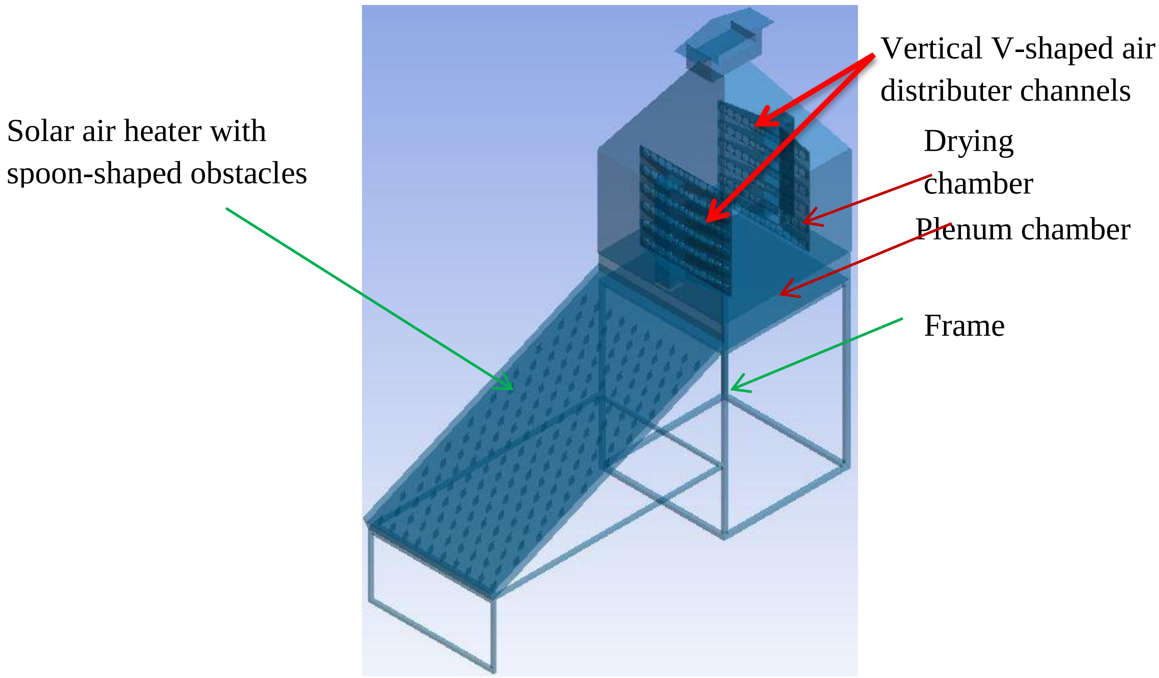

Figure 4. 9: Pictorial view of the conceptual model of the solar dryer

The solar collector with spoon-shaped obstacles has the same size as the conventional solar collector. However, to improve the performance of the solar dryer a modification has been applied through an experimental and theoretical investigation. A CFD model is also proposed to optimize the performance of the drying chamber using a vertical air distributer along all the trays.

4.8 Mechanisms of heat and mass transfer modes in a solar dryer

There are mainly three types of heat transmission involved in the solar air heating process. Solar radiation can penetrate through the glass cover and is then captured by an absorbent sheet. The glass cover also convects heat to the ambient by convection and radiation mode of heat transfer. Heat is lost from the SAH due to heat conduction that occurs through the bottom (base plate) wall. By using a thick layer of insulation materials, this loss can be minimized. The heat received by the SAH is convected to the air in the duct. The heat energy from the heated air is transported by convection to the drying materials (products) (Yao et al., 2022).

Since drying is a mass transfer process consisting of the removal of water from the drying material, internal heat transfer in solar dryers includes mass transfer. Convective and radiative heat transmissions are the the inside system transmission mechanisms (Daş et al., 2021). Figure

4.10 and Figure 4.11 provides the various heat and mass transfer mechanisms in a solar collector and drying chamber, respectively.

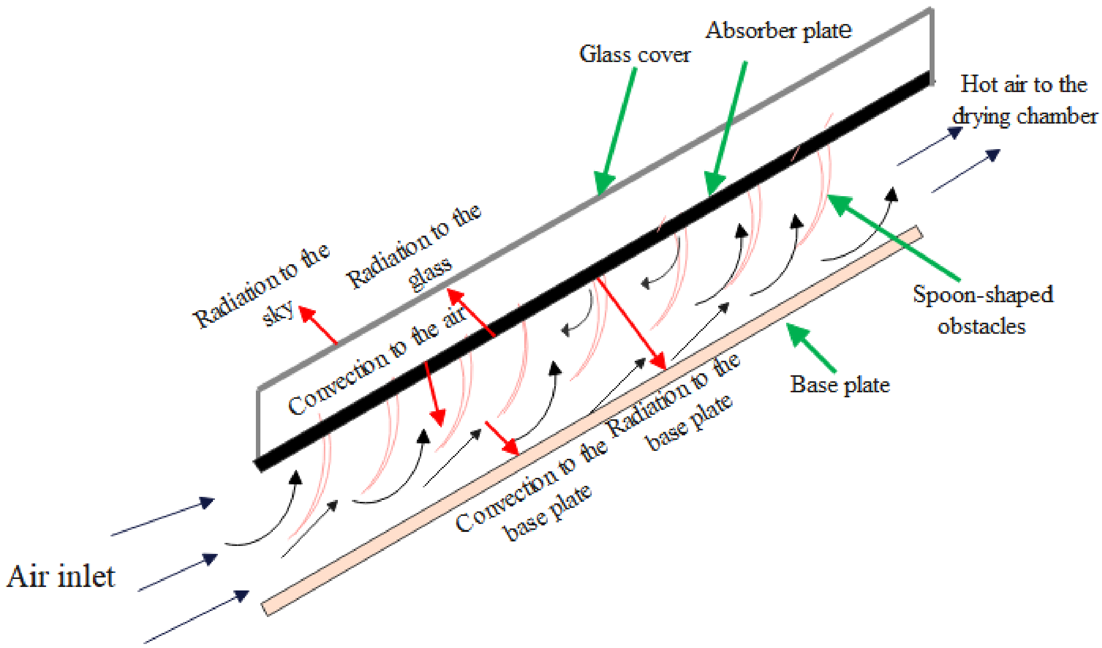

Figure 4. 10: Heat transfer processes within the solar collector

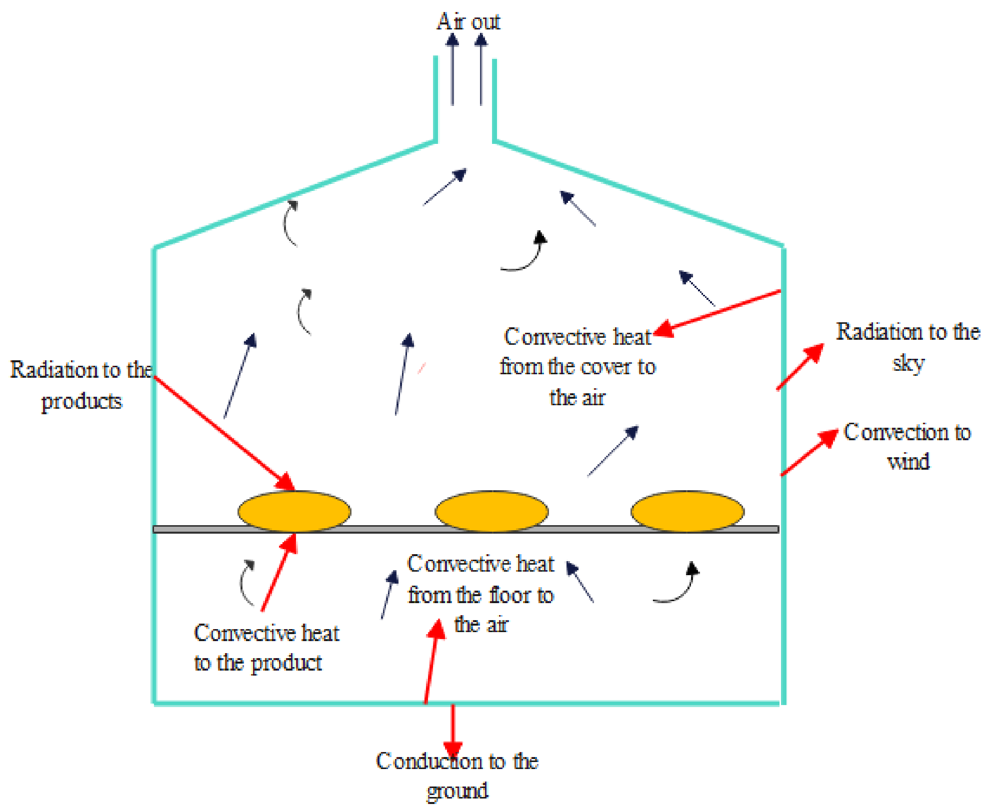

Figure 4. 11: Heat transfer processes within the drying chamber

4.9 Energy and exergy analysis

Energy and exergy evaluation of the components of solar air dryer components was carried out on the basis of the general equations for the conservation of mass and energy.

4.9.1 Energy analysis

The use of energy analysis is required to understand the fundamental design and efficiency of the thermal system.

4.9.1.1 Energy balance of solar air heater

The following simplifying assumptions are used to model the solar air heater. These are:

- The thermal performance of the solar air heater is a steady state.
- The sky can be considered as a black body.
- Heat losses driven by the wind and thermal radiation from the insulation are considered to be negligible.
- The base plate and side walls of the SAH are considered perfectly insulated.
- The convective heat-transfer coefficients for the ranges of functional temperature are assumed constant.
- The mass flow is streamlined flow and constant
- The inlet air temperature is approximately equal to the surrounding air temperature.
- There is no heat generation

Equation (4.47) is used to determine the solar radiation collected by the SAH and given by (Abdelkader et al., 2020).

$$Q_c = A_c \tau_g \alpha_c I(t) \tag{4.47}$$

Where I(t) is the solar radiation influx and τ_g is the transmissivity of the glass cover.

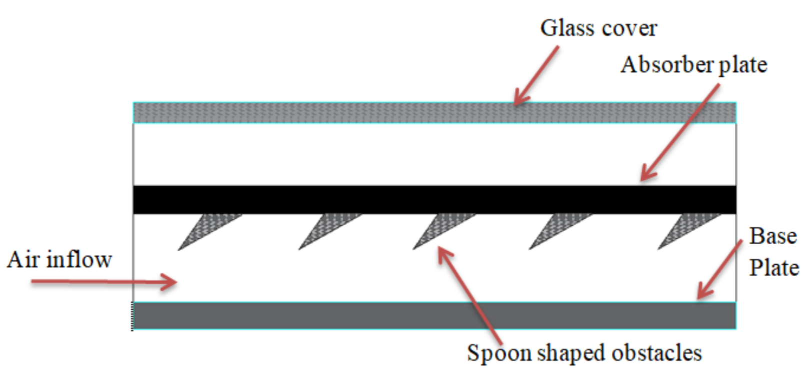

Figure 4. 12: Solar collector airflow

Energy balance for the Glass cover:

Energy absorbed by the glass cover top surface	+	Energy absorbed by the glass cover bottom surface	=	Energy stored in the glass	+	Energy loss from the top surface of the glass

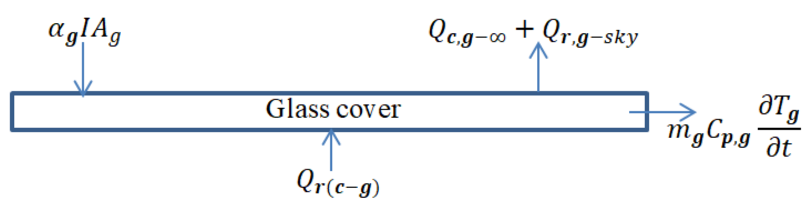

Figure 4. 13: Heat energy balance of glass cover

The glass cover absorptivity is α_g, hence the energy gain is $\alpha_g I$. From Figure 4.13 the energy balance for the glass cover is given by the equation (4.48):

$$\alpha_g I(t) + h_{r,c-g}\left(T_c - T_g\right) = h_{r,g-sky}\left(T_g - T_\infty\right) + (mC_p)_g \frac{\partial T_g}{\partial t} \tag{4.48}$$

Where, α_g is absorptance of glass, I is solar radiation on a tilted surface, $h_{r,c-g}$is radiative heat transfer from the absorber plate to the glass cover, $h_{c,g-air}$ is convective heat transfer from the glass cover to the air, $h_{r,g-sky}$ is radiative heat transfer from the glass to the sky, m is the mass of the glass, and C_p is the specific heat capacity of the glass.

Energy balance for the absorber plate:

Energy absorbed by the collector	=	Energy stored in the collector	+	Energy loss from the collector

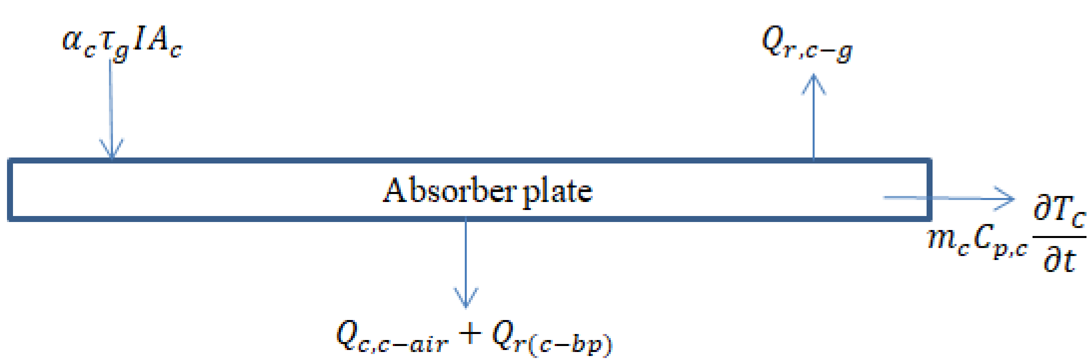

Figure 4. 14: Heat energy balance of the absorber plate

Hence, the absorber plate energy balance is given by:

$$\alpha_c \tau_g I(t) = h_{c,c-air}(T_c - T_{air}) + h_{r,c-bp}(T_c - T_{bp}) + (mC_p)_c \frac{\partial T_c}{\partial t} \quad (4.49)$$

Where, $\alpha_c$is the absorbtance of the collector, τ_g is the transmissivity of the glass, $h_{c,c-air}$ is the convective heat transfer from the collector to the air, and $h_{r,c-bp}$ is the radiative heat transfer between the collector and the base plate.

For airflow:

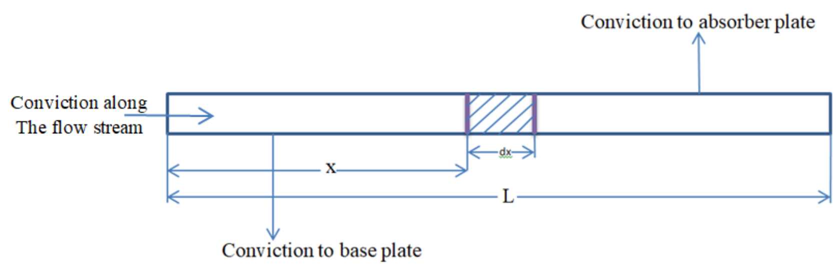

Figure 4. 15: Heat energy balance of the air stream

$$h_{c,c-air}(T_c - T_{air}) = (mC_p)_{air} \frac{\partial T_{air}}{\partial t} + h_{c,air-bp}(T_{air} - T_{bp}) - \frac{(\dot{m}C_p)_{air}}{W} \frac{\partial T_{air}}{\partial x} \quad (4.50)$$

Where $h_{c,c-air}$ is the convective heat transfer between the collector and the air, $h_{c,air-bp}$ is the convective heat transfer between the air and the base plate, and W is the width of the collector.

For the bottom plate:

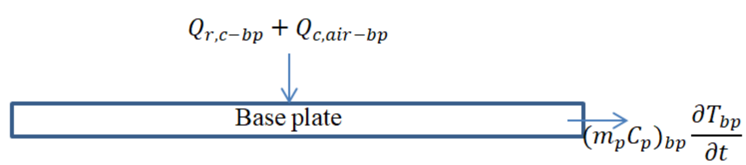

Figure 4. 16: Heat energy balance of the base plate

$$h_{r,c-bp}(T_c - T_{bp}) + h_{c,air-bp}(T_{air} - T_{bp}) = (mC_p)_{bp} \frac{\partial T_{bp}}{\partial t} \quad (4.51)$$

Where, $h_{r,c-bp}$ is the radiative heat transfer between the collector and the base plate, $h_{c,air-bp}$ is the convective heat transfer between the air and the base plate.

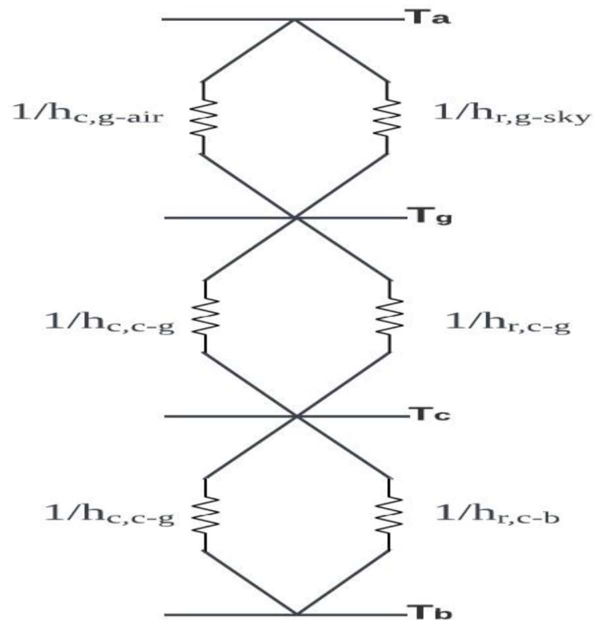

Figure 4. 17: Thermal resistance diagram of solar air heater

4.9.1.2 Energy balance for the drying chamber

The following assumptions are taken to develop the mathematical model for the drying chamber:

- ✓ No layering of the air exists inside the dryer.
- ✓ The specific heat of air and cover is constant.
- ✓ Radiative heat transfers from the floor to the cover and from the floor to the product are negligible

Energy balance for the cover of the chamber

The expression for the energy balance on the cover of the chamber can be written as:

Rate of thermal energy accumulation in the cover = Convection-induced rate of thermal energy transfer between the air inside the dryer and the cover + Rate of radiation-induced thermal energy transfer between the cover and the sky + Convection-induced rate of thermal energy transfer between the atmospheric air and the cover + Rate of radiation-induced thermal energy transfer between the product and the cover + Rate of solar radiation absorbed by the cover. The energy balance for the cover of the chamber is given by:

$$m_{co}C_{p,co}\frac{\partial T_{co}}{\partial t} = h_{c,co-ad}A_{co}(T_{ad} - T_{co}) + h_{r,co-sky}A_{co}\left(T_{sky} - T_{co}\right) + h_wA_{co}(T_\infty - T_{co}) + h_{r,co-p}A_p\left(T_p - T_{co}\right) + A_{co}\alpha_{co}I(t) \tag{4.52}$$

Where, $m_{co}$is the mass of the cover, $C_{p,co}$ is the specific heat of the cover, $h_{c,co-ad}$ is the convective heat transfer between the cover and the air in the chamber, $h_{r,co-sky}$ is the radiative heat transfer between the cover and the sky, and h_w is the wind heat transfer.

Equation 4.52 can be solved using Runge-Kutta method using the following steps as:

i. Choose a time step Δt and an initial condition for T_{co}

ii. Iterate the following steps for each time step until the desired time is reached.

iii. Calculate the values of:

$$h_c = h_{c,co-ad}A_{co}(T_{ad} - T_{co}) \tag{4.52a}$$

$$h_r = h_{r,co-sky}A_{co}\left(T_{sky} - T_{co}\right) + h_{r,co-p}A_p\left(T_p - T_{co}\right) \tag{4.52b}$$

$$h_w = h_w A_{co}(T_\infty - T_{co}) \tag{4.52c}$$

iv. Calculate the rate of change of temperature at the current time step:

$$\frac{\partial T_{co}}{\partial t} = \frac{h_c+h_r+h_w}{m_{co}C_{p,co}} \tag{4.52d}$$

v. Calculate the temperature at the next time step using Runge-Kutta method:

- Calculate the intermediate value, $k_1 = \Delta t \times \frac{\partial T_{co}}{\partial t}$ (4.52e)
- Calculate the intermediate value, $k_2 = \Delta t \times \frac{\partial T_{co}}{\partial t} + \frac{k_1}{2}$ (4.52f)
- Calculate the intermediate value, $k_3 = \Delta t \times \frac{\partial T_{co}}{\partial t} + \frac{k_2}{2}$ (4.52g)
- Calculate the intermediate value, $k_4 = \Delta t \times \frac{\partial T_{co}}{\partial t} + k_3$ (4.52h)

vi. Update the temperature at the next time step:

$$T_{co} = T_{co} + \frac{k_1+2k_2+2k_3+k_4}{6} \tag{4.52i}$$

vii. Update the time $t = t + \Delta t$ (4.52j)

viii. Repeat step (iii) to (vii) until the desired time is reached.

Energy balance of the air inside the dryer

The expression for the energy balance of the air inside the chamber can be written as:

Rate of thermal energy accumulation in the air inside the drying chamber = Convection-induced rate of thermal energy transfer between the product and the air + Rate of thermal energy transfer between the cover and the air due to convection + Rate of sensible heat transmission from the product to the air + Rate of thermal energy gained in the air chamber due to inflow and outflow of the air in the chamber + Rate of overall heat transfer from the air inside dryer to the surrounding atmosphere. The energy balance for the air inside the dryer is given by:

$$m_{ad}C_{pa}\frac{dT_{ad}}{dt} = A_p h_{c,p-ad}\left(T_p - T_{ad}\right) + A_{co}h_{c,co-ad}(T_{co} - T_{ad}) + D_p A_p C_{pd}\rho_p\left(T_p - T_{ad}\right)\frac{dM_p}{dt} + \rho_a V_{out}C_{pa}T_{out} - \rho_a V_{in}C_{pa}T_{in} + U_c A_c(T_\infty - T_{ad}) \quad (4.53)$$

Where, m_{ad} is the mass of the air inside the chamber, $h_{c,p-ad}$ is convective heat transfer between the product and the air inside the chamber, $h_{c,co-ad}$ is the convective heat transfer between the cover and the air inside the chamber, D_p is the depth of product, and A_p is area of the product.

Equation 4.53 can be solved using Runge-Kutta method using the following steps as:

i. Choose a time step Δt and an initial condition for $T_{ad}(0)$, $M_p(0), T_p(0)$.

ii. Define the constants: $A_p, A_{co}, D_p, \rho_p, \rho_{a,}V_{in}, V_{out}, U_c, A_c, C_{pa}, C_{pd}, T_{out}, T_{in}, and\ T_\infty$

iii. Calculate the intermediate values for each time step n (starting from n=0):

$$\frac{dT_{ad}}{dt} = A_p h_{c,p-ad}\left(T_p - T_{ad}\right) + A_{co}h_{c,co-ad}(T_{co} - T_{ad}) + D_p A_p C_{pd}\rho_p\left(T_p - T_{ad}\right) \quad (4.53a)$$

$$\frac{dM_p}{dt} = \rho_a V_{out}C_{pa}T_{out} - \rho_a V_{in}C_{pa}T_{in} + U_c A_c(T_\infty - T_{ad}) \quad (4.53b)$$

iv. Calculate the intermediate values using these derivatives:

$$T_{ad,intermediate} = T_{ad}(n) + \frac{\Delta t}{2} \times \frac{dT_{ad}}{dt} \quad (4.53c)$$

$$M_{p,intermediate} = M_p(n) + \frac{\Delta t}{2} \times \frac{dM_p}{dt} \quad (4.53d)$$

$$T_{p,intermediate} = T_p(n) + \frac{\Delta t}{2} \quad (4.53e)$$

v. Calculate the derivatives at the intermediate values:

$$\frac{dT_{ad,intermediate}}{dt} = A_p h_{c,p-ad}(T_{p,intermediate} - T_{ad,intermediate} + A_{co}h_{c,co-ad}\left(T_{co} - T_{ad,intermediate}\right) + D_p A_p C_{pd}\rho_p\left(T_{p,intermediate} - T_{ad,intermediate}\right) \quad (4.53f)$$

$$\frac{dM_{P,intermediate}}{dt} = \rho_a V_{out}C_{pa}T_{out} - \rho_a V_{in}C_{pa}T_{in} + U_c A_c\left(T_\infty - T_{ad,intermediate}\right) \quad (4.53g)$$

vi. Calculate the final values using the derivatives at the intermediate values:

$$T_{ad}(n+1) = T_{ad}(n) + \Delta t\frac{dT_{ad,intermediate}}{dt} \quad (4.53h)$$

$$M_P(n+1) = M_P(n) + \Delta t\frac{dM_{P,intermediate}}{dt} \quad (4.53i)$$

$$T_p(n+1) = T_P(n) + \Delta t(T_{P,intermediate}) \quad (4.53j)$$

vii. Repeat step (iv), (v), and (vi) until the desired time is reached.

Product energy balance

The expression for the energy balance on the product is given by:

Rate of thermal energy accumulation in the product inside the drying chamber = Convection-induced rate of thermal energy transfer between the air and product + Rate of radiation-induced thermal energy transfer between the cover and the product + Thermal energy loss rate from the product as a result of sensible and latent heat loss + product thermal energy absorption rate**.** The energy balance on the product gives:

$$m_p\left(C_{pg}+C_{pl}M_p\right)\frac{\partial T_p}{\partial t}=$$
$$A_p h_{c,p-ad}\left(T_{ad}-T_p\right)+A_p h_{r,p-co}\left(T_{co}-T_p\right)+D_p A_p \rho_p\left[L_p C_{pp}\left(T_{ad}-T_p\right)\right]\frac{\partial M_p}{\partial t}+$$
$$F_p\alpha_p I A_c\tau_c \qquad (4.54)$$

Where, C_{pg} is the specific heat capacity of the product when water is in vapor, C_{pl} is the specific heat capacity when water is in a liquid state.

Equation 4.54 can be solved using Runge-Kutta method using the following steps as:

i. Choose a time step Δt and an initial condition for $M_p(0)\ and\ T_p(0)$.

ii. Define the constants in the equation

iii. Calculate the derivatives:

$$\frac{\partial T_p}{\partial t}=A_p h_{c,p-ad}\left(T_{ad}-T_p\right)+A_p h_{r,p-co}\left(T_{co}-T_p\right)+D_p A_p \rho_p\left[L_p C_{pp}\left(T_{ad}-T_p\right)\right] \qquad (4.54a)$$

$$\frac{\partial M_p}{\partial t}=F_p\alpha_p I A_c\tau_c \qquad (4.54b)$$

iv. Calculate the intermediate values

$$k_1=\Delta t\frac{\partial T_p}{\partial t} \qquad (4.54c)$$

$$l_1=\Delta t\frac{\partial M_p}{\partial t} \qquad (4.54d)$$

$$k_2=\Delta t\frac{\partial T_p}{\partial t}+\frac{k_1}{2} \qquad (4.54e)$$

$$l_2=\Delta t\frac{\partial M_p}{\partial t}+\frac{l_1}{2} \qquad (4.54f)$$

$$k_3=\Delta t\frac{\partial T_p}{\partial t}+\frac{k_2}{2} \qquad (4.54g)$$

$$l_3=\Delta t\frac{\partial M_p}{\partial t}+\frac{l_2}{2} \qquad (4.54h)$$

$$k_4=\Delta t\frac{\partial T_p}{\partial t}+k_3 \qquad (4.54i)$$

$$l_4 = \Delta t \frac{\partial M_p}{\partial t} + l_3 \quad (4.54j)$$

v. Update T_p and M_p values:

$$T_p = T_p + \frac{k_1+2k_2+2k_3+k_4}{6} \quad (4.54k)$$

$$M_p = M_p + \frac{k_1+2k_2+2k_3+k_4}{6} \quad (4.54l)$$

vi. Repeat step (iv) and (v) for desired number of time steps.

Energy balance on the floor

The expression for the energy balance of the floor is given by:

Rate of thermal energy accumulation on the floor = Convection-induced rate of thermal energy transfer between the air and the floor + Conduction-induced rate of thermal energy transfer between the floor and the ground + Rate of solar radiation absorption on the floor. The energy balance on the floor gives:

$$m_{fl}C_{pfl}\frac{\partial T_{fl}}{\partial t} = A_{fl}h_{c,fl-ad}\left(T_{ad} - T_{fl}\right) + A_{fl}h_{d,fl-gr}\left(T_{gr} - T_{fl}\right) + (1 - F_p)\,\alpha_{fl}IA_{fl}\tau_c \quad (4.55)$$

Equation 4.55 can be solved using Runge-Kutta method using the following steps as:

i. Initialize the time step size, Δt, and set the initial condition, $T_{fl}(0)$.

ii. For each time step, perform the following calculations:

- Calculate the intermediate values:

$$k_1 = \Delta t(f\left(t, T_{fl}(t)\right)) \quad (4.55a)$$

$$k_2 = \Delta t\left(f\left(t + \frac{\Delta t}{2}, T_{fl}(t) + \frac{k_1}{2}\right)\right) \quad (4.55b)$$

$$k_3 = \Delta t\left(f\left(t + \frac{\Delta t}{2}, T_{fl}(t) + \frac{k_2}{2}\right)\right) \quad (4.55c)$$

$$k_4 = \Delta t\left(f\left(t + \Delta t, T_{fl}(t) + k_3\right)\right) \quad (4.55d)$$

iii. Update the tempertature at the current time step:

$$T_{fl}(t + \Delta t) = T_{fl}(t) + \frac{k_1+2k_2+2k_3+k_4}{6} \quad (4.55e)$$

- Increment the time $t = t + \Delta t$ (4.55f)

iv. Repeat step (ii) and (iii) until the desired time is reached.

In the above algorithm $f\left(t, T_{fl}\right)$ represents the right hand side of the given equation:

$$f(t, T_{fl}) =$$

$$A_{fl}h_{c,fl-ad}(T_{ad} - T_{fl}) + A_{fl}h_{d,fl-gr}(T_{gr} - T_{fl}) + (1 - F_p)\ \alpha_{fl}IA_{fl}\tau_c A_{fl}h_{c,fl-ad}(T_{ad} - T_{fl}) + A_{fl}h_{d,fl-gr}(T_{gr} - T_{fl}) + (1 - F_p)\ \alpha_{fl}IA_{fl}\tau_c \quad (4.55g)$$

4.9.2 Mass balance equation

The expression for the moisture in and outflow from the drying compartment can be written as (Serm, 2012):

The rate of moisture accumulation in the air which is inside the chamber = Rate of moisture inflow into the drying chamber due to the entrance of ambient air - Rate of moisture outflow from the drying chamber due to exit of air from the chamber + Rate of product moisture removal inside the dryer

$$\rho_a V \frac{dRH}{dt} = A_{in}\rho_a RH_{in}V_{in} - A_{out}\rho_a RH_{out}V_{out} + D_p A_p \rho_p \frac{dM_p}{dt} \quad (4.56)$$

Equation 4.56 can be solved using Runge-Kutta method using the following steps as:

i. Calculate the intermediate values at the beginning of the time steps:

$$k_1 = f(t, RH)dt \quad (4.56a)$$

Here $f(t, RH)$ represents the right hand side of the equation.

ii. Calculate the intermediate values at the mid point of the time step using the previously calculated k_1:

$$k_2 = f(t + \frac{dt}{2}, RH + \frac{k_1}{2})dt \quad (4.56b)$$

iii. Calculate another set of intermediate values at the mid point:

$$k_3 = f(t + \frac{dt}{2}, RH + \frac{k_2}{2})dt \quad (4.56c)$$

iv. Finally, calculate the values at the end of the time step:

$$k_4 = f(t + dt, RH + k_3)dt \quad (4.56d)$$

Now, we can update the solution for the next time step:

$$RH_{new} = RH + \frac{k_1 + 2k_2 + 2k_3 + k_4}{6} \quad (4.56e)$$

v. Repeat these steps for each time step until the desired time interval is covered.

4.9.3 Heat transfer and heat loss coefficients

According to (Aboghrara *et al.*, 2017), the radiative heat transfer coefficient between the cover and the sky ($h_{r,co-sky}$) is given by:

$$h_{r,co-sky} = \varepsilon_{co}\sigma\left(T_{co}^2 + T_{sky}^2\right)\left(T_{co} + T_{sky}\right) \tag{4.57}$$

Where $\sigma = 5.67 \times 10^{-8} W/m^2K^4$ is the Stefan–Boltzmann constant.

Radiative heat transfer coefficient from the product to the cover ($h_{r,p-co}$) is given by (Aboghrara et al., 2017):

$$h_{r,p-co} = \varepsilon_p\sigma\left(T_p^2 + T_{co}^2\right)\left(T_p + T_{co}\right) \tag{4.58}$$

The sky temperature T_{sky} (K) is given by (Aboghrara et al., 2017).

$$T_{sky} = T_\infty - 6 \tag{4.59}$$

Convective heat transfer coefficient between the glass and ambient air by the wind (h_w) is given by (Aboghrara et al., 2017):

$$h_w = 5.7 + 3.8V_w \tag{4.60}$$

V_w is the wind velocity of the ambient air and is given by (Aboghrara et al., 2017):

$$V_w = 1.5\,{}^{m}/_{s}$$

The convective heat transfer coefficient (h_c) inside the drying chamber for the cover and floor is given by (Duffie and Beckman, 2013):

$$h_{c,fl-ad} = h_{c,co-ad} = h_c = \frac{N_u k_a}{D_h} \tag{6.61}$$

Where D_h is given by (Bekele et al., 2014):

$$D_h = \frac{4WD}{2(W+D)} \tag{4.62}$$

Where Re is the Reynolds number which is given by (Bekele et al., 2014):

$$Re = \frac{D_h V_{ad} \rho_a}{\mu} \tag{4.63}$$

$$U_c = \frac{k_{co}}{\delta_{co}} \tag{4.64}$$

The drying chamber efficiency is given by:

$$\eta_{ds} = \frac{m_w h_{fg}}{A_c I t_d} \tag{4.65}$$

4.10 Exergy analysis

Exergy is the maximum amount of work that can be produced by a flow of matter, heat, or work as it reaches equilibrium with a reference environment. According to the second law, a part of the exergy entering a thermal system is lost due to irreversibility once inside the system (Panwar et al., 2012).

4.10.1 Exergy by heat transfer, Q

Exergy transfer by heat between two heat sources at different temperatures is given by the following relation (Cengel and Boles, 2010):

$$X_{heat} = \left(1 - \frac{T_L}{T_H}\right) Q \tag{4.66}$$

4.10.2 Exergy transfer by work, W

The exergy transfer by work can simply be expressed as (Cengel and Boles, 2010):

$$X_{work} = P_o(V_2 - V_1) \tag{4.67}$$

4.10.3 Exergy transfer by mass, *m*

When mass in the amount of *m* enters or leaves a system is given by (Cengel and Boles, 2010):

$$X_{mass} = m\psi \tag{4.68}$$

Where,

$$\psi = (h - h_o) - T_o(s - s_o) + \frac{V^2}{2} + gz \tag{4.69}$$

Exergy out and exergy in are the sum of exergy of heat (Q), exergy of mass (m), and exergy of work.

$$X_{in} = X_{heat,in} + X_{work,in} + X_{mass,in} \tag{4.70}$$

$$X_{out} = X_{heat,out} + X_{work,out} + X_{mass,out} \tag{4.71}$$

The following assumptions are taken into account when doing exergy analysis:

- The flow is assumed to be steady.
- The effects of the kinetic and the potential energy are neglected.
- The effect of moisture content on the heat capacity of the air is neglected.
- The exergy loss in the product is neglected.
- The change in the pressure between the inlet and outlet is neglected.

4.10.4 Exergy analysis of the solar air heater

Under steady state conditions, the exergy balance equation is given by (Sudhakar & Cheralathan, 2020):

$$\sum \dot{X}_{in} - \sum \dot{X}_{out} = \sum \dot{X}_{des} \tag{4.72}$$

Exergy to the system due to solar radiation is given by (Fudholi, Sopian, Yazdi, et al., 2014).

$$\dot{X}_{rad} = \left(1 - \frac{T_\infty}{T_{as}}\right) \dot{Q}_{in} \tag{4.73}$$

Here, T_{as} is the apparent sun temperature for the source of exergy. Its value is taken as 4500K for this study.

$$\dot{X}_{in,f} = \dot{m}_{air} C_{pa} \left[\left(T_{i,SAH} - T_{\infty} \right) - T_{\infty} ln \left(\frac{T_{i,SAH}}{T_{\infty}} \right) \right] \quad (4.74)$$

$$\dot{X}_{out,f} = \dot{m}_{air} C_{pa} \left[\left(T_{out,SAH} - T_{\infty} \right) - T_{\infty} ln \left(\frac{T_{out,SAH}}{T_{\infty}} \right) \right] \quad (4.75)$$

The exergy lost inside the SAH is the difference between the exergy inflow and outflow and is given by:

$$\dot{X}_{in,f} - \dot{X}_{out,f} = \left(1 - \frac{T_{\infty}}{T_{as}} \right) \dot{Q}_{in} - \dot{m}_{air} C_{pa} \left[\left(T_{i,SAH} - T_{out,SAH} \right) - T_{out,SAH} ln \left(\frac{T_{i,SAH}}{T_{out,SAH}} \right) \right] \quad (4.76)$$

$$\dot{X}_{des} = \left(1 - \frac{T_{\infty}}{T_{as}} \right) \dot{Q}_{in} - \dot{m}_{air} C_{pa} \left[\left(T_{i,SAH} - T_{out,SAH} \right) - T_{out,SAH} ln \left(\frac{T_{i,SAH}}{T_{out,SAH}} \right) \right] \quad (4.77)$$

The exergy efficiency is given by (Akpinar and Koçyiğit, 2010).

$$\eta_{\dot{X},SAH} = 1 - \frac{\dot{X}_{des}}{\dot{X}_{in,SAH}} \quad (4.78)$$

4.10.5 Exergy analysis of the drying chamber

The exergy flow into and from the drying chamber is given by equations (4.79) and (4.80), respectively (Fudholi *et al.*, 2014).

$$\dot{X}_{in,dc} = \dot{m}_{air} C_{pa} \left[\left(T_{in,dc} - T_{\infty} \right) - T_{\infty} ln \left(\frac{T_{in,dc}}{T_{\infty}} \right) \right] \quad (4.79)$$

$$\dot{X}_{out,dc} = \dot{m}_{air} C_{pa} \left[\left(T_{out,dc} - T_{in,dc} \right) - T_{in} ln \left(\frac{T_{out,dc}}{T_{in,dc}} \right) \right] \quad (4.80)$$

The exergy destroyed in the drying chamber is given by:

$$\dot{X}_{des} = \dot{X}_{rad} + \dot{X}_{in,dc} - \dot{X}_{out,dc} \quad (4.81)$$

Substituting equations (4.73), (4.79), and (4.80) into (4.81) yields:

$$\dot{X}_{des} = \left(1 - \frac{T_{\infty}}{T_{as}} \right) \dot{Q}_{in} + \dot{m}_{air} C_{pa} \left[\left(T_{in,dc} - T_{out,dc} \right) - T_{out,dc} ln \left(\frac{T_{in,dc}}{T_{out,dc}} \right) \right] \quad (4.82)$$

The exergy efficiency of the drying chamber is the ratio between the exergy outflow to the exergy inflow of the chamber and is expressed as:

$$\eta_{\dot{X},dc} = \frac{\dot{m}_{air} C_{pa} \left[\left(T_{out,dc} - T_{in,dc} \right) - T_{in} ln \left(\frac{T_{out,dc}}{T_{in,dc}} \right) \right]}{\left(1 - \frac{T_{\infty}}{T_{as}} \right) \dot{Q}_{in}} \quad (4.83)$$

4.11 CFD investigation

The analysis was conducted using the CFD code ANSYS FLUENT 21R2 in three primary stages: pre-processing, solver, and post-processing.

4.11.1 Pre-processing

The initial model assumptions (steady, unsteady, inviscid, laminar, turbulent, etc.), interest domain identification, geometry development, mesh generation, and boundary conditions are all included in the pre-processing stage analysis.

4.11.1.1 Geometry creation

3D geometry of the multi-grain solar dryer was developed in ANSYS 21R2 design module. The geometry of the solar dryer with two vertical air distributors was also created and shown in Figure 4.18.

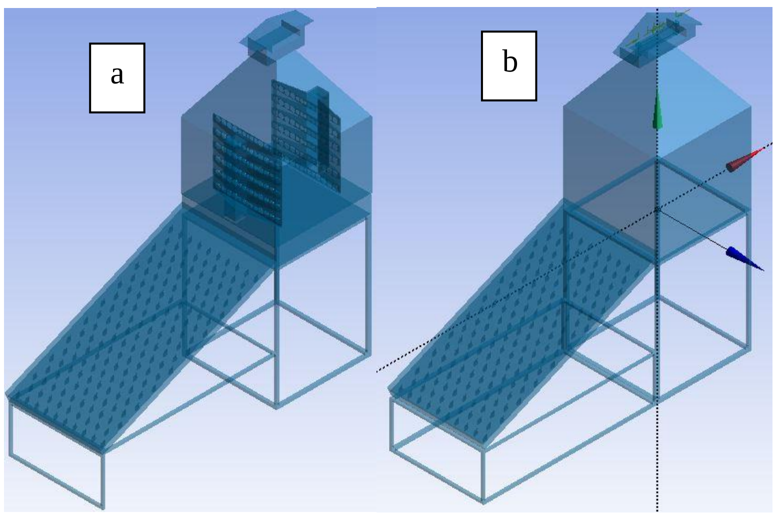

Figure 4. 18: 3D geometry of the solar dryer (a) with vertical air distributor channels (b) without the channels

The solar dryer with vertical air distributors (4.18a) contains five main parts, the solar collector, the drying chamber, the plenum, and two vertical air distributor channels.

4.11.1.2 Mesh generation

Figure 4.19 shows the mesh for the geometry, which was created using the unstructured tetrahedral meshing that is advised for models with complex flow domains.

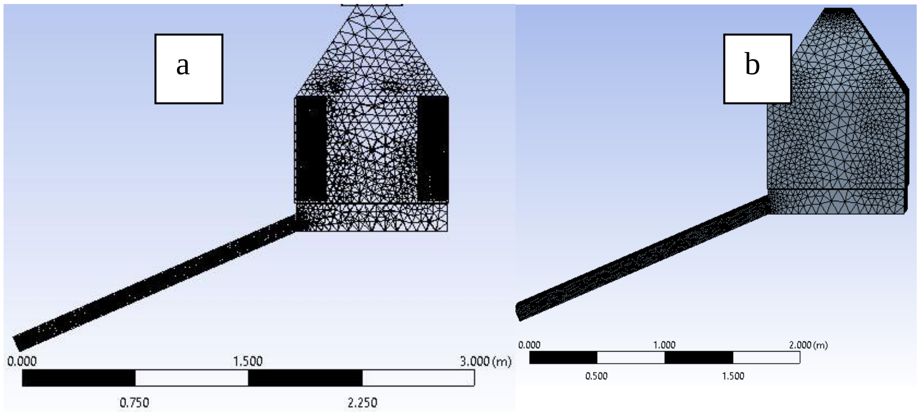

Figure 4. 19: Mesh of the muti-grain solar dryer (a) with vertical air distributor channels (b) without the channels

The fluent user manual states that the minimum orthogonal quality determines the mesh quality. Orthogonal quality ratings have a scale from 0 to 1, with lower values indicating cells of worse quality. As observed in Figure 4.20, the mesh quality is greater than 0.01 and the average value is significantly higher.

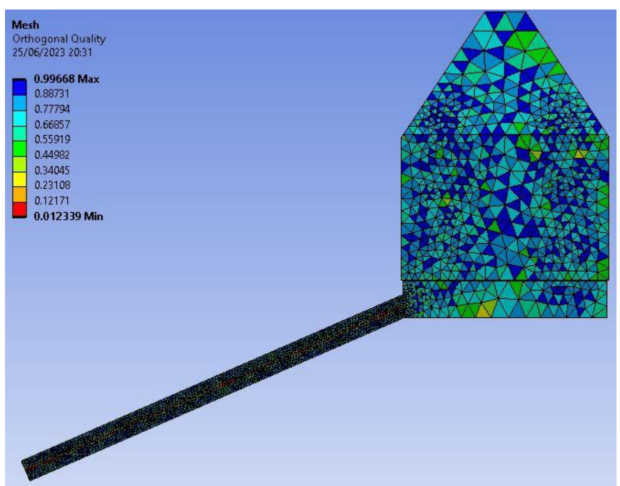

Figure 4.20: The quality of the mesh for the muti-grain solar dryer with vertical air distributor channels

4.11.1.3 Model setup

ANSYS FLUENT 2021R2 was used to do a steady-state pressure-based simulation. A SIMPLE algorithm is selected to solve the momentum equation to create a new pressure distribution by formulating a pressure equation. Velocity is corrected and a new flux set is solved by the SIMPLE algorithm. A standard k-epsilon model was employed for the simulation to determine flow characteristics, and a second-order upwind discretization scheme was used to solve equations of convection terms for each governing equation. The governing transport equation for the standard k-epsilon model is defined as:

$$\frac{\partial(\rho k)}{\partial t} + \frac{\partial}{\partial x_i}(\rho k u_i) = \frac{\partial}{\partial x_j}\left[\left(\mu + \frac{\mu_t}{\sigma_k}\right)\frac{\partial k}{\partial x_j}\right] + G_k + G_b - \rho\epsilon - Y_M + S_k \tag{4.85}$$

$$\frac{\partial(\rho\epsilon)}{\partial t} + \frac{\partial}{\partial x_i}(\rho\epsilon u_i) = \frac{\partial}{\partial x_j}\left[\left(\mu + \frac{\mu_t}{\sigma_\epsilon}\right)\frac{\partial \epsilon}{\partial x_j}\right] + C_{1\epsilon}\frac{\epsilon}{k}(G_k + C_{3\epsilon}G_b) - C_{2\epsilon}\rho\frac{\epsilon^2}{k} + S_\epsilon \tag{4.86}$$

Where, G_k represents the generation of turbulence kinetic energy due to the mean velocity gradients, G_b is the generation of turbulence kinetic energy due to buoyancy, Y_M represents the contribution of the fluctuating dilatation in compressible turbulence to the overall dissipation rate, $C_{1\epsilon}$, $C_{2\epsilon}$, and $C_{3\epsilon}$ are constants, σ_k and σ_ϵ are the turbulent Prandtl numbers for k and ϵ, respectively, S_k and S_ϵ are user-defined source terms.

4.11.1.4 Boundary conditions

Properties of the thermodynamic state of materials and boundary conditions were set following the setup of the CFD models. Using CFD code ANSYS FLUENT 2021R2, the finite volume method is employed to solve continuity, momentum, and energy in the steady-state domain. Design boundary conditions are then applied which are adjacent to fluid zones in the ray tracing calculation. A uniform mass flow rate of 0.02 kg/s was employed at the inlet, with the direction of flow being normal to the inlet opening and the outlet as a pressure outlet.

A uniform heat flux equivalent to the solar radiation falling on the surface in June is given and the simulation is conducted for eight hours. Inside duct air temperature 300K is taken. The transparent cover was described as a semi-transparent solid wall and no-slip condition was set, whereas the other walls were regarded as opaque solid walls and no-slip conditions.

4.11.2 Mesh independence study

The selection of an appropriate mesh affects how the flow equations are solved. The mesh displays the discretization of a computational domain into a finite number of control volumes. It is frequently impossible to use a greater range of mesh sizes due to memory and computing speed constraints. At a minimum, a fine enough mesh is essential to ensure that the solution is accurate. The average outlet temperature of the drying chamber was selected as the primary parameter to analyze the mesh independence because it indicates the overall performance of the system. Element size of 25mm and 10 mm for the drying chamber and absorber plate respectively was selected for the simulation depending on the percentage error obtained in Table 4.7.

Table 4. 7: Results of grid independence study

Mesh	Element size (mm)		Average temperature at the outlet of the drying chamber (K)	Percentage error (%)
	Absorber plate	Drying chamber		
1	25	10	356.72	-
2	31.25	12.5	354.03	0.754
3	39.06	15.62	349.51	1.276
4	48.28	19.53	341.82	2.2
5	60.35	24.41	332.69	2.67

4.11.3 Material properties

The various materials utilized for the various components of the design are listed in Table 4.9 along with their thermophysical properties.

Table 4. 8: Materials selected for the numerical analysis

Part	Material	Thickness (mm)	Thermal conductivity (W/Mk)	Specific heat (J/kg.K)	Density (kg/m^3)
Glass cover	Glass	4	2.01	750	2579
Absorber plate	Galvanized iron	1	80.2	449	7874
Obstacles	Aluminum	0.5	202.4	871	2719
Air	-	-	0.00242	1005.43	1.225
Absorber side walls	Galvanized iron	10	80.2	449	7874
Drying chamber	Galvanized iron	0.5	80.2	449	7874

CHAPTER FIVE

EXPERIMENTAL SETUP AND PROCEDURE

The construction of the experimental setup and the experimental procedure for a forced convection solar dryer are covered in this chapter. The working principle of the system and final assembly of the experimental setup supported with photographs and measuring devices used is also presented.

5.1 Fabrication process

To construct the experimental prototype and measure the system variables, various construction materials, and solar dryer components are purchased from the local market. The building materials of the experimental setup were chosen based on their local accessibility and affordability.

5.1.1 Construction of the flat plate solar air heater

The solar collector is the most important component of a solar dryer which collects useful solar energy and distributes the heat to the air passing through it. Galvanized iron and tin sheet metals were used to build a rectangular box having a size of 2.02m×1.02m×0.112m (length, width, and height). The insulation is made with thick foam of 20 mm thickness on the base plate and canned by sheet metal. The base plate is a 2 m × 1 m steel sheet with 1 mm thickness.

Figure 5. 1: View of a) solar collector from the inlet side b) anti-rust painted absorber plate

As an absorber plate, a 2 m x 1 m x 0.001 m thick black ink-painted galvanized iron sheet is employed, spaced 50 mm from the base plate and the glass cover. The glazing is positioned on top of the flat plate collector with a size of 2 m x 1 m x 0.004 m in thickness. As seen in Figure

5.1, the collector is installed towards the south and slanted at a 24° angle. The spaces are then filled with silica gel to prevent leakage.

For effective improvement of thermal performance, spoon-shaped obstacles are mounted on the absorber plate in a staggered configuration. Some of the fluid will be trapped by the obstacles back as it hits the obstacles, causing the flow to split close to the obstacles. Some of the fluid will turn back as it passes the obstacles and creates a secondary flow. After a certain amount of flow length near the obstacles, the fluid will reattach. This results in the creation of vortices next to the obstacles. The creation of vortices increases the turbulence intensity and enables more fluid to come into contact with the absorber plate for a longer time, increasing heat transfer to the fluid.

5.1.2 Construction of the drying chamber

The solar energy striking the solar collector is absorbed as thermal energy and gets into the drying chamber where the grains are kept. The drying chamber, where the food product is placed for drying, receives the heat energy from the sun and an enhanced solar collector. Its body is made of sheet metal of thickness 0.8mm and is coated black to increase heat gain, while its framework is made of steel bar and angle iron. According to design guidelines, the drying chamber has a size of 0.90 m x 1.00 m x 0.90 m (length x width x height) and five equally spaced trays, which is shown in Figure 5.2. The moistened hot air is expelled from the chamber through a trapezoidal-shaped cover that is positioned at its top. A door on the backside of the chamber is utilized for loading and unloading. The wire mesh of the trays is selected with tiny holes (Figure 5.2) of a better porosity to reduce the pressure drop and improve heat transfer throughout the dryer. Each tray was kept on an angle iron that was fixed to the interior walls of the chamber.

Figure 5. 2: Construction of the drying chamber with a tray

5.1.3 Construction of system supporter structure

The supporting structure was built as to support the system and with the required inclination for solar radiation. The entire supporting structure has been anti-rust coated to extend its lifespan as it is exposed to the effect of the environment.

5.2 Experimental Setup

A forced convection indirect solar dryer has been designed, developed, and installed to conduct an experimental investigation on its heat transfer characteristics and drying performance. Figure 5.3 shows the entire experimental setup of the solar air drying system employed for the current experimental study.

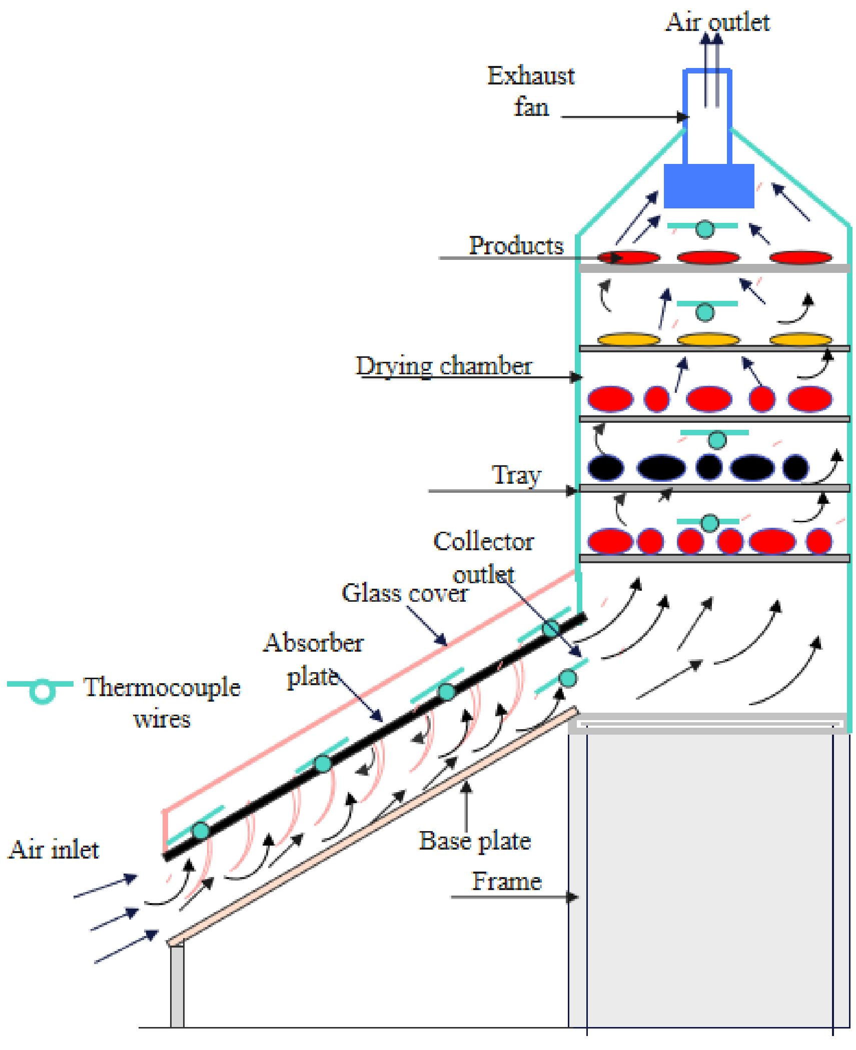

Figure 5. 3: Experimental setup of the system

The air dryer consists of an exhaust fan, a solar collector, and a drying chamber. Air from the ambient passes through the rectangular duct employing a fan driven by 30 W power, AC 220 V/50Hz motor mounted at the exit of the drying chamber. A sheet of window glass (4 mm thick) was used to cover the SAH, leaving an air gap of 50 mm between the glass and the absorber plate in order to reduce top loss. The bottom side of the absorber plate was roughened with spoon-shaped obstacles in a staggered arrangement. Obstacle parameters are determined by obstacles height (e), obstacles base (b), obstacles longitudinal and transverse pitch ($P_l$and P_t) and obstacles twisting angle (angle of incidence) (α). Relative obstacle height (e/H), relative obstacle longitudinal pitch ($P_l/$e), relative obstacles transverse pitch ($P_t/$b) and obstacles angle of incidence (α) is the general formats in which the parameters have been stated. The value of relative obstacle height is selected based on a percentage of airflow blockage. The value of obstacle transverse and longitudinal pitch is defined on the basis of considering flow separation and reattachment length. The angle of twist or angle of attack is selected based on creating turbulence. Referring to (Bekele et al., 2014; Vengadesan & Senthil, 2020), the following parameter values were selected for the optimal thermal performance of a solar air heater duct with spoon-shaped obstacles mounted on the absorber plate. The specified parameter values are: $P_l = 98$mm, $P_t = 100$mm, e = 25 mm, $P_l/$e = 3.9, $P_t/$b = 1.67, e/H = 0.50 and α = 30^o. The figure below shows the photographic view of the absorber plate with spoon-shaped obstacles mounted at an angle of attack of 30^o.

Figure 5. 4: Photographic view of the absorber plate with spoon-shaped obstacles mounted for e/H = 0.50 at an angle of attack 30^o

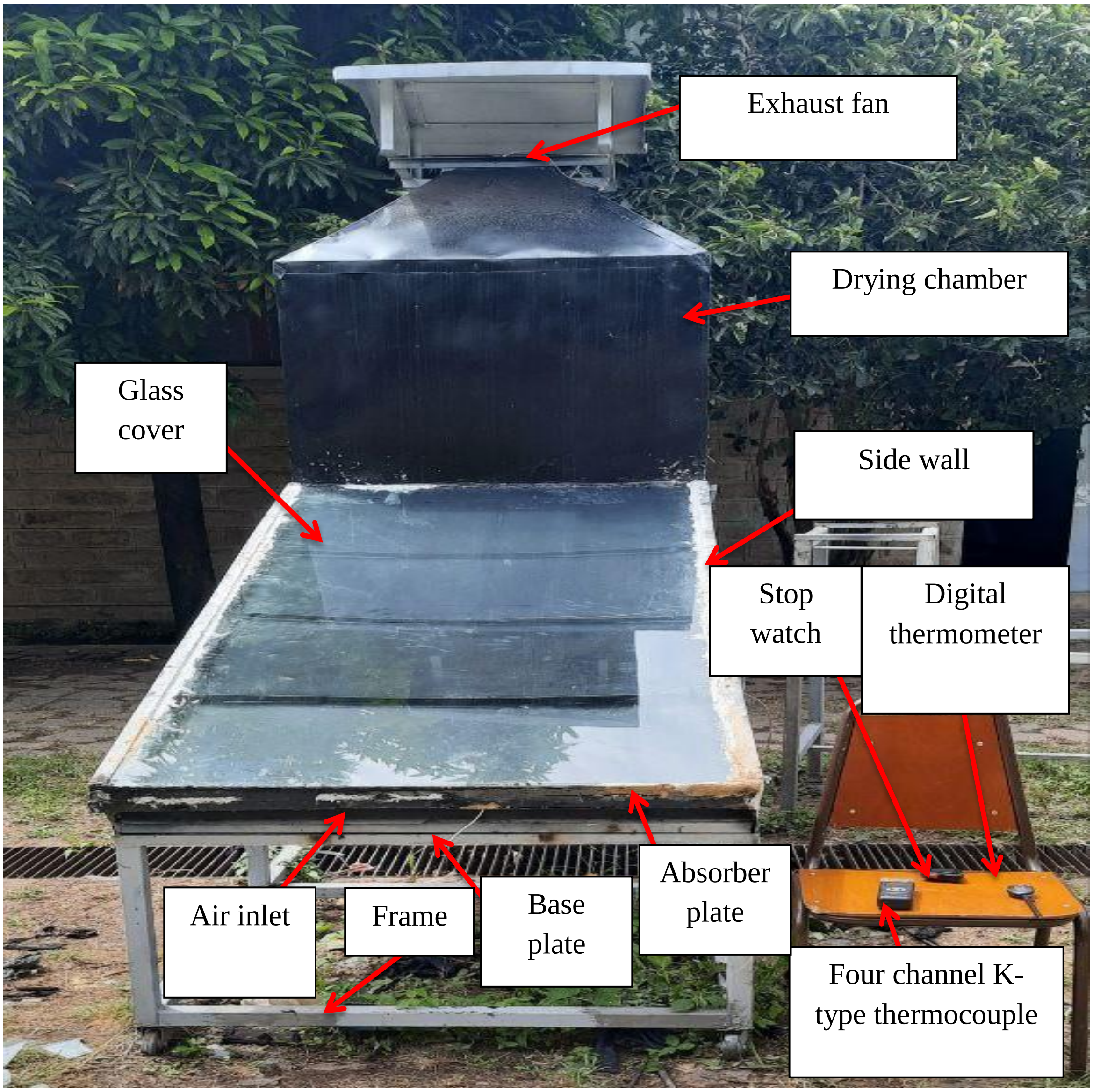

Figure 5. 5: Pictorial view of the experimental setup

5.3 Experimental Procedure

The experimental investigation was performed under two different conditions:

i. Solar collector without spoon-shaped obstacles

ii. Solar collector with spoon-shaped obstacles

The experimental setup with necessary instrumentation was developed and tested its performance from May 29 to June 7 months of 2023 with a modified and conventional solar collector. The items needed for making Miten Shiro were produced before the experiment began. All of the thermocouples were carefully examined before the experiment began to ensure that they were indicating the ambient temperature. The thermocouples can read values between -200 to 1350 °C. A detailed calibration process of the thermocouple has been carried out and presented in Appendix B.

The first experiment is done on a conventional solar dryer; five thermocouples are placed on the absorber plate at the inlet, outlet, and middle at an equal distance. Additionally, four thermocouples are placed inside the drying chamber trays and one at the outlet of the chamber. The second experiment was carried out to investigate the effect of obstacles on the performance of SAH while 6 kg of the grains is loaded to dry. In this experiment, obstacles in the shape of spoons were mounted on the bottom side of the absorber plate. To calculate the amount of moisture that has been lost from the ingredients during a two-hour period, samples of the ingredients were measured using a digital weight balance. In all of the experiments, the solar air heater input and output temperatures as well as the drying chamber temperature were monitored every 30 minutes.

5.4 Description of the instruments

The instruments used for the measuring of the parameters and their specifications are summarized in this section. For a better comprehension of the results and to assess the improvement of them, it is critical to record the experimental conditions. Due to a lack of measurement instruments, the meteorological parameters (solar radiation, ambient temperature, and wind) were taken from the Ethiopian National Metrological Agency, Adama branch. A K-type thermocouple and thermometer were used to measure the temperatures of the surrounding air, the absorber plate, the product, and the glass. Percentage errors, accuracies, and ranges of instruments were summarized in Appendix C.

5.5 Impacts of the proposed modification

The effect of spoon-shaped air flow obstacles mounted on the absorber plate was examined experimentally and numerically. To increase the impingement of air with the high temperature absorber plate which in turn increases the heat transfer to the air, the effect of spoon-shaped obstacles was examined. The 10 mm base of the obstacle effect to increase the flow re-attachment and flow distribution intensity was studied by CFD simulation. A drying chamber with a vertical air distributor channel was examined numerically and compared with the drying chamber without the air distributor. To increase the air distribution over all the trays with equal temperature V-shaped air distributor channel was examined.

CHAPTER SIX

RESULTS AND DISCUSSIONS

Several experiments were carried out on the dryer after it had been constructed to determine its performance with and without spoon-shaped obstacles. In this chapter, the theoretical and experimental results obtained from the solar dryer designed are presented. The experiment is conducted from June 3-5 and from June 14-16 in 2023.

6.1 Solar radiation intensity variations with time

During the experimental days, the sky was almost clear. The tabulated and plotted graph presented in Figure 6.1 shows the estimated monthly average hourly incident solar radiation on a tilted surface for a June month corresponding to local time.

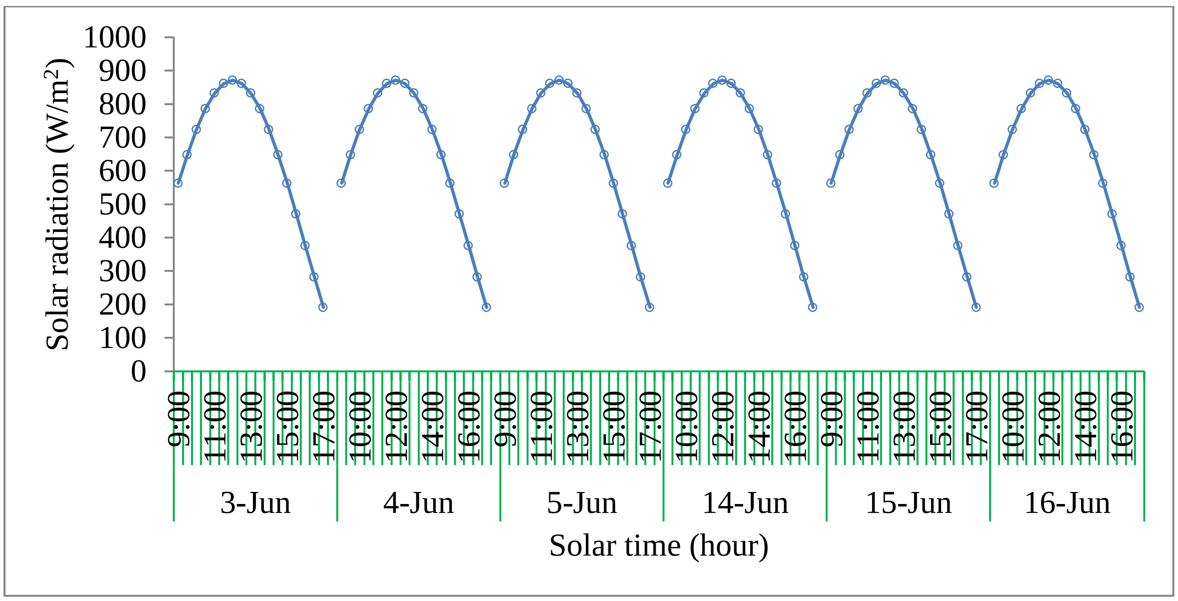

Figure 6. 1: Estimated solar radiation for the climatic condition of Adama in June month

The average maximum and minimum solar radiation intensity reached 871.242 W/m^2 and 191.028 W/m^2 at 12:00 and 17:00 hours, respectively, with an average of 648.305 W/m^2.

6.2 Experimental results of the SAH

The experimental analysis of conventional and modified solar dryers was carried out and the various results obtained during experimentations were recorded in a 30-minute interval. The temperature of the ambient, absorber plate, air, and product was measured and noted for reference in Appendix A-1 and A-2.

6.2.1 Measured variation of ambient temperature

The convection and radiation losses from the top surfaces are influenced by the surrounding temperature. Additionally, affects the conduction losses through the insulation material stacked at the bottom surface of the solar dryer. Furthermore, the ambient temperature affects the drying efficiency of the system. Figure 6.2 shows the hourly variation in ambient temperature that was observed during the experiment.

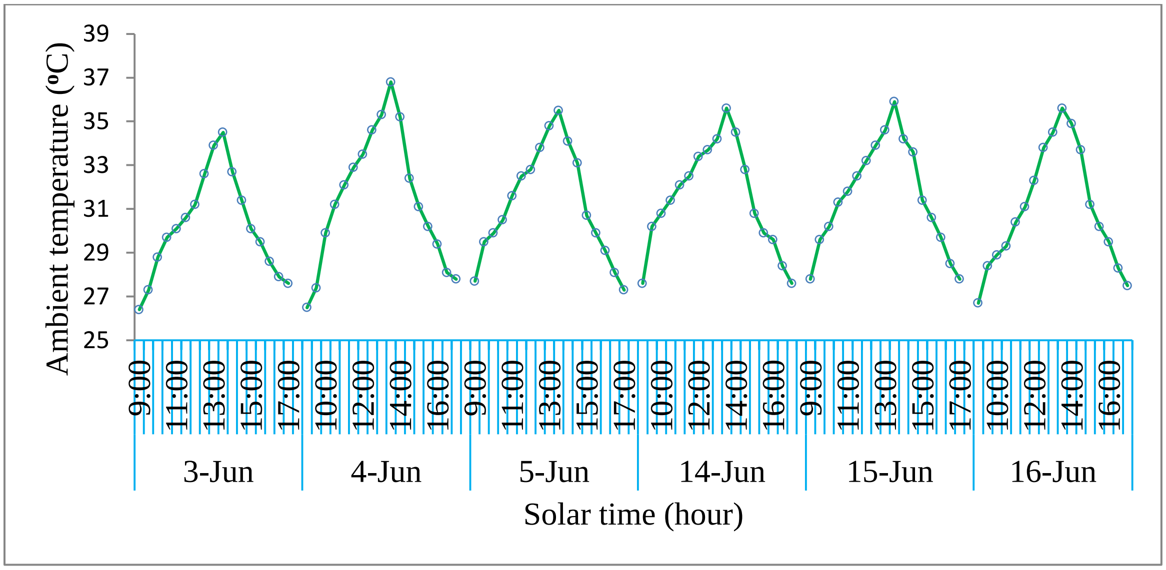

Figure 6. 2: Variations of ambient temperatures observed during experimentation

During the experiment, the ambient temperature varied from about 25.6 to 35.8 ^{o}C. It is also observed that the ambient temperature is nearly the same across all the experimental days and conditions.

6.2.2 Temperature variation

Both conventional and modified solar air heaters' average ambient, absorber plate, and air outlet temperature variations were examined and noted with local time. Figure 6.3 and Figure 6.4 shows the observed variation corresponding to the local time.

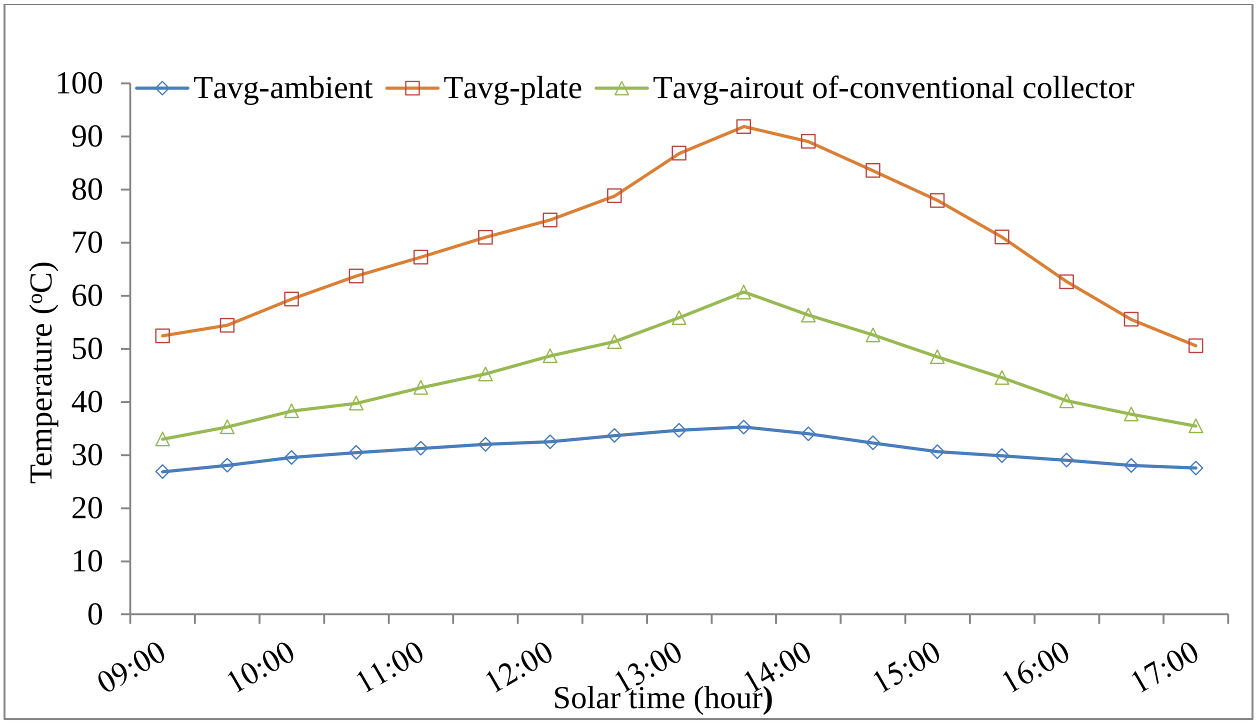

Figure 6. 3: Average Temperature Variation of conventional solar collector

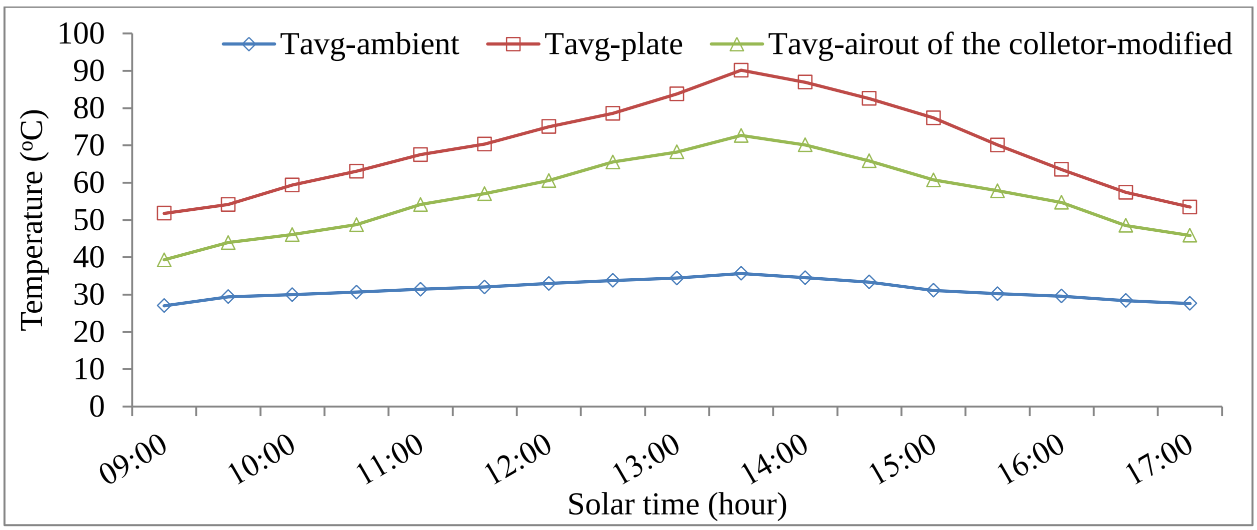

Figure 6. 4: Average Temperature Variation of modified solar collector

The temperature variations between the inlet air and the exit air following the local time for both conventional and modified SAHs are also shown in Figures 6.3 and 6.4. The temperature differences for both collectors increase throughout the day until they reach their peak at 13:30 and then begin to fall. The conventional and continuous spoon-shaped roughed SAHs under 0.02 kg/s mass flow rate have the biggest average temperature difference of 25.4 °C and 37 °C, respectively at 13:30.

6.2.3 Useful heat gain

The experimental test of conventional and modified solar air heaters is carried out from June 3-5 and June 14-16 respectively. Figure 6.5 shows the comparison of the hourly variation of the average useful heat gain of conventional and spoon-shaped SAH during experimental analysis. The useful heat gain initially increases, reaches a peak value after solar noon, and then starts to fall. This is because the temperature change and the useful heat gain are both highly reliant on incident solar radiation. It is noted that the modified SAH recorded a maximum average useful heat gain of 743.7 W with a minimum useful heat gain of 247.23 W, whereas the conventional SAH recorded an average maximum useful heat gain of 511.21 W. With a mass flow rate of 0.02 kg/s, the average useful heat gain for modified and conventional SAH, respectively, was 438.692 W and 231.111 W. The maximum and minimum useful heat was gained at 13:30 and 9:00, respectively.

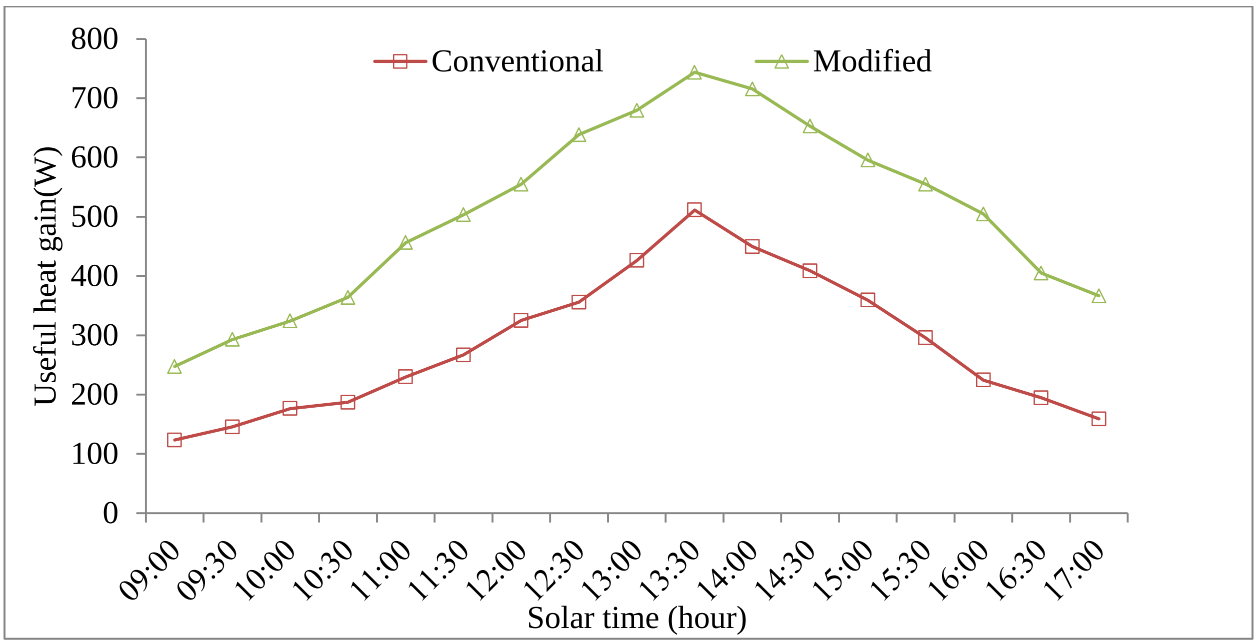

Figure 6.5: Comparison of useful heat gain of the SAH with and without spoon-shaped obstacles

6.2.4 Thermal efficiency

Figure 6.6 compares the average thermal efficiency of the conventional and modified collectors during the experimental days in hourly variations. The average thermal efficiency continued to rise until 13:30 before it started to fall. The average maximum thermal efficiency of 62% and 42.6% were obtained by modified and conventional solar collectors respectively. The increase in efficiency is correlated with both the intensity of solar radiation and the change in air temperature in the collector. The average thermal efficiency has ranged from 10.27% to 42.6% and from 20.6% to 62% for conventional and modified SAH respectively. The maximum thermal efficiency of the modified solar air heater was almost similar to the earlier research study reported by (Mahmood et al., 2015).

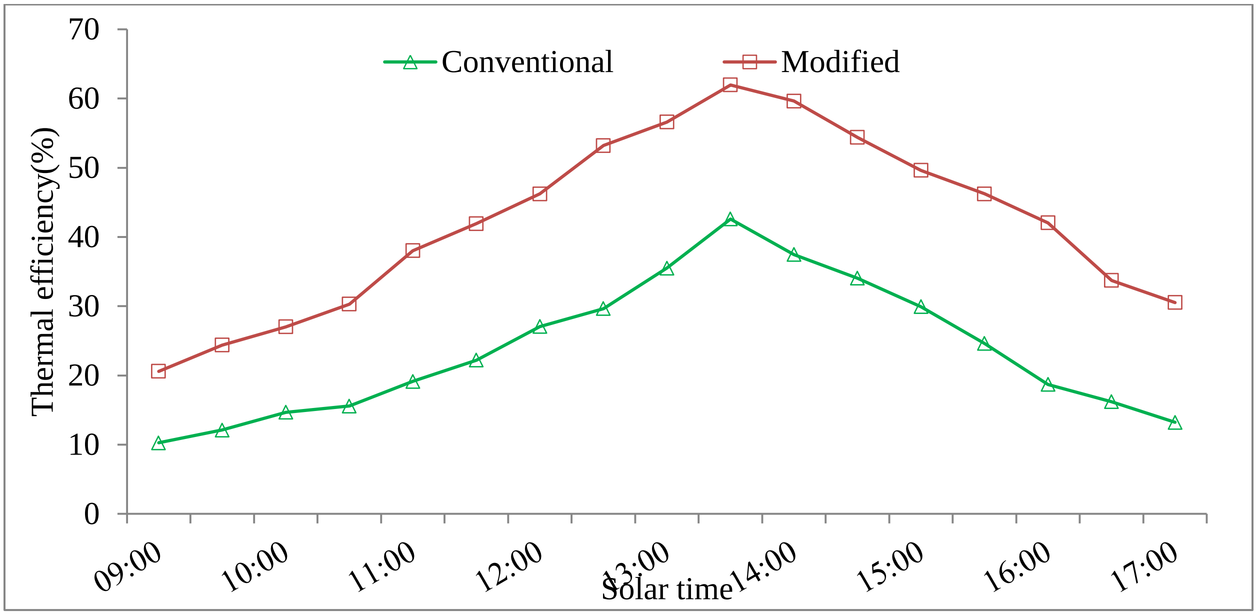

Figure 6. 6: Comparison of thermal efficiency of the SAH with and without spoon-shaped obstacles

6.2.5 Exergy efficiency

The comparison of the exergy efficiency of conventional and modified SAH observed during the experiment was shown in Figure 6.7. For determining the losses in a solar collector, the exergy performance of the collector was evaluated based on the second law of thermodynamics. The average maximum and minimum exergy efficiencies utilizing conventional SAH were determined to be 1.67% and 0.104%, respectively. While the obtained average maximum and minimum exergy efficiencies for a spoon-shaped SAH were 3.44% and 0.42%, respectively. It was noted that conventional and modified SAHs attained average exergy efficiencies of 0.62% and 1.78% respectively.

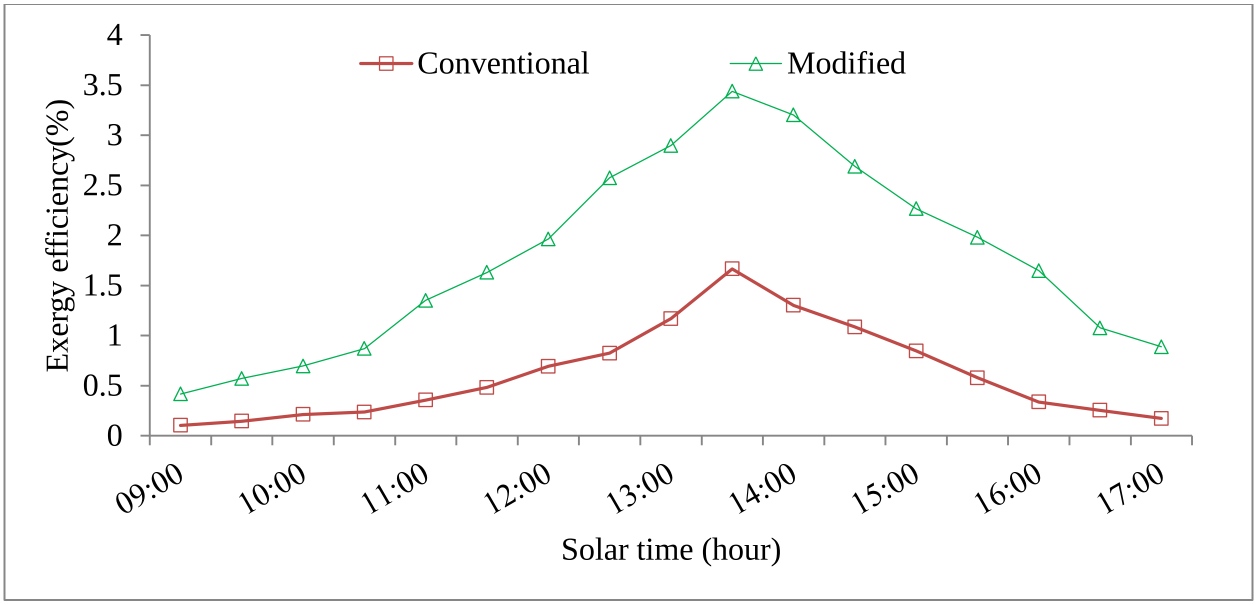

Figure 6. 7: Comparison of exergy efficiency of the SAH with and without spoon-shaped obstacles

6.3 Comparison of various performance parameters of the drying chamber with conventional and enhanced solar collector

The performance of a drying chamber with a single-pass smooth solar air heater and with spoon-shaped obstacles is also carried out in this investigation. In this sub-section, the influence of a solar air heater with spoon-shaped obstacles on the performance of the drying chamber is described and discussed by comparing it with a drying chamber integrated with a smooth solar air heater. The next subsections contain an investigation and discussion of experimental values for various performance characteristics of the drying chamber with conventional and enhanced collectors.

6.3.1 Comparison of drying chamber inlet, outlet, and product temperature variation

Figure 6.8 indicates the variation of drying chamber inlet, outlet, and product temperature with conventional and modified collector corresponding to local time. The temperature variations of the drying chamber integrated with both of the collectors increase throughout the day until they reach their peak at 13:30 and then begin to fall. The biggest average inlet, product, and outlet temperature difference between the drying chamber integrated with conventional and continuous spoon-shaped roughed SAHs under 0.02 kg/s mass flow rate was 14.2 ^{o}C, 13.2 ^{o}C, and 14 ^{o}C, respectively. The average maximum inlet, product, and outlet temperature of the drying chamber utilizing enhanced SAH were determined to be 72.6 ^{o}C, 81.8 ^{o}C, and 80.8 ^{o}C respectively. While the obtained average maximum inlet, product, and outlet temperature of the drying chamber integrated with a conventional SAH were 60.7 ^{o}C, 71.9 ^{o}C, and 69.9 ^{o}C respectively. It was noted that the drying chamber integrated with spoon-shaped obstacles mounted SAH attained average inlet, outlet, and product temperatures of 56.47 ^{o}C, 64.66 ^{o}C, and 65.82 ^{o}C, respectively.

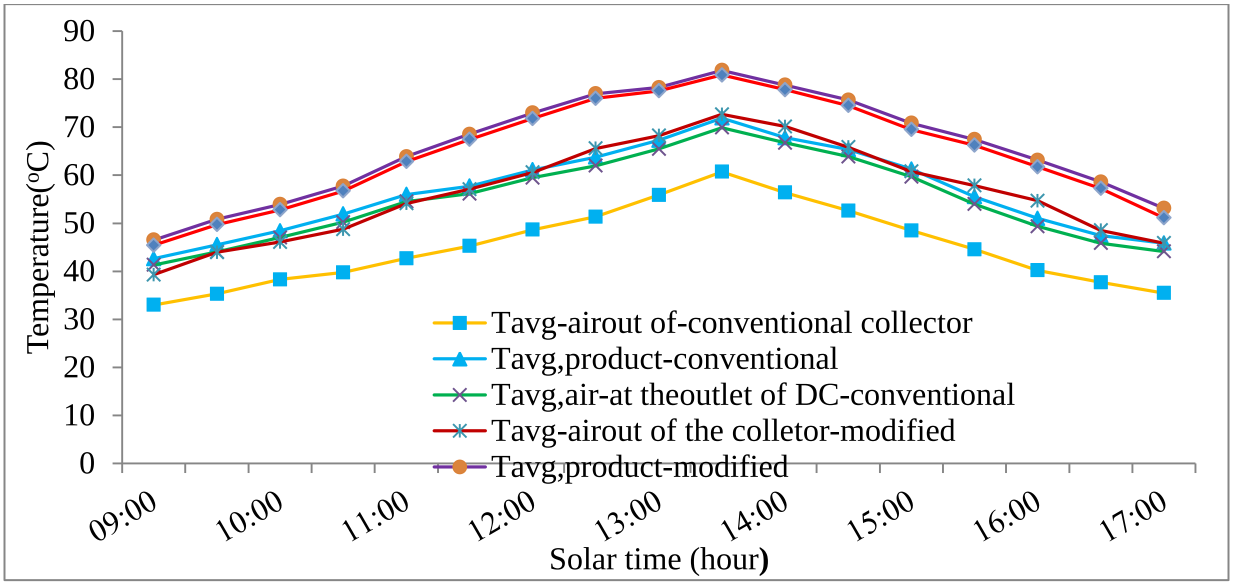

Figure 6. 8: Comparison of drying chamber inlet, outlet, and product temperature variation integrated with a SAH with and without spoon-shaped obstacles

6.3.2 Comparison of useful heat gain of the drying chamber

The comparison of the useful heat gain of the drying chamber integrated with a conventional and modified SAH observed during the experiment was shown in Figure 6.9. The useful heat gains first rise, peak around solar noon, and then start to fall. The maximum average useful heat gain of the drying chamber was 225.79 W and 187.91 W with and without spoon-shaped obstacles. It has been found that the average useful heat gain of the drying chamber integrated with a spoon-shaped SAH is 18.71 W to 40.16 W higher than a drying chamber integrated with a smooth solar collector with an average value of 30.89 W. An average useful heat gain value of 170.9 W and 140 W were found with and without enhanced solar collectors.

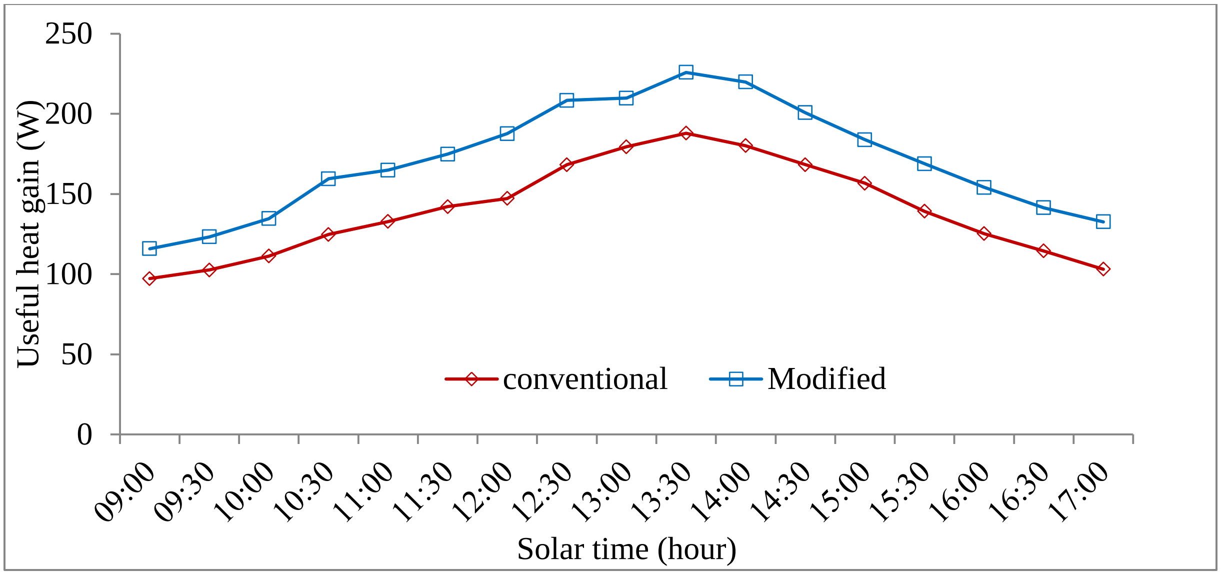

Figure 6. 9: Comparison of drying chamber useful heat gain variation integrated with a SAH with and without spoon-shaped obstacles

6.3.3 Comparison of thermal efficiency of the drying chamber

Figure 6.10 shows the comparison between the experimentally determined hourly changes of the drying chamber average thermal efficiency integrated with spoon-shaped obstacles installed SAH and conventional SAH.

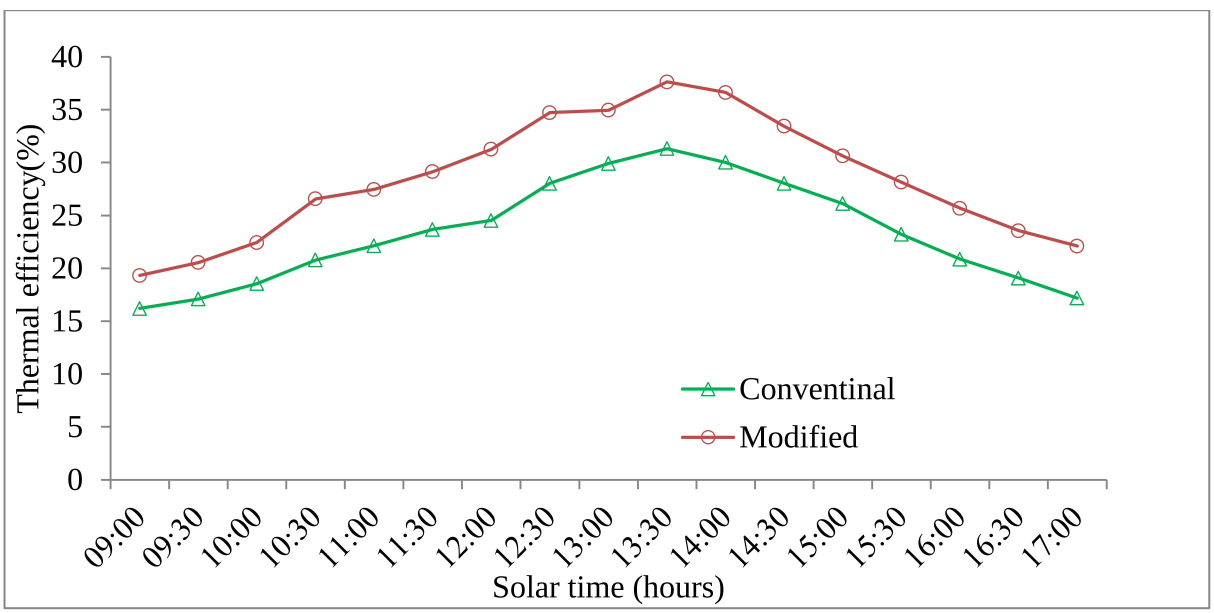

Figure 6. 10: Comparison of drying chamber thermal efficiency variation integrated with a SAH with and without spoon-shaped obstacles

A maximum value of average thermal efficiency of 31.3% is achieved at 13:30 hours in the case of a drying chamber paired with a conventional SAH, while a maximum value of average thermal efficiency of 37.63% is attained at the same time with a modified SAH. It is observed that for both conventional and modified collector integrated drying chambers, the average thermal efficiency increases over time and reaches its maximum value at 13:30 hours. Its value starts to decline after 13:30 hours in both the cases of conventional and modified collector integrated drying chambers. This corresponds to the fact that the increase in efficiency is correlated with both the intensity of solar radiation and the change in air temperature in the collector. It has been found that the average thermal efficiency of the drying chamber integrated with a spoon-shaped SAH is 3.12% to 6.61% higher than a drying chamber integrated with a smooth solar collector with an average value of 5.15%. An average thermal efficiency value of 28.49% and 23.34% were found with and without enhanced solar collectors.

6.3.4 Comparison of exergy efficiency of the drying chamber

For determining the losses in the drying chamber, its exergy performance was evaluated based on the second law of thermodynamics. The exergy efficiency for both conventional and modified collector integrated drying chambers observed during the experimental investigation was shown in Figure 6.11.

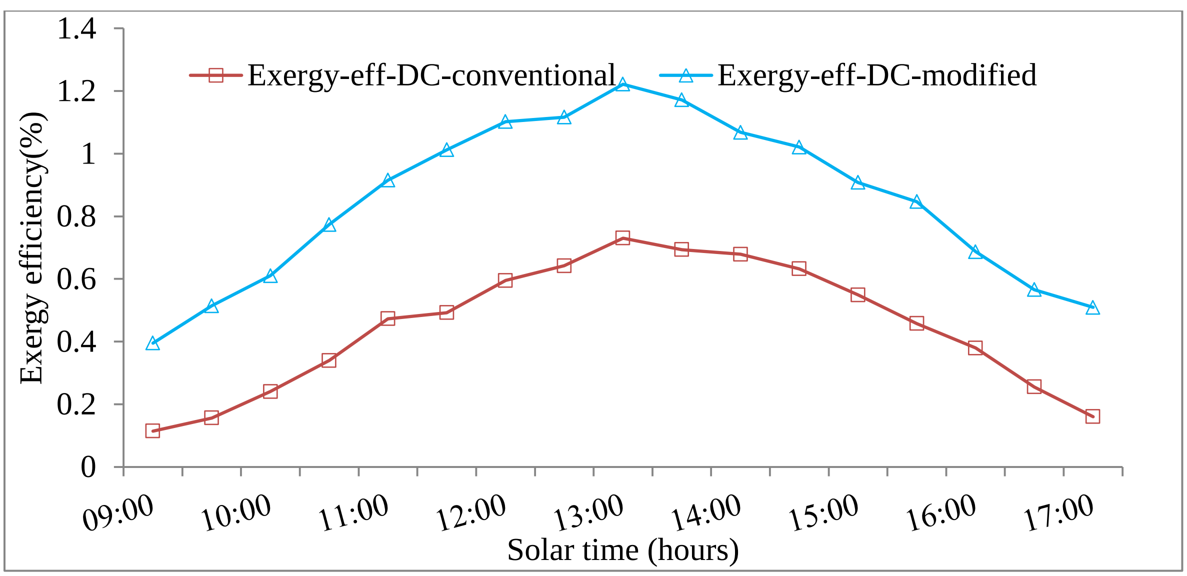

Figure 6. 11: Comparison of drying chamber average exergy efficiency variation integrated with a SAH with and without spoon-shaped obstacles

A maximum value of average exergy efficiency of 0.73% is obtained, while with a modified SAH, a maximum value of average exergy efficiency of 1.23% is achieved. An average exergy efficiency value of 0.85% and 0.45% were found with and without enhanced solar collectors.

6.4 Product moisture content variation

Figure 6.12 illustrates how the moisture content of the ingredients varies with drying time for conventional, modified solar dryers, and open sun drying. The weight of the grains was measured, and the weight loss was calculated within two hours intervals to determine the moisture content. The moisture content of the product samples was reduced from their initial value to the final value in 18 hours in the drying chamber integrated with enhanced SAH and in 24 hours (three days) in the drying chamber integrated with conventional SAH. The final moisture content value of the multi-grain product was achieved after 34 hours (4 days and 2 hours) by open-sun drying.

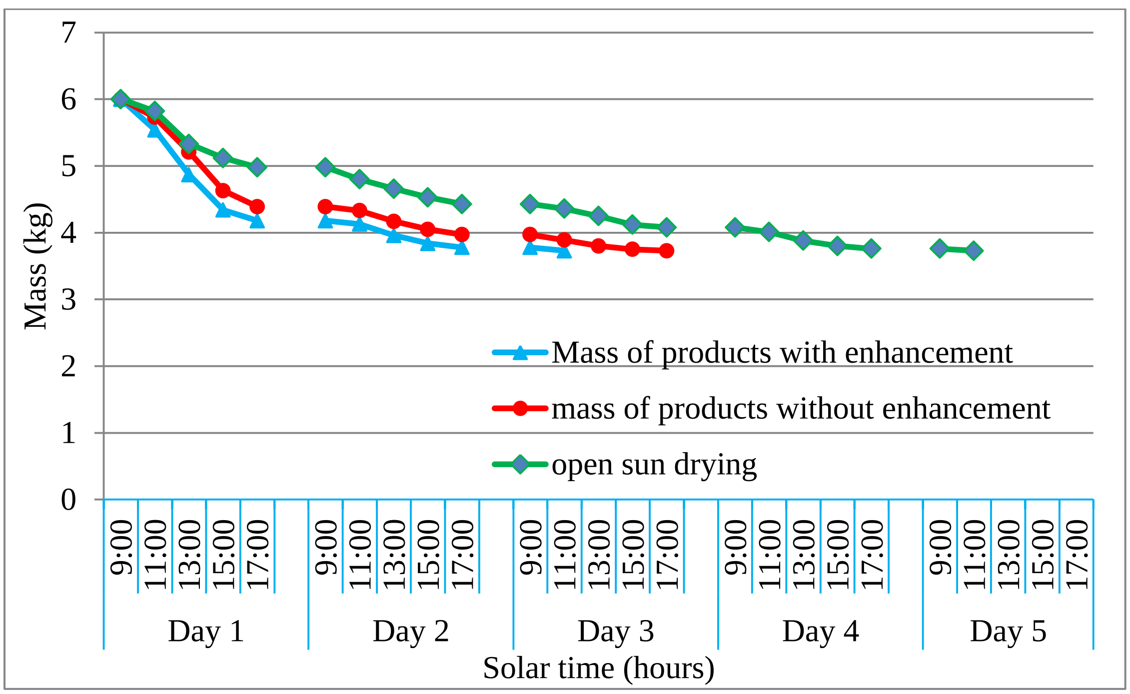

Figure 6. 12: Comparison of product moisture content variation

The first day of the drying process showed a high level of moisture removal, and as the drying process progressed, the rate of moisture removal started to decrease. This occurred because there was less moisture to be extracted toward the end.

It is observed that the drying chamber integrated with the enhanced collector appears to have the fastest drying rate for the products. The highest moisture removal from the ingredients is achieved at noon when the intensity of solar radiation and the product temperature were at their highest.

6.5 Overall efficiency of the system

The overall area of the system was 3 m^2 consisting of a 2 m^2 collector area and a 1 m^2 drying chamber. The average intensity of the solar radiation incident on the surface of the solar collector in June was estimated to be 648 W/m^2. The solar dryer was used every day for 8 hours, using 30 W to power the exhaust fan. The moisture content of 6 kg of products was reduced to their final moisture content by evaporating 2.27 kg of moisture in total. The latent heat of the vaporization of water was determined using Equation (4.5), and it was found to be 2358.4 kJ/kg at a drying average air temperature of 60 °C. Equation (4.3) is used to compute the amount of energy needed to evaporate 2.27 kg of moisture, and the result is 5353.6 kJ. The total energy input to the dryer during the entire drying period was 85.9 MJ and 114.6 MJ for conventional and modified dryers which is determined from equation (4.45). Applying equation (4.44), the specific energy consumption of the drying system was determined to be 10.51 kWh/kg and 14.02 kWh/kg of moisture. For the enhanced collector solar dryer, the exhaust fan used 0.238 kWh of electrical energy per kg of moisture removed, which was only 2.26% of the total specific energy consumed. Thus, solar energy provided 97.74% of the total energy required to dry the ingredients in the newly designed and constructed solar dryer. Equation (4.46) is used to calculate the overall efficiency of the drying system integrated with the enhanced collector, which was found to be 6.23%.

6.6 CFD simulation results

For a solar dryer with and without a vertical air distributor channel, CFD simulation of fluid flow characteristics at a constant mass flow rate has been performed in ANSYS FLUENT 21R2. Flow behavior analysis of drying air inside the modified solar collector was performed. Result comparison was taken between a drying chamber with and without a vertical air distributor channel.

6.6.1 Solar collector

Air flow distribution were used to examine the fluid flow characteristics of a modified solar collector. The velocity distribution on the plane were taken parallel to the direction of air flow.

Figure 6.13 shows the 3D velocity streamlines created on a plane parallel to the flow direction through the solar air heater.

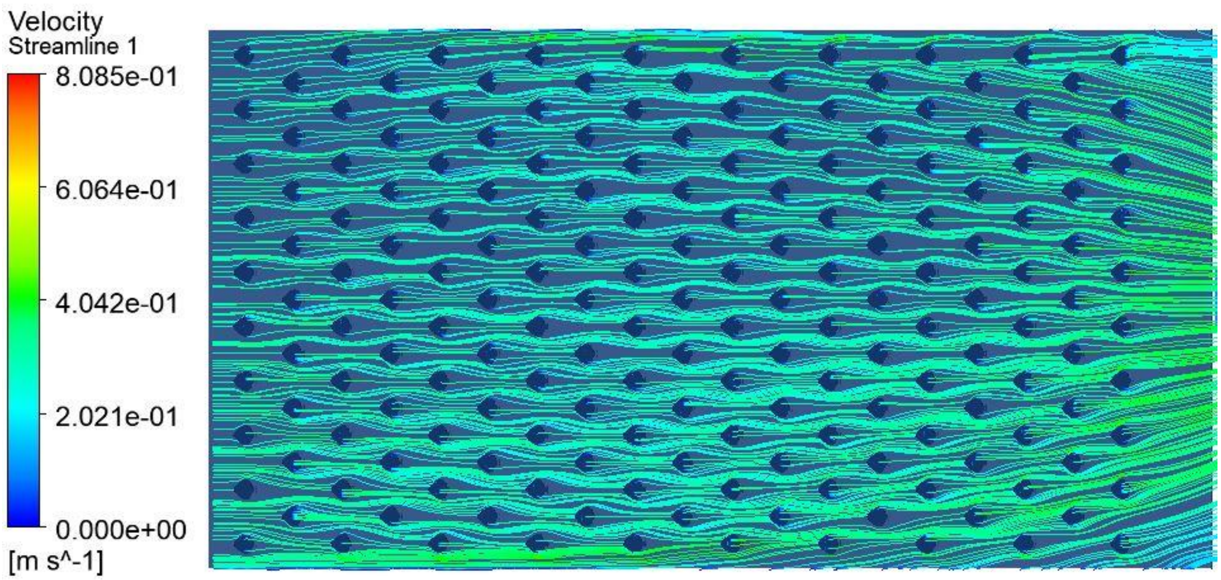

Figure 6. 13: 3D velocity streamline plot in the solar air heater

As it is observed, the intensity of air was evenly distributed throughout the heater which increases the convective heat transfer between the absorber plate and the air. Thus, as it is observed from Figure 6.13, the obstacle base geometry played a vital role to increase the flow separation and for the re-attachment of flow. The airflow blockage of the obstacles also creates good turbulence, flow separation, and re-attachment.

6.6.2 Drying chamber

The drying chamber is modeled with two vertical V-shaped air distributor channels and without channels. The goal is to show the air velocity distribution across the entire drying chamber for uniform drying. The fluid flow characteristics performance investigation of a solar dryer drying chamber with and without a vertical V-shaped air distributor channel has been carried out.

The 3D velocity streamlines developed for the drying chamber combined with two vertical V-shaped air distributors and without air distributors, respectively, are shown in Figures 6.14 and 6.15 on different planes.

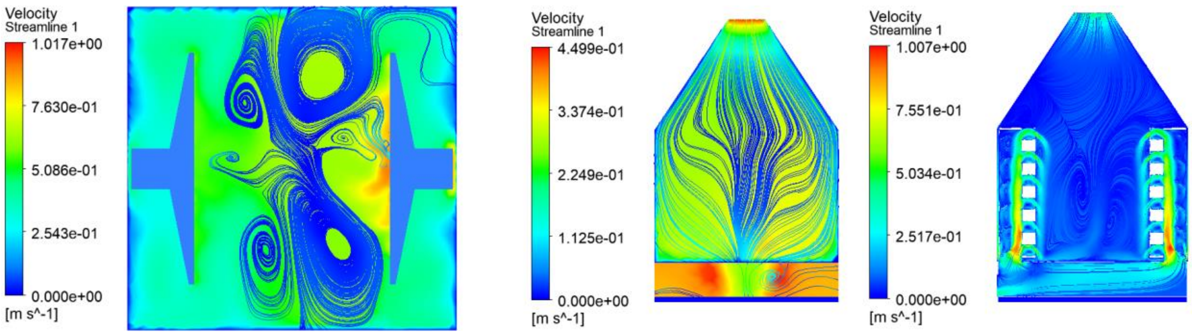

Figure 6. 14: Velocity streamlines of the drying chamber integrated with two vertical V-shaped air distributors

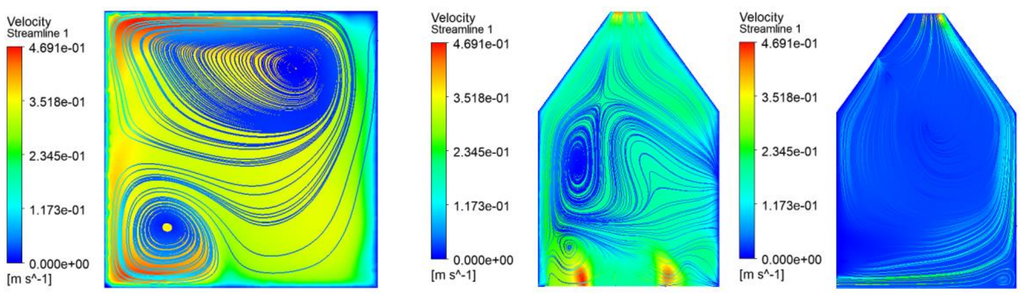

Figure 6. 15: Velocity streamlines of the drying chamber without the distributors

As it is observed, the intensity of air in the drying chamber integrated with two vertical V-shaped air distributors showed better distribution throughout the drying chamber. The effectiveness of the vertical air distributers, which are newly utilized in this dryer, is demonstrated by a uniform temperature distribution. A non-uniform flow is observed in the drying chamber without the air distributors. The high intensity of air distribution in the drying chamber with vertical air distributors is essential for fast, even, and high quality drying of the products and is fulfilled by the new model.

6.7 Result summary

The results obtained from the experimental and numerical analysis are summarized in this sub-section as follows:

The average useful heat gain of the conventional and modified SAH was 231.111 W and 438.69 W, respectively. The average maximum thermal efficiency and exergy efficiency utilizing conventional SAH were determined to be 42.6% and 1.67%, respectively. Conversely, 62% and 3.44% of the values were attained by the modified solar air heater. The average maximum inlet, product, and outlet temperature of the drying chamber utilizing enhanced SAH were determined to be 72.6 ^{o}C, 81.8 ^{o}C, and 80.8 ^{o}C respectively. While the obtained average maximum inlet, product, and outlet temperature of the drying chamber integrated with a conventional SAH were 60.7 ^{o}C, 71.9 ^{o}C, and 69.9 ^{o}C respectively. The maximum average useful heat gain, thermal, and exergy efficiency value of 187.91 W, 31.3%, and 2.12%, was achieved respectively by the drying chamber with conventional SAH. Contrarily, 225.79 W, 37.63%, and 3.91% were obtained respectively by the drying chamber with modified SAH. The final moisture content value of the multi-grain product was achieved after 34, 24, and 18 hours by the open sun, conventional, and modified solar dryer, respectively. The overall efficiency of the drying system integrated with the enhanced collector was found to be 6.23%. The spoon-shaped obstacles produce very good flow characteristics for temperature enhancement. The drying chamber integrated with two V-shaped vertical air distributors attained a uniform airflow intensity throughout its domain.

CHAPTER SEVEN

CONCLUSIONS AND RECOMMENDATIONS

Conclusions

The present work investigated the experimental performance of a single pass active solar dryer with a spoon-shaped obstacle mounted absorber plate which is used to dry different grains for miten Shiro preparation. Additionally, computational fluid dynamics numerical simulation was also carried out for comparison of drying chamber performance with and without vertical V-shaped air distributors. The components of the solar dryer are constructed from locally available materials. A theoretical and experimental performance investigation was conducted twice, once with a spoon-shaped obstacle mounted absorber plate and once with a conventional smooth solar collector that had not been modified. Energy and exergy efficiency analyses were carried out to evaluate the performance of the solar dryer components and the overall system. Data from the experiment, which includes temperature and product mass measurements were recorded every 30 minutes and 2 hours, respectively. The theoretical analysis and experimental findings were in good agreement. The experimental and theoretical analysis of the solar dryer led to the following conclusions:

In the case of the experimental analysis:

- The maximum average temperature difference between the inlet and the outlet obtained by the modified solar collector had an increment of 5.04 ^{o}C to the conventional collector.
- The modified solar air heater demonstrated an average useful heat gain, thermal efficiency, and exergy efficiency increment of 207.581 W, 17.34%, and 0.8514%, respectively, in the experimental performance comparison between conventional and modified solar air heaters.
- The drying chamber integrated with the modified solar collector demonstrated an average useful heat gain and thermal efficiency increment of 25.61 W and 4.24%, respectively, in the experimental performance comparison between the drying chamber integrated with the conventional and modified solar collector.
- The moisture content of the product samples was reduced from their initial value to the final value in 18 hours in the drying chamber integrated with enhanced SAH and in 24 hours (three days) in the drying chamber integrated with conventional SAH.

- The final moisture content value of the multi-grain product was achieved after 34 hours (4 days and 2 hours) by open-sun drying.
- The overall efficiency of the drying system integrated with the enhanced collector was found to be 6.23%.
- The experimental results showed the modified active mode solar dryer performed better than the conventional and open sun drying methods.
- The thermal performance of the selected obstacle geometry has increased noticeably.
- Finally, it has been found that miten Shiro ingredient solar drying could be a practical way to preserve and maintain the quality of dried ingredients.

In the case of numerical results:

- Higher turbulence, flow separation, and re-attachment of airflow were observed by the new feature of spoon-shaped obstacles, which results in higher heat transfer.
- The CFD result showed that the airflow intensity distribution increases using vertical air distributor channels.
- The findings showed that using vertical V-shaped air distribution channels can improve the performance of the drying system by increasing the uniformity of drying air distribution.

Recommendations

In the present study, theoretical and experimental investigation on the performance of active mode single pass solar dryer using spoon-shaped obstacles mounted absorber plates for drying miten Shiro grains has been carried out. The conclusion section highlights the most important findings of the research. However, there are many opportunities for more studies to enhance system performance. The followings are some potential future research areas and suggestions:

- In this work, the drying of miten Shiro ingredients was examined using an active solar dryer. Thus, future work should focus on solar dryers integrated with photovoltaic sources.
- Since solar radiation is not accessible all year long, integrating the system with alternative renewable energy sources like biomass and biogas can be explored.
- As solar radiation varies depending on the season of the year, the performance of the drier should be measured throughout different seasons of the year.

- A small-scale performance investigation has been done in this work. As a result, the dryer can be further studied for applications on a broad scale.

REFERENCES

Abdelkader, T. K., Zhang, Y., Gaballah, E. S., Wang, S., Wan, Q., and Fan, Q. (2020). Energy and exergy analysis of a flat-plate solar air heater coated with carbon nanotubes and cupric oxide nanoparticles embedded in black paint. *Journal of Cleaner Production*, *250*, 119501. https://doi.org/10.1016/j.jclepro.2019.119501

Abdu, Y. (2021). Experimental performance investigation of double pass solar air heater with baffles for red chilli drying. Unpublished, MSc. Thesis submitted to Adama Science and Technology University, 1-122

Abo-Elfadl, S., Hassan, H., and El-Dosoky, M. (2020). Study of the performance of double pass solar air heater of a new designed absorber: An experimental work. *Solar Energy*, *198*, 479–489. https://doi.org/10.1016/j.solener.2020.01.091

Aboghrara, A. M., Baharudin, B., Alghoul, M. A., Adam, N. M., Hairuddin, A. A., and Hasan, H. A. (2017). Performance analysis of solar air heater with jet impingement on corrugated absorber plate. *Case Studies in Thermal Engineering*, *10*, 111–120. https://doi.org/10.1016/j.csite.2017.04.002

Abubakar, S., Umaru, S., Anafi, F. O., and Abubakar, A. S. (2018). Design and Performance Evaluation of a Mixed-Mode Solar Crop Dryer. *FUOYE Journal of Engineering and Technology*. https://doi.org/10.46792/fuoyejet.v3i1.133

Abuşka, M. (2018). Energy and exergy analysis of solar air heater having new design absorber plate with conical surface. *Applied Thermal Engineering*, *131*, 115–124. https://doi.org/10.1016/j.applthermaleng.2017.11.129

Agrawal, A., and Sarviya, R. (2014). A review of research and development work on solar dryers with heat storage. *International Journal of Sustainable Energy*, *35*(6), 583–605. https://doi.org/10.1080/14786451.2014.930464

Akarslan, F. (2012). Solar-Energy Drying Systems. *Modeling and Optimization of Renewable Energy Systems*. https://doi.org/10.5772/39207

Alam, T., & Kim, M. H. (2017). Performance improvement of double-pass solar air heater – A state of art of review. *Renewable and Sustainable Energy Reviews*, *79*, 779–793. https://doi.org/10.1016/j.rser.2017.05.087

Amer, B., Hossain, M., and Gottschalk, K. (2010). Design and performance evaluation of a new hybrid solar dryer for banana. *Energy Conversion and Management*, *51*(4), 813–820. https://doi.org/10.1016/j.enconman.2009.11.016

Atalay, H. (2019). Performance analysis of a solar dryer integrated with the packed bed thermal energy storage (TES) system. *Energy*, *172*, 1037–1052. https://doi.org/10.1016/j.energy.2019.02.023

Atalay, H. (2020). Assessment of energy and cost analysis of packed bed and phase change material thermal energy storage systems for the solar energy-assisted drying process. *Solar Energy*, *198*, 124–138. https://doi.org/10.1016/j.solener.2020.01.051

Ayensu, A. (1997). Dehydration of food crops using a solar dryer with convective heat flow. *Solar Energy*, *59*(4–6), 121–126. https://doi.org/10.1016/s0038-092x(96)00130-2

Bakari, R., Minja, R. J. A., and Njau, K. N. (2014). Effect of Glass Thickness on Performance of Flat Plate Solar Collectors for Fruits Drying. *Journal of Energy*, *2014*, 1–8. https://doi.org/10.1155/2014/247287

Bekele, A., Alemu, D., and Mishra, M. (2013). Large-scale solar water heating systems analysis in Ethiopia: a case study. *International Journal of Sustainable Energy*, *32*(4), 207–228. https://doi.org/10.1080/14786451.2011.605951

Bekele, A., Mishra, M., and Dutta, S. (2014). Performance characteristics of solar air heater with surface mounted obstacles. *Energy Conversion and Management*, *85*, 603–611. https://doi.org/10.1016/j.enconman.2014.04.079

Daş, M., Aliç, E., and Akpinar, E. K. (2021). Detailed analysis of mass transfer in solar food dryer with different methods. *International Communications in Heat and Mass Transfer*, *128*, 105600. https://doi.org/10.1016/j.icheatmasstransfer.2021.105600

Elkhadraoui, A., Kooli, S., Hamdi, I., and Farhat, A. (2015). Experimental investigation and economic evaluation of a new mixed-mode solar greenhouse dryer for drying of red pepper and grape. *Renewable Energy*, *77*, 1–8. https://doi.org/10.1016/j.renene.2014.11.090

El-Sebaii, A., and Shalaby, S. (2012). Solar drying of agricultural products: A review. *Renewable & Sustainable Energy Reviews*, *16*(1), 37–43. https://doi.org/10.1016/j.rser.2011.07.134

Esen, H. (2008). Experimental energy and exergy analysis of a double-flow solar air heater having different obstacles on absorber plates. *Building and Environment*, *43*(6), 1046–1054. https://doi.org/10.1016/j.buildenv.2007.02.016

Fudholi, A., Sopian, K., Othman, M. H. D., and Ruslan, M. H. (2014). Energy and exergy analyses of solar drying system of red seaweed. *Energy and Buildings*, *68*, 121–129. https://doi.org/10.1016/j.enbuild.2013.07.072

Fudholi, A., Sopian, K., Yazdi, M. R. H., Ruslan, M. H., Gabbasa, M., & Kazem, H. A. (2014). Performance analysis of solar drying system for red chili. *Solar Energy*, *99*, 47–54. https://doi.org/10.1016/j.solener.2013.10.019

Hap, N. van. (2022, May 29). *Heat Transfer in Double-Pass Solar Air Heater: Mathematical Models and Solution Strategy*. IntechOpen. https://www.intechopen.com/online-first/82016

Ho, C. D., Chang, H., Wang, R. C., and Lin, C. S. (2012). Performance improvement of a double-pass solar air heater with fins and baffles under recycling operation. *Applied Energy*, *100*, 155–163. https://doi.org/10.1016/j.apenergy.2012.03.065

Jin, W., Wu, J., Jia, N., Lei, J., Ji, W., and Xie, G. (2021). Effect of shape and distribution of pin-fins on the flow and heat transfer characteristics in the rectangular cooling channel. *International Journal of Thermal Sciences*, *161*, 106758. https://doi.org/10.1016/j.ijthermalsci.2020.106758

Kannan, N., and Vakeesan, D. (2016). Solar energy for future world: - A review. *Renewable and Sustainable Energy Reviews*, *62*, 1092–1105. https://doi.org/10.1016/j.rser.2016.05.022

Karney, C., and Deakin, R. (2009). F.W. Bessel (1825): The calculation of longitude and latitude from geodesic measurements. *Astronomische Nachrichten*, *331*(8), 852–861. https://doi.org/10.1002/asna.201011352

Khadraoui, A. E., Bouadila, S., Kooli, S., Farhat, A., and Guizani, A. (2017). Thermal behavior of indirect solar dryer: Nocturnal usage of solar air collector with PCM. *Journal of Cleaner Production*, *148*, 37–48. https://doi.org/10.1016/j.jclepro.2017.01.149

Khoukhi, M., Maruyama, S., Komiya, A., and Behnia, M. (2006). Flat-Plate Solar Collector Performance with Coated and Uncoated Glass Cover. *Heat Transfer Engineering*. https://doi.org/10.1080/01457630500343009

Kumar, A., and Layek, A. (2019). Energetic and exergetic performance evaluation of solar air heater with twisted rib roughness on absorber plate. *Journal of Cleaner Production*, *232*, 617–628. https://doi.org/10.1016/j.jclepro.2019.05.363

Kumar, P., and Singh, D. (2020). Advanced technologies and performance investigations of solar dryers: A review. *Renewable Energy Focus*, *35*, 148–158. https://doi.org/10.1016/j.ref.2020.10.003

Kumar, R., Nadda, R., Kumar, S., Razak, A., Sharifpur, M., Aybar, H. S., Saleel, C. A., and Banapurmath, N. R. (2022). Influence of artificial roughness parametric variation on thermal performance of solar thermal collector: An experimental study, response surface analysis and ANN modelling. *Sustainable Energy Technologies and Assessments*, *52*, 102047. https://doi.org/10.1016/j.seta.2022.102047

Lakshmi, D., Muthukumar, P., Layek, A., and Nayak, P. K. (2019). Performance analyses of mixed mode forced convection solar dryer for drying of stevia leaves. *Solar Energy*, *188*, 507–518. https://doi.org/10.1016/j.solener.2019.06.009

Lamrani, B., and Draoui, A. (2020). Thermal performance and economic analysis of an indirect solar dryer of wood integrated with packed-bed thermal energy storage system: A case study of solar thermal applications. *Drying Technology*, *39*(10), 1371–1388. https://doi.org/10.1080/07373937.2020.1750025

Lingayat, A. B., Chandramohan, V., Raju, V., and Meda, V. (2020). A review on indirect type solar dryers for agricultural crops – Dryer setup, its performance, energy storage and important highlights. *Applied Energy*, *258*, 114005. https://doi.org/10.1016/j.apenergy.2019.114005

Mahian, O., Kianifar, A., Heris, S. Z., Wen, D., Sahin, A. Z., and Wongwises, S. (2017). Nanofluids effects on the evaporation rate in a solar still equipped with a heat exchanger. *Nano Energy*, *36*, 134–155. https://doi.org/10.1016/j.nanoen.2017.04.025

Mahmood, A., Aldabbagh, L. B. Y., and Egelioğlu, F. (2015). Investigation of single and double pass solar air heater with transverse fins and a package wire mesh layer. *Energy Conversion and Management*, *89*, 599–607. https://doi.org/10.1016/j.enconman.2014.10.028

Maleki, S. a. M., Hizam, H., and Gomes, C. (2017). Estimation of Hourly, Daily and Monthly Global Solar Radiation on Inclined Surfaces: Models Re-Visited. Energies, 10(1), 134. https://doi.org/10.3390/en10010134

Mavromatidis, L. E., Mankibi, M. E., Michel, P., & Santamouris, M. (2012). Numerical estimation of time lags and decrement factors for wall complexes including Multilayer Thermal Insulation, in two different climatic zones. *Applied Energy*, *92*, 480–491. https://doi.org/10.1016/j.apenergy.2011.10.007

Mohammed, S., Fatumah, N., and Shadia, N. (2020). Drying performance and economic analysis of novel hybrid passive-mode and active-mode solar dryers for drying fruits in East Africa. *Journal of Stored Products Research*, *88*, 101634. https://doi.org/10.1016/j.jspr.2020.101634

Mohana, Y., Mohanapriya, R., Anukiruthika, T., Yoha, K., Moses, J. A., and Anandharamakrishnan, C. (2020). Solar dryers for food applications: Concepts, designs, and recent advances. *Solar Energy*, *208*, 321–344. https://doi.org/10.1016/j.solener.2020.07.098

Mohanraj, M., and Chandrasekar, P. (2008). Drying of copra in a forced convection solar drier. *Biosystems Engineering*, *99*(4), 604–607. https://doi.org/10.1016/j.biosystemseng.2007.12.004

Muhammad, M., Muhammad, I. B., Sidik, N. a. C., and Yazid, M. D. (2016). Thermal performance enhancement of flat-plate and evacuated tube solar collectors using nanofluid: A review. *International Communications in Heat and Mass Transfer*, *76*, 6–15. https://doi.org/10.1016/j.icheatmasstransfer.2016.05.009

Musembi, M. N., Kiptoo, K. S., and Nakajo, Y. (2016). Design and analysis of solar dryer for Mid-Latitude Region. *Energy Procedia*, *100*, 98–110. https://doi.org/10.1016/j.egypro.2016.10.145

Mustayen, A., Mekhilef, S., and Saidur, R. (2014). Performance study of different solar dryers: A review. *Renewable and Sustainable Energy Reviews*, *34*, 463–470. https://doi.org/10.1016/j.rser.2014.03.020

Muzathik, A., Nik, W. B. W., Khan, I. A., Samo, K., Sopian, K., and Alghoul, M. A. (2011). DAILY GLOBAL SOLAR RADIATION ESTIMATE BASED ON SUNSHINE HOURS. *International Journal of Mechanical and Materials Engineering*, *6*(1), 75–80.https://dissem.in/p/32921373/daily-global-solar-radiation-estimate-based-on sunshine-hours

Naphon, P. (2005). Effect of porous media on the performance of the double-pass flat plate solar air heater. *International Communications in Heat and Mass Transfer*, *32*(1–2), 140–150. https://doi.org/10.1016/j.icheatmasstransfer.2004.11.001

Nwosu, N. P. (2010). Employing exergy-optimized pin fins in the design of an absorber in a solar air heater. *Energy*, *35*(2), 571–575.

https://doi.org/10.1016/j.energy.2009.10.027

Omojaro, A., and Aldabbagh, L. (2010). Experimental performance of single and double pass solar air heater with fins and steel wire mesh as absorber. *Applied Energy*, *87*(12), 3759–3765. https://doi.org/10.1016/j.apenergy.2010.06.020

Ozgen, F., Esen, M., and Esen, H. (2009). Experimental investigation of thermal performance of a double-flow solar air heater having aluminium cans. *Renewable Energy*, *34*(11), 2391–2398. https://doi.org/10.1016/j.renene.2009.03.029

Paneri, A., Wong, I. L., and Burek, S. (2019). Transparent insulation materials: An overview on past, present and future developments. *Solar Energy*, *184*, 59–83. https://doi.org/10.1016/j.solener.2019.03.091

Panwar, N. L., Kaushik, S., and Kothari, S. (2012). A review on energy and exergy analysis of solar dying systems. *Renewable & Sustainable Energy Reviews*, *16*(5), 2812–2819. https://doi.org/10.1016/j.rser.2012.02.053

Poblete, R., and Painemal, O. (2020). Improvement of the solar drying process of sludge using thermal storage. *Journal of Environmental Management*, *255*, 109883. https://doi.org/10.1016/j.jenvman.2019.109883

Rajaseenivasan, T., Ravi Prasanth, S., Salamon Antony, M., and Srithar, K. (2017). Experimental investigation on the performance of an impinging jet solar air heater. *Alexandria Engineering Journal*, *56*(1), 63–69. https://doi.org/10.1016/j.aej.2016.09.004

Sarbu, I. (2017). Solar Collectors. In *Elsevier eBooks* (pp. 29–97). https://doi.org/10.1016/b978-0-12-811662-3.00003-7

Sasongko, S. B., Suherman, S., Djaeni, M., Perdanianti, A. M., and Utari, F. D. (2020). Effects of drying temperature and relative humidity on the quality of dried onion slice. *Heliyon*, *6*(7), e04338. https://doi.org/10.1016/j.heliyon.2020.e04338

Sharma, A., Chen, C., and Vu Lan, N. (2009). Solar-energy drying systems: A review. *Renewable and Sustainable Energy Reviews*, *13*(6–7), 1185–1210. https://doi.org/10.1016/j.rser.2008.08.015

Singh, P., and Gaur, M. K. (2020). Review on development, recent advancement and applications of various types of solar dryers. *Energy Sources, Part A: Recovery, Utilization, and Environmental Effects*, 1–21. https://doi.org/10.1080/15567036.2020.1806951

Singh, P., and Gaur, M. S. (2021). Environmental and economic analysis of novel hybrid active greenhouse solar dryer with evacuated tube solar collector. *Sustainable Energy Technologies and Assessments*, *47*, 101428. https://doi.org/10.1016/j.seta.2021.101428

Sudhakar, P., and Cheralathan, M. (2020b). Thermal performance enhancement of solar air collector using a novel V-groove absorber plate with pin-fins for drying agricultural products: an experimental study. *Journal of Thermal Analysis and Calorimetry*, *140*(5), 2397–2408. https://doi.org/10.1007/s10973-019-08952-9

Tibebu, T. B. (2015, November 12). *Design, construction and evaluation of performance of solar dryer for drying fruit*. http://ir.knust.edu.gh/handle/123456789/8185

Varun, Saini, R., and Singal, S. (2007). A review on roughness geometry used in solar air heaters. Solar Energy, 81(11), 1340–1350. https://doi.org/10.1016/j.solener.2007.01.017

Venkatachalam, C., Samuel, G., Mariam, and Solomon, G. (2019). Dataset of solar energy potential assessment for Adama city (Ethiopia). *Data in Brief*, *24*, 103879.

https://doi.org/10.1016/j.dib.2019.103879

Vengadesan, E., and Senthil, R. (2020). A review on recent developments in thermal performance enhancement methods of flat plate solar air collector. *Renewable* and *Sustainable Energy Reviews*, *134*, 110315. https://doi.org/10.1016/j.rser.2020.110315

Yao, Y., Pang, Y. X., Manickam, S., Lester, E., Wu, T., and Pang, C. H. (2022). A review study on recent advances in solar drying: Mechanisms, challenges and perspectives. *Solar Energy Materials and Solar Cells*, *248*, 111979. https://doi.org/10.1016/j.solmat.2022.111979

APPENDIXES

APPENDIX-A: Experimental observation of the conventional and modified solar dryers

Table A- 1: Experimental observation of the conventional solar dryer

	solar time	Tam	Tplate	Tair,out	Tpro	Tout,dc
3-Jun	9:00	26.4	53.2	32.1	38.1	37.5
	9:30	27.3	54.3	33.9	41.2	40.7
	10:00	28.8	57.6	36.7	43.7	43.1
	10:30	29.7	61.9	38.3	49.3	48.7
	11:00	30.1	64.4	40.2	52.1	51.5
	11:30	30.6	68.8	41.6	54.5	54.1
	12:00	31.2	72.3	46.7	59.2	58.6
	12:30	32.6	76.8	49.8	62.9	62.4
	13:00	33.9	81.4	55.2	67.9	67.2
	13:30	34.5	87.6	60.8	73.5	72.8
	14:00	32.7	85.2	55.6	65.7	65.1
	14:30	31.4	83.4	52.4	64.2	63.1
	15:00	30.1	77.6	48.1	59.1	58.2
	15:30	29.5	71.5	44.2	55.3	54.6
	16:00	28.6	62.4	39.8	48.9	48.3
	16:30	27.9	55.8	37.5	44.1	43.5
	17:00	27.6	50.7	35.2	40.8	40.1
4-Jun	9:00	26.5	53.3	34.2	33.6	36.7
	9:30	27.4	54.6	35.3	34.7	41.2
	10:00	29.9	60.9	39.3	38.7	45.7
	10:30	31.2	64.7	41.4	40.9	48.5
	11:00	32.1	68.9	47.4	46.8	53.1
	11:30	32.9	72.1	50.3	49.8	54.8
	12:00	33.5	75.2	55.7	55.2	60.1
	12:30	34.6	79.5	61.5	61.1	62.9
	13:00	35.3	86.9	67.5	67.1	67.8
	13:30	35.8	92.6	73.4	72.9	69.7
	14:00	35.2	90.4	67.5	66.9	65.2
	14:30	32.4	84.1	60.4	59.6	64.1
	15:00	31.1	77.7	54.7	54.1	59.5
	15:30	30.2	69.4	48.4	47.5	53.9
	16:00	29.4	59.7	41.2	40.6	49.2
	16:30	28.1	55.1	39.3	38.3	44.1
	17:00	27.8	48.7	37.1	36.4	41.4
5-Jun	9:00	27.7	50.8	34.8	33.9	38.6

	9:30	29.5	54.4	37.8	36.7	40.2
	10:00	29.9	59.6	40.4	39.2	46.3
	10:30	30.5	64.5	41.4	40.9	46.2
	11:00	31.6	68.5	46.7	45.9	52.1
	11:30	32.5	72.1	50.2	49.5	56.2
	12:00	32.8	75.3	56.5	55.9	59.7
	12:30	33.8	80.1	61.4	60.7	62.6
	13:00	34.8	92.2	67.5	67.1	68.9
	13:30	35.5	95.4	70.9	70.5	75.2
	14:00	34.1	91.6	67.1	66.8	73.8
	14:30	33.1	83.2	60.3	59.8	64.3
	15:00	30.7	78.5	55	54.2	58.9
	15:30	29.9	72.2	47.8	47.1	53.4
	16:00	29.1	65.8	41.9	40.9	48.6
	16:30	28.1	55.7	39.8	38.7	46.3
	17:00	27.3	52.3	37.8	36.5	41.3

Table A- 2: Experimental Observation of the Modified solar dryer

	solar time	Tam	Tplate	Tair,out	Tpro	Tout,dc
13-Jun	9:00	27.6	53.1	38.6	48.6	47.7
	9:30	30.2	57.2	43.4	52.8	52.1
	10:00	30.8	60.9	45	56.2	55.6
	10:30	31.4	63.4	47.9	59.4	58.7
	11:00	32.1	70.7	50.1	66.4	66
	11:30	32.5	73.8	57.2	71.8	71.4
	12:00	33.4	78.9	61.5	75.9	75.2
	12:30	33.7	85.4	65.3	81.9	81.3
	13:00	34.2	87.9	65.4	84.4	83.9
	13:30	35.6	91.5	69.5	87.8	87.4
	14:00	34.5	89.5	67.2	87.2	86.7
	14:30	32.8	87.4	64.3	84.3	83.8
	15:00	30.8	82.4	57.2	78.1	77.5
	15:30	29.9	80.3	54.1	74.9	74.3
	16:00	29.6	75.3	50.7	66.8	66.1
	16:30	28.4	70.2	46.1	57.9	57.2
	17:00	27.6	63.1	43.2	53.2	52.3
14-Jun	9:00	27.8	52.1	40.1	48.9	47.8
	9:30	29.6	56.8	43.8	54.6	53.7
	10:00	30.2	60.3	46.8	57.1	56.3
	10:30	31.3	64.6	49.4	61.5	62.1

	11:00	31.8	72.3	53.1	69.1	68.4
	11:30	32.5	75.4	56.2	73.2	72.8
	12:00	33.2	79.4	60.6	76.5	76.1
	12:30	33.9	84.4	64.5	80.7	80.3
	13:00	34.6	87.8	69.2	84.3	83.9
	13:30	35.8	90.7	73.4	85.1	84.7
	14:00	34.2	87.1	67.3	84.9	84.5
	14:30	33.6	83.6	64.5	81.1	80.5
	15:00	31.4	77.5	59.7	74.4	73.8
	15:30	30.6	72.4	55.2	69.5	68.7
	16:00	29.7	67.9	51.1	64.1	63.2
	16:30	28.5	61.1	45.2	58.4	57.2
	17:00	27.8	56.9	43.6	54.1	52.8
15-Jun	9:00	25.6	52.7	39.2	49.5	48.4
	9:30	28.4	60.5	45.2	56.9	56
	10:00	28.9	67.8	47.8	59.8	59.1
	10:30	29.3	70.7	49.6	63.2	62.5
	11:00	30.4	74.3	55.2	69.3	68.6
	11:30	31.1	77.9	57.6	70.6	69.9
	12:00	32.3	82.7	60.5	76.1	75.4
	12:30	33.8	86.4	62.4	81.4	80.7
	13:00	34.5	88.9	63.6	85.3	84.8
	13:30	35.6	90.2	69.1	85.3	84.6
	14:00	34.9	87.3	67.3	81.9	81.2
	14:30	33.7	83.5	64.3	77.4	76.8
	15:00	31.2	79.5	58.8	72.7	71.8
	15:30	30.2	72.3	53.2	69.2	68.5
	16:00	29.5	65.2	50.6	62.4	61.7
	16:30	28.3	63.4	45.1	57.9	57.2
	17:00	27.5	60.4	42.6	54.8	53.7

APPENDIX-B: Thermocouple calibration

The calibration test for a four-channel K-type digital thermocouple was conducted with a standard thermocouple by using a 1 liter of water boiling test for 15 minutes.

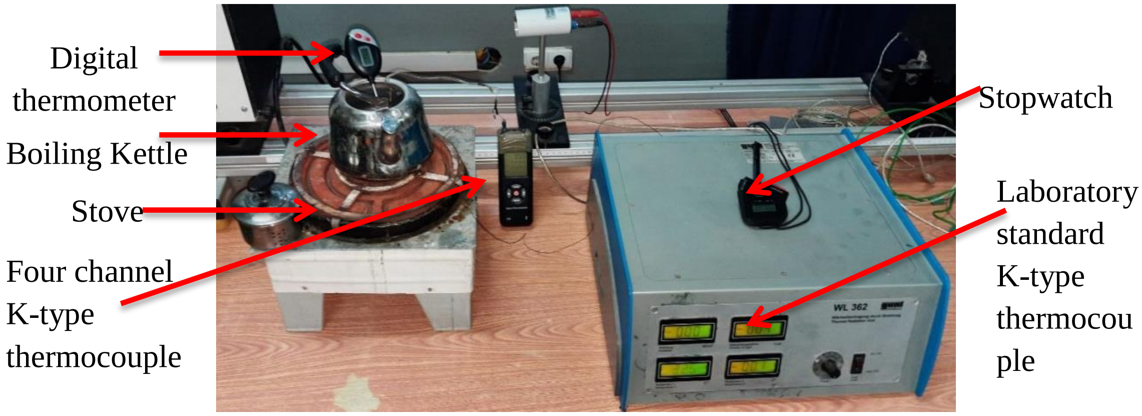

Figure B- 1: Calibration setup with standard and K-type thermocouples

Table B-1 shows the data recorded with the help of a standard thermocouple and a K-type thermocouple during calibration.

Table B- 1: Water temperature measuring test by using a K-type thermocouple

Time (minute)	$T_{1,\ water}$ (Standard thermocouple) (^{o}C)	$T_{2,\ water}$ (four-channel K-type Thermocouple) (^{o}C)	Uncertainty (%) $[(T_{1,\ water} - T_{2,\ water})/T_{1,\ water}] \times 100$
Initial water temperature	30.4	30.1	0.98684
1	32.3	31.9	0.61919
3	43.6	43.2	0.91743
5	51.6	51.3	0.58139
7	58.7	58.5	0.34071
9	67.7	67.3	0.59084
11	77.4	77.1	0.38759
13	87.1	86.8	0.34443
15	95.5	95.1	0.41884

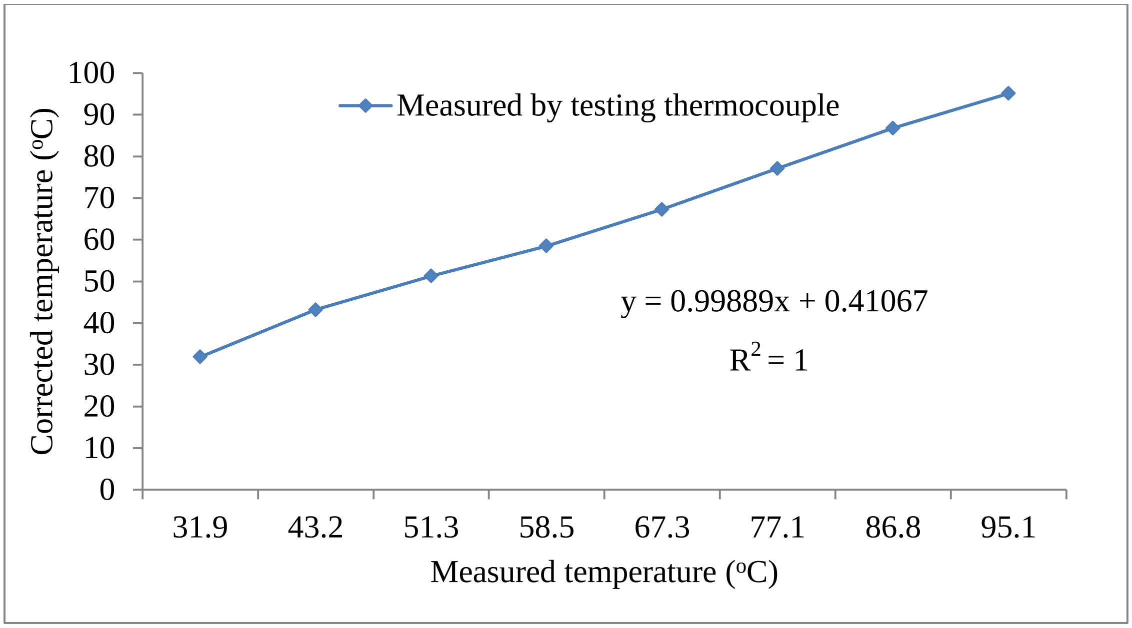

Figure B- 2: Measured Temperature versus Corrected temperature

Appendix-C: Description of Measuring Instruments Used and Their Accuracy

Four channel digital thermocouple, digital thermometer, and digital weight balance are the main measuring instruments used during experimentation. Table C-1 shows their accuracy, usage, range, and error.

Table C- 1: Description of measuring instruments used

Instrument	Model	Range	Accuracy	Error	Usage
Thermocouple	K-type thermocouple	0-1500 °C	±0.1 °C	0.4%	To measure components temperature
Thermometer	Digital thermometer	-50–200 °C	±0.1 °C	0.4%	To measure the ambient temperature
Digital weight balance		0 – 2 kg	±0.0001g		To measure product mass

Appendix-D: Description of the exhaust fan used

Table D- 1: Specifications of the exhaust fan used

Size	Voltage	Power
200mm	AC 20V/50Hz	30 W

Figure D- 1: Exhaust fan used

Appendix-E: Cost analysis

Table E- 1: Cost Analysis

S. No.	Cost description		Quantity	Unit price (ETB)	Total amount (ETB)
	Material	Specification			
1.	Galvanized iron sheet	1m × 2m	1	1000	1000
2.	Tin sheet metal	1m × 2m	1	600	600
3.	Glass cover	1m × 2m	1	3000	3000
4.	Square steel pipes	Total 8 m	2 with different diameters	-	1800
5.	Silica gel	1 gallon	2	450	900
6.	Paint	1 gallon	2	300	600
7.	Insulating material	1m × 2m	1	500	500

8.	Exhaust fan	Size: 200mm, Power: 30 W	1	2000	3000
9.	Tray	0.9m × 1m	5	150	750
10.	Manufacturing cost	-	-	-	2000
		Total			14,150

Appendix-F: Product preparation

Roasted Beans, peas, and chickpeas were washed and prepared for drying. Onion, garlic, and ginger were chopped and prepared for drying.

Figure F- 1: Product preparation

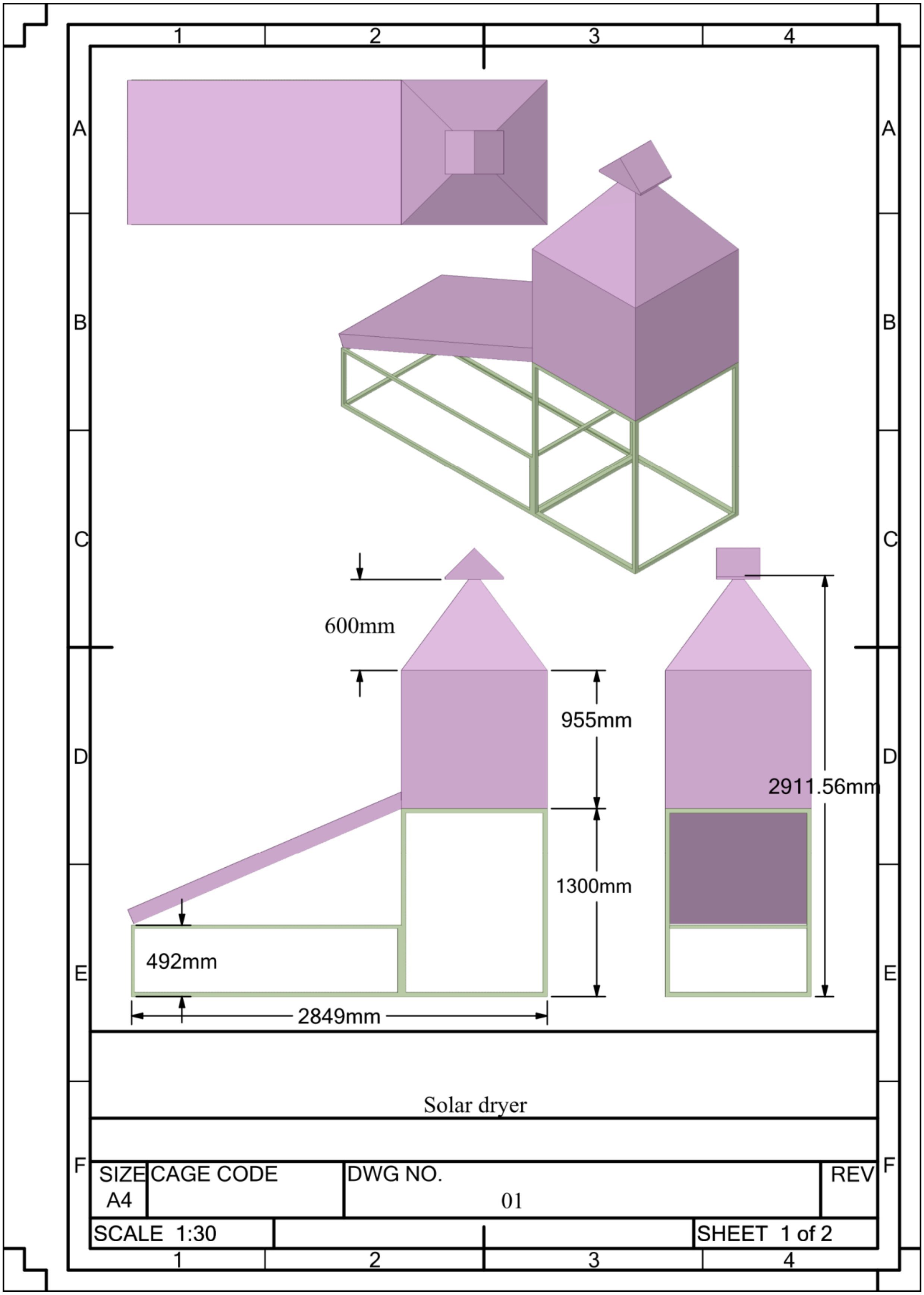
1
2
3
4
A
B
C
D
E
F
600mm
955mm
1300mm
2911.56mm
492mm
2849mm
Solar dryer
SIZE
A4
CAGE CODE
DWG NO.
01
REV
SCALE 1:30
SHEET 1 of 2

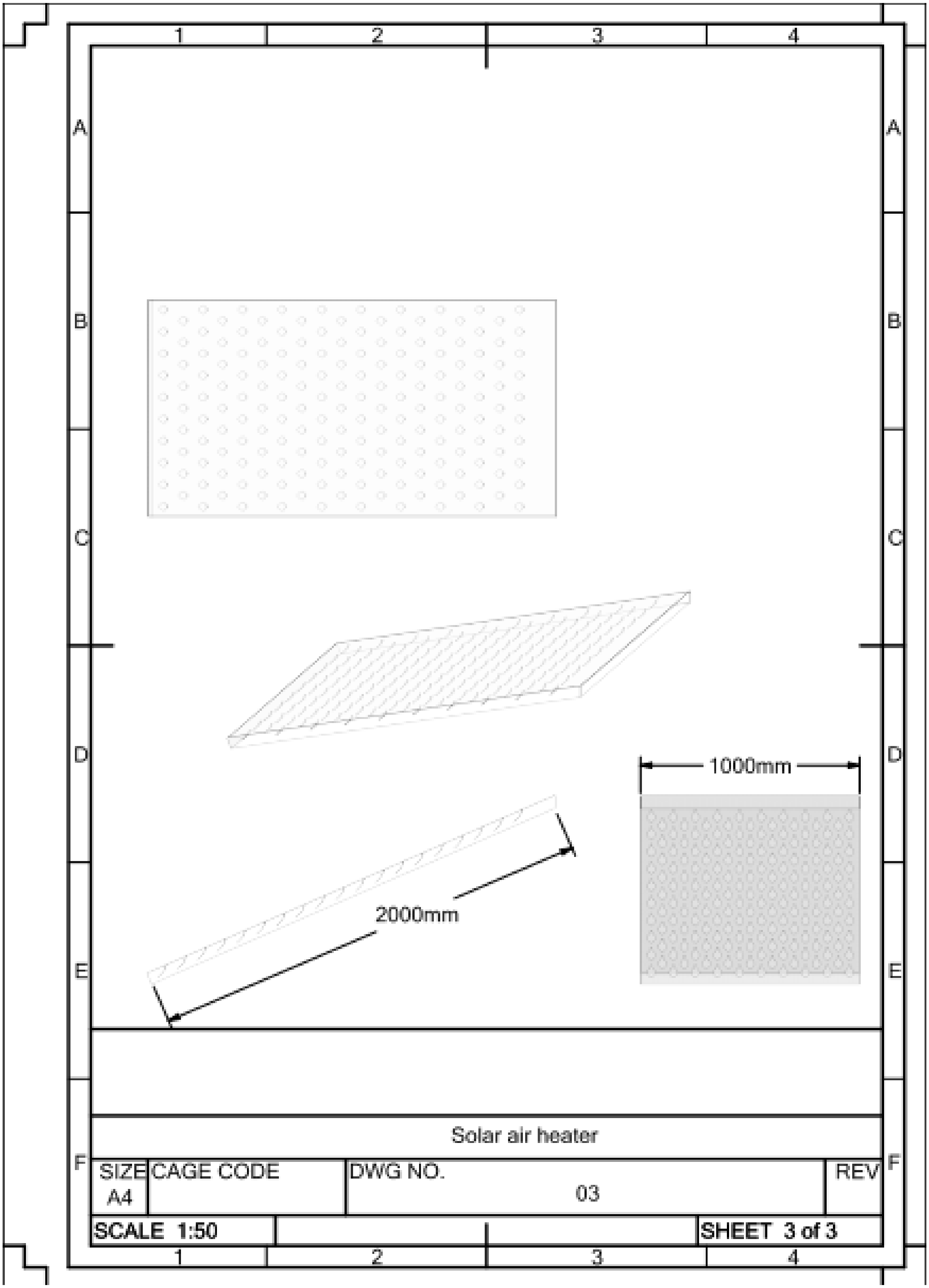
1000mm
2000mm
Solar air heater
SIZE A4
CAGE CODE
DWG NO. 03
REV
SCALE 1:50
SHEET 3 of 3

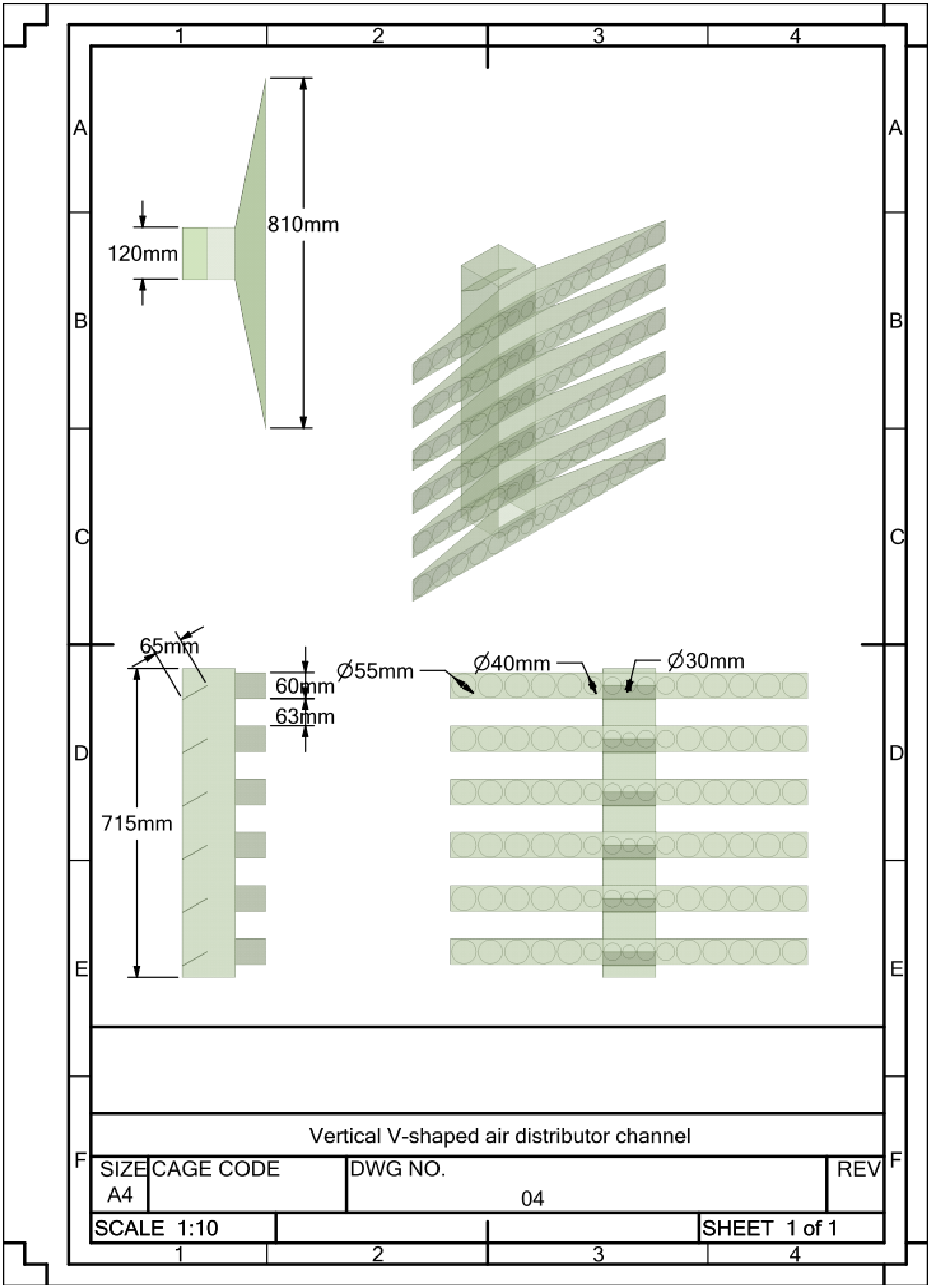
1
2
3
4
A
B
C
D
E
F
810mm
120mm
65mm
60mm
63mm
715mm
∅55mm
∅40mm
∅30mm
Vertical V-shaped air distributor channel
SIZE
A4
CAGE CODE
DWG NO.
04
REV
SCALE 1:10
SHEET 1 of 1

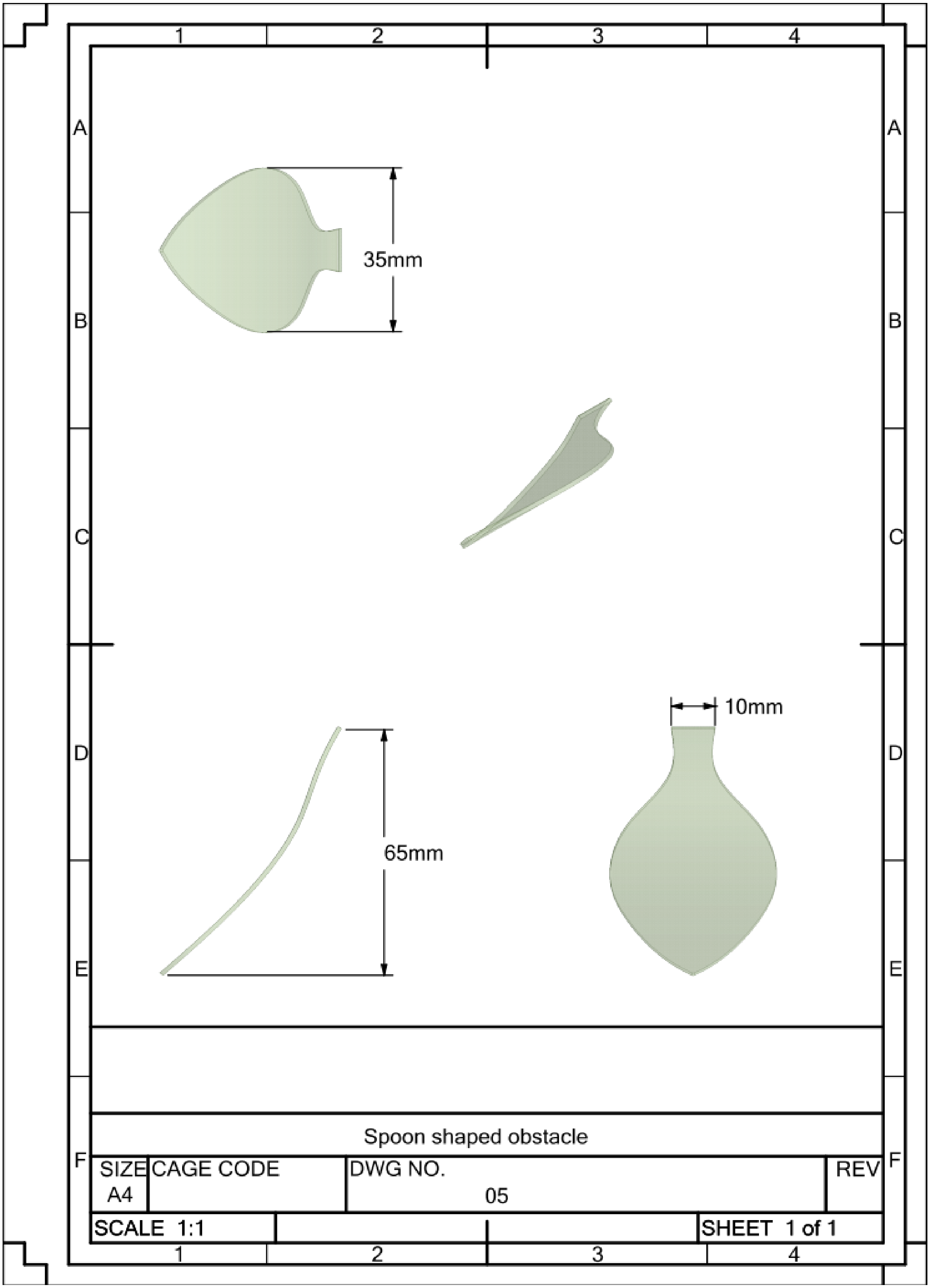
1
2
3
4
A
B
C
D
E
F
35mm
10mm
65mm
Spoon shaped obstacle
SIZE
A4
CAGE CODE
DWG NO.
05
REV
SCALE 1:1
SHEET 1 of 1